FINITE-WAVELENGTH INSTABILITY COUPLED TO A GOLDSTONE MODE: THE NIKOLAEVSKIY EQUATION

Eman Simbawa, MMath.

Thesis submitted to the University of Nottingham
for the degree of Doctor of Philosophy

December 2011

Abstract

The Nikolaevskiy equation is considered as a simple model exhibiting spatiotemporal chaos due to the coupling of finite-wavelength patterns to a long-wavelength mode (Goldstone mode). It was originally proposed as a model for seismic waves and is also considered as a model for various physical phenomena, including electroconvection, reaction-diffusion systems and transverse instabilities of travelling fronts for chemical reactions. This equation has attracted the attention of several researchers due to its rich dynamical properties and physical applications. We are interested in studying this equation closely by means of numerical computations and asymptotic analysis.

In this thesis we reinstate the dispersive terms, in contrast to most research regarding the Nikolaevskiy equation, and study the effect on the stability of spatially periodic solutions, which take the form of travelling waves. It is shown that dispersion can stabilise the travelling wave solutions, which emerge at the onset of instability of the spatially uniform state. The secondary stability plots exhibit high sensitivity on the degree of dispersion and can sometimes be remarkably complicated. Dispersive amplitude equations are derived: numerical simulations manifest behaviour similar to the non-dispersive case but there is a drift of the pattern with a certain speed.

Another aspect of this thesis is analysing systems similar to the Nikolaevskiy equation, where they incorporate a Goldstone mode and possess the same symmetries. We conclude that such systems share with the Nikolaevskiy equation the fact that roll solutions are unstable at the onset of instability. We also study the amplitude equations of these systems numerically and deduce that statistical measures of their solutions depend on the ratio of the curvatures of the dispersion relation near the finite-wavelength and long-wavelength modes. Finally, we consider a system coupling a Swift-Hohenberg equation to a large-scale mode. The result of this study shows that there can be stable stationary wave solutions, in contrast to the Nikolaevskiy equation.

To all the mothers in the world who are juggling their dreams and their family

Acknowledgements

I want to express my deepest gratitude to Allah Almighty for all His blessings, His graciousness and His Mercifulness, and for empowering me with the strength and perseverance to continue this challenging journey.

To the King Abdul Aziz University, my educational and financial sponsor, thank you for being generous and for making this journey possible.

To my academic supervisors, Dr. Stephen Cox and Dr. Paul Matthews, my educators and mentors, thank you for your unconditional patience, your genuine encouragement and your sincere non-judgmental and professional outlook. Thank you for providing me with the opportunity to learn from your expertise and for disclosing your profound knowledge unstintingly. I appreciate your thorough help and constructive criticism that has enabled me to transform my work, progress and academic writing into a meaningful reality. I am so grateful.

To the Staff of the School of Mathematical Sciences at the University of Nottingham, I appreciate your consistent support and helpfulness. Thank you for being friendly and for being easily approachable; that made all the difference!

To my loving parents Mona Hammoudah and Ahmed Simbawa, my role models, you have set an extraordinary example for me. Thank you for your continuous encouragement and your boundless prayers. To my soul mate, my husband, Mohammed, thank you for giving me the space, the freedom and the independence to accomplish and fulfil my dream. You constantly empowered me to go on in hard times; words cannot express my appreciation to you. To my beloved children, Tawfiq and Yomna, the joy of my life; thank you for boosting me with your captivating positive energy to continue the journey. To my brother Ayman, thank you for encouraging and supporting me throughout this journey. To all of my family and friends in Jeddah, thank you for tolerating my remoteness (of living overseas) for the sake of academic achievement. Last but not least, to my wonderful friends in Nottingham, thank you for making me feel amongst my family and making Nottingham feel like home.

Contents

Chapter 1

Introduction

In the last few decades spatiotemporal chaos has started to attract considerable attention. The Nikolaevskiy equation is considered as a simple pattern forming-dissipative model with finite-wavelength instability exhibiting chaos directly at onset. Although it is a simple model, there are still some unanswered questions regarding the behaviour of the system, which is strongly influenced by the presence of a long-wavelength Goldstone mode (growth rate vanishes at zero wavenumber for any value of the bifurcation parameter). Our motivation is to understand the properties of the solution by means of analytical and numerical approaches. Before we introduce our work, some background information about the Nikolaevskiy equation and some related pattern forming systems will be presented, in addition to a literature review.

1.1 Background

The main pattern forming partial differential equation (PDE) studied in this thesis is the Nikolaevskiy equation. Throughout the thesis other models will be present which are the Ginzburg-Landau, Swift-Hohenberg and Kuramoto-Sivashinsky equations. This section will be devoted to presenting the Nikolaevskiy equation in addition to these equations, with brief descriptions and some main properties.

1.1.1 The Nikolaevskiy equation

In 1989 V. N. Nikolaevskiy [45] proposed a model for longitudinal seismic waves as follows:

$$\frac{\partial v}{\partial t} + v\frac{\partial v}{\partial x} = \sum_{p=1}^{n} A_{p+1}\frac{\partial^{p+1} v}{\partial x^{p+1}}, \tag{1.1}$$

where v is the displacement velocity and A_{p+1} are constants. In reviewing the literature, a standard rescaled form is considered where only the dissipative terms $\dfrac{\partial^2 u}{\partial x^2}$ and $\dfrac{\partial^6 u}{\partial x^6}$ and the destabilising term $\dfrac{\partial^4 u}{\partial x^4}$ are kept and the other spatial derivatives are ignored. Equation

(1.1) then becomes

$$\frac{\partial u}{\partial t} + u\frac{\partial u}{\partial x} = -\frac{\partial^2}{\partial x^2}\left[r - \left(1 + \frac{\partial^2}{\partial x^2}\right)^2\right] u, \tag{1.2}$$

and is known as the Nikolaevskiy equation (see for example [14, 79]). In numerical simulations, this PDE is generally solved in some finite domain $0 \leq x \leq l$ with periodic boundary conditions. Furthermore, r and l are the free parameters of the problem.

An equivalent form of (1.2) was also used in some studies; for example, [22, 62, 68]. This form is

$$\frac{\partial \phi}{\partial t} + \left(\frac{\partial \phi}{\partial x}\right)^2 = -\frac{\partial^2}{\partial x^2}\left[r - \left(1 + \frac{\partial^2}{\partial x^2}\right)^2\right] \phi. \tag{1.3}$$

The only difference between (1.2) and (1.3) is the nonlinear term. However, by differentiating (1.3) with respect to x and putting $2\phi_x = u$ we obtain (1.2). Thus the two equations are equivalent, and it is a personal choice to consider either one of them. It is worth mentioning that (1.3) is similar to the Kuramoto-Sivashinsky equation [8, 41] with an additional term involving the sixth spatial derivative, and this may be a reason for preferring this form over (1.2). In this thesis we study (1.2), and we refer to it as "the Nikolaevskiy equation".

The Nikolaevskiy equation has Galilean symmetry: $x \mapsto x + Vt$, $u \mapsto u + V$ (where V is a constant), which implies that the spatial average of u may be set to zero. This is because $\dfrac{d}{dt}\displaystyle\int_0^l u dx = 0$, and therefore the spatial average of u: $\langle u \rangle = \dfrac{1}{l}\displaystyle\int_0^l u dx$ is a constant, which can be chosen to be zero. This is since the addition of a constant to a solution of the Nikolaevskiy equation corresponds to transforming to a moving frame of reference. Moreover, the Galilean symmetry will lead to the existence of a large-scale mode, corresponding to wavenumbers near zero, in the weakly nonlinear regime. In addition to the previous symmetry, (1.2) satisfies the space translation symmetry: $x \mapsto x+$constant and the time translation symmetry: $t \mapsto t+$constant. Both of these symmetries mean that any shift in space or time will give the same behaviour as a solution to (1.2). The final symmetry we have is the reflection symmetry: $x \mapsto -x$ and $u \mapsto -u$. This kind of symmetry is only satisfied if the equation consists of even spatial derivatives, and thus it applies to (1.2). On the other hand, (1.1) involves both odd and even derivatives, and consequently, the reflection symmetry is broken.

In attempting to characterise the behaviour of the solution of (1.2) we first consider a linearised version of this equation around the steady state solution $u \equiv 0$. Then we calculate solutions proportional to $e^{\mathrm{i}kx+\lambda t}$, where k is the wavenumber and λ is the growth rate. After substituting in (1.2) and linearising, we obtain the dispersion relation which behaves as follows: for small positive r there exists a narrow band of unstable wavenumbers centred at the critical wavenumber (see the solid line in figure 1.1). In addition to this, we have a stable but slow neutral mode near $k = 0$ (large-scale mode). If $r = 0$, then we have neutral

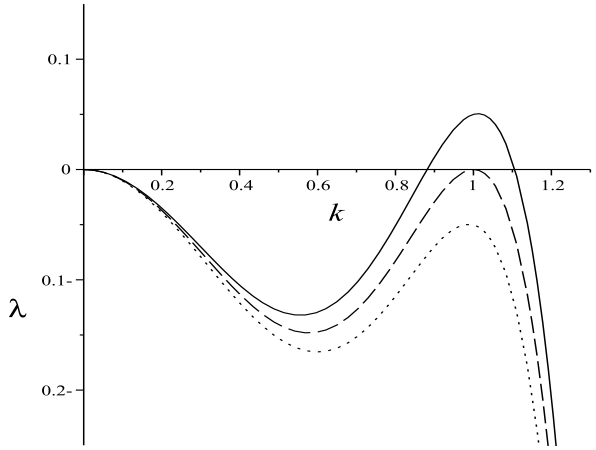

Figure 1.1: The growth rate of the linear Nikolaevskiy equation for $r = 0.05$ (solid line), $r = 0$ (dashed line) and $r = -0.05$ (dotted line).

stability at the critical wavenumber (dashed line in figure 1.1). If r is negative, then all modes are linearly damped and the steady state solution is stable as shown in figure 1.1 (dotted line). Hence r is the stability control (bifurcation) parameter, where the solution $u \equiv 0$ becomes unstable as r increases through zero. Therefore, we are interested in studying the properties of the solution just beyond the onset of instability; that is, when r is small. Thus we introduce the notation

$$r = \epsilon^2 \ll 1.$$

This notation is consistent with [14, 40, 47, 48, 79]. However, a considerable amount of the literature uses ϵ instead of r in (1.2); for example, [52, 68, 72, 80]. Therefore, the research done using ϵ may seem different from our results; nevertheless, they are indeed equivalent.

1.1.2 Pattern forming systems

1.1.2.1 The Ginzburg-Landau equation

The Ginzburg-Landau equation [3, 16] is given as follows:

$$\frac{\partial A}{\partial T} = A + (1 + \mathrm{i}a)\frac{\partial^2 A}{\partial X^2} - (1 + \mathrm{i}b)|A|^2 A.$$

Here $A(X, T)$ is a complex amplitude with slow space and time scales: $X = \epsilon x$ and $T = \epsilon^2 t$. The coefficients a and b are real. The Ginzburg-Landau equation arises as an amplitude equation describing the slow time and space scales near the onset of pattern formation close to the threshold of the first instability. If the system undergoes supercritical bifurcation with translation and reflection symmetries and finite-wavelength instability (occurring with a nonzero wavenumber), then the Ginzburg-Landau equation is an appropriate amplitude equation exemplifying the modulation of waves [43, 53]. If a and b are both nonzero, then

the envelope A will take the form of a travelling wave. On the other hand, if a and b are both zero then the unstable modes are waves growing in time and stationary in space.

It is important to stress that in the case of long-wavelength instability, corresponding to wavenumber near zero, the Ginzburg-Landau equation is no longer valid. Depending on the symmetries of the model and the linear dispersion relation, the nonlinear dynamics are governed by different order parameter equations [42]. This case also arises in the Nikolaevskiy equation where finite-wavelength instability is coupled to a large-scale mode. This will result in a different amplitude equation from the known Ginzburg-Landau equation [40].

1.1.2.2 The Swift-Hohenberg equation

The Swift-Hohenberg equation is a widely studied pattern forming system. It is considered as a simple model PDE for pattern formation. It was originally derived by Swift and Hohenberg [59] as a model for thermal convection. The Swift-Hohenberg equation has also been related to various physical contexts. Some of these applications are lasers [38], flame fronts [25], magnetoconvection [15], Rayleigh-Bénard convection [59] and optical bistability [65, 66].

The Swift-Hohenberg model is defined by the PDE

$$\frac{\partial w}{\partial t} = \left[r - \left(1 + \frac{\partial^2}{\partial x^2} \right)^2 \right] w - sw^2 - w^3,$$

where r is the convection parameter and $s \geq 0$ since we have the symmetry: $w \mapsto -w$ and $s \mapsto -s$. Unlike the Nikolaevskiy equation the sixth spatial derivative does not appear in this equation. Furthermore, this equation has different nonlinear terms than the Nikolaevskiy equation: here the nonlinear terms are proportional to w^2 and w^3.

The stability analysis of the steady state solution $w = 0$ shows that for small r the long-wavelength modes are all damped. Moreover, there exists a band of unstable wavenumbers corresponding to finite-wavelength instability [5] (see figure 1.2). This will lead to the formation of roll solutions and thus the Swift-Hohenberg equation can be reduced, by the usual scaling for the weakly nonlinear analysis, to the Ginzburg-Landau equation, which describes the modulation of rolls [16]. The stability of rolls will be given by the Eckhaus stability condition [73].

1.1.2.3 The Kuramoto-Sivashinsky equation

Another widely known pattern forming system is the Kuramoto-Sivashinsky equation

$$\frac{\partial v}{\partial t} + v\frac{\partial v}{\partial x} = -\frac{\partial^2 v}{\partial x^2} - \frac{\partial^4 v}{\partial x^4}. \tag{1.4}$$

This equation was proposed by Kuramoto and Tsuzuki [36] as a model for phase dynamics in reaction-diffusion systems. In addition to this, Sivashinsky [55] derived this equation to

model small thermal diffusive instabilities in laminar flame fronts. This equation arises also among other physical applications including chemical reaction waves [81], plasma ion mode instabilities [37], fluctuations in liquid films on inclines [57], propagation of combustion fronts in gases [56] and others.

There is another form of the Kuramoto-Sivashinsky equation known as the damped or stabilised Kuramoto-Sivashinsky equation [5, 16, 19, 41, 77], which may be rescaled to the form

$$\frac{\partial v}{\partial t} + v\frac{\partial v}{\partial x} = \left[r - \left(1 + \frac{\partial^2}{\partial x^2}\right)^2\right] v. \tag{1.5}$$

Here r is the stability control parameter. The damped Kuramoto-Sivashinsky equation is used to exhibit the transition from periodic stationary states to spatiotemporal chaos as r approaches 1 [19]. Note that for $r = 1$, both forms of the Kuramoto-Sivashinsky equation given in (1.4) and (1.5) are equivalent (by rescaling) and so we can consider any form in this case.

The damped Kuramoto-Sivashinsky equation shares the same linear terms as the Swift-Hohenberg equation; however, the nonlinear term is different. Therefore, they both have the same dispersion relation. Figure 1.2 represents the growth rate of the linearised damped Kuramoto-Sivashinsky equation. As shown in the figure, the zero solution is unstable to perturbations with finite wavenumbers. Therefore, similarly to the Swift-Hohenberg equation, rolls exist and the damped Kuramoto-Sivashinsky equation can be reduced to the Ginzburg-Landau equation [16] leading to the Eckhaus instability [41].

The Swift-Hohenberg and damped Kuramoto-Sivashinsky equations are both pattern forming systems exhibiting finite-wavelength instability. Therefore, by using the well-known scaling for pattern forming systems, they can both be reduced to the Ginzburg-Landau equation for small r. In contrast, the Nikolaevskiy equation has an anomalous scaling, which leads to coupled amplitude equations different from the Ginzburg-Landau equation. This is due to the Galilean invariance responsible for the appearance of a large-scale mode significantly changing the behaviour of the solution.

1.2 Pattern forming systems coupled to a large-scale mode

In the Nikolaevskiy equation there is a coupling between finite-wavelength instability and a large-scale neutral mode. The mode interaction strongly affects the nonlinear behaviour, although the large-scale mode is (slowly) linearly damped, as shown in figure 1.1. Due to this coupling, the system destabilises dramatically, and the steady spatially periodic patterns are replaced with a spatiotemporally chaotic state (see for example figure 1.3). The influence of the large-scale mode on the dynamics of the solution was also studied in different contexts.

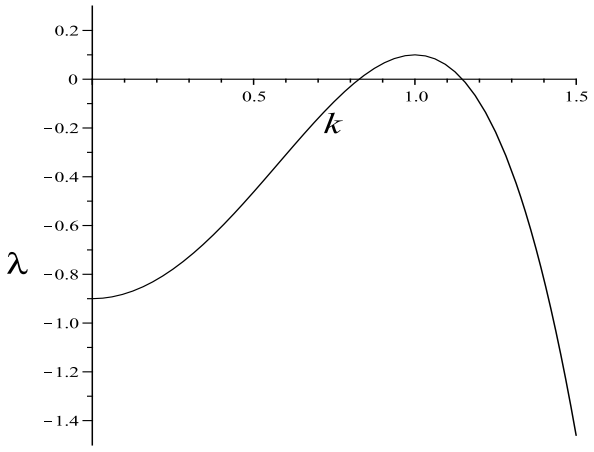

Figure 1.2: Dispersion relation of the Swift-Hohenberg and damped Kuramoto-Sivashinsky equations as a function of the wavenumber k with $r = 0.1$.

An interesting example of such coupling appears in a system of the complex Swift-Hohenberg equation coupled to a Goldstone mode for flame fronts [25], where they found that the strong coupling modifies the stability of travelling waves. In particular, the travelling wave patterns are destabilised and this leads to the transition to spatiotemporal chaos. Another coupled Swift-Hohenberg equation and a Goldstone mode was presented and studied in [51]. Due to this coupling, the periodic patterns are unstable to zigzag instability and a chaotic behaviour arises. Lega *et al.* [38] discovered that the coupling of the Swift-Hohenberg model for lasers to a large-scale mode leads to the appearance of higher order instabilities. Moreover, this also results in the shrinkage of the Busse balloon [9] for the stability of travelling wave solutions. The influence of the coupling of the neutral mode on the Swift-Hohenberg equation will be investigated in this thesis. The stability analysis reveals a new type of modulational instability of waves.

1.3 Previous work on the Nikolaevskiy equation

In this section we shall introduce previous research concerning the Nikolaevskiy equation (1.2) in terms of theoretical and numerical results in addition to applications.

1.3.1 Numerical simulations

There have been extensive numerical simulations performed regarding the Nikolaevskiy equation. These simulations exhibit chaotic dynamics in both space and time as r increases through zero. In particular, immediately after the instability onset, the system becomes "turbulent" [32] even at extremely small values of r [71]. The spatially uniform stationary state directly transforms to dynamical chaos, which is called soft-mode turbulence [68, 70].

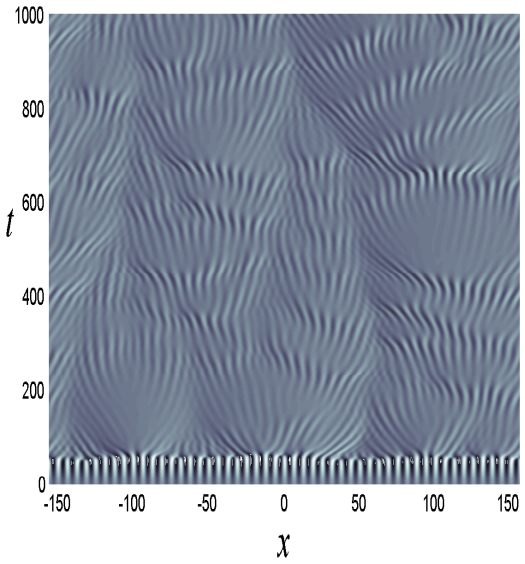

Figure 1.3: Space-time numerical simulation of the solution of the Nikolaevskiy equation with $r = 0.05$.

This is due to the interaction of the finite-wavelength and long-wavelength instabilities. The neutral mode destabilises the stationary spatially periodic patterns resulting from the finite-wavelength instability, and thus all roll solutions are unstable in sufficiently large domains [72].

A typical example of a numerical solution showing the evolution of chaotic disturbances of the Nikolaevskiy equation for positive r ($r = 0.05$) is displayed in figure 1.3. Here the total integration time of the simulation is 1000, the number of grid points is 512 and the domain size is $l = 100\pi$ allowing fifty rolls in the domain. A cosine wave with small amplitude and wavenumber $k = 1$ plus small random noise is used as the initial data. The numerical simulation is carried out using a pseudo-spectral scheme for spatial discretisation [21, 67] and a second-order exponential time differencing method for time integration [13] (the *Matlab* code is given in appendix B). As exhibited in the simulation, immediately after onset, the rolls become unstable as they are replaced with a chaotic state where there is no development of arranged structures.

The numerical simulations performed regarding the Nikolaevskiy equation revealed the spatiotemporal chaotic state of the solution. This raised the interest in trying to explain this kind of behaviour analytically. Thus reducing the Nikolaevskiy equation to amplitude equations helps answer this question.

1.3.2 Amplitude equations and properties

In order to obtain information about the complicated dynamics of the solution of (1.2) near a bifurcation point, it should be reduced to amplitude equations describing slow modulations in space and time of the envelope of the finite-wavelength pattern. These equations are derived using an expansion of the solution of the full equation in the control parameter. Specifically, this involves writing the leading-order term as a product of a pattern and a slowly varying amplitude. Moreover, the space and time variables are replaced with slower scales to allow the development of self-consistent amplitude equations. After substituting the asymptotic expansion of the solution in (1.2) and equating coefficients of higher harmonics along with solvability conditions we obtain the required amplitude equations.

The scaling used to derive these equations must be tested against numerical computations. This scaling is different from the conventional case where the pattern forming system with finite-wavelength instability is described at onset by the usual Ginzburg-Landau equation [43, 53]. There were several attempts before the right scaling was achieved because it is not a straightforward case. Indeed, the numerical computations, which are needed to confirm the correct scaling, should be done near the onset in a large domain to contain all of the unstable modes. Also because of the slow evolution of the solution the computations need to be done over a long period of time. Therefore, due to these expensive computations, the data were limited; and therefore the scaling was controversial.

One of the first analytical attempts to find the amplitude equations was in [39]. Malomed derived coupled generalized Ginzburg-Landau equations for the slowly varying amplitude of the rolls and the real neutral mode. Due to the symmetry features of (1.2) (Galilean invariance), an equation for the large-scale mode is included [12]. These amplitude equations predicted the existence of a finite range of stability of rolls. This result is in fact wrong because it was shown later that all steady spatially periodic patterns are unstable [40, 72]. This contradiction arises since the equations found in [39] are not asymptotically self-consistent: they do not result from a systematic expansion in the powers of small r. Furthermore, these equations need to be supplemented with higher-order correction terms. Therefore, some terms are omitted from the dispersion relation, which gives a wrong result regarding the stability of rolls.

Calculating the root mean square (rms) of the solution of (1.2) (averaged over a long time) against the value of the supercriticality parameter r is a sufficient way for finding the correct scaling. In [32] and [71] it was suggested that the rms of u is scaled as 1 and $1/2$ power of r, respectively. These results are inaccurate since in [32] the domain size is small, which may not contain all of the unstable modes. Moreover, the rms of u is calculated for

large values of r ($0.05 \leq r \leq 1.2$) and in this case the exponent has not yet converged to the correct value. On the other hand, the result in [71] was established for a single value of r, which is not enough to conclude a general result for the scaling.

Finally, a successful attempt to reduce (1.2) to asymptotically consistent coupled amplitude equations was conducted in [40]. The amplitude equations capturing the dynamics of (1.2) show that the amplitude of the solution is scaled as $r^{3/4}$. This scaling is different from the usual Ginzburg-Landau equation where the amplitude of the solution is scaled as $r^{1/2}$. This anomalous scaling has been tested against numerical computations, in particular, to the rms of the solution of (1.2). The result found in [40] is that the rms of u is proportional to $r^{3/4}$ for $0.01 < r < 0.1$, and later in [62] the same result was found for a wider range in r ($0.001 < r < 0.1$). If $r > 0.1$, the amplitude equations found in [40] are no longer valid to describe the behaviour of the solution of (1.2). This is because when $r = 0.1$ the long-wavelength and finite-wavelength instabilities become indistinguishable. Therefore, as r increases the Nikolaevskiy chaos becomes similar to the Kuramoto-Sivashinsky chaos where the long-wavelength instability is dominant [52, 62] (see figure 2.1 given later in chapter 2).

The amplitude equations found in [40] stimulated further investigations. In particular, the scaling used to derive these equations was closely considered by [47, 79], where they extracted the large-scale mode and the slowly varying amplitude from the calculated solution of (1.2) by using Fourier filters. Then they computed the time-averaged rms of both modes for $10^{-5} \leq r \leq 0.04$. The result shows that the scaling of the complex amplitude is consistent with [40]. In contrast, the large-scale mode has a different scaling from [40]. This difference suggests adding extra r-dependent terms to the amplitude equations found in [40]. Thus the modified amplitude equations provide a better representation of the Nikolaevskiy chaos according to [47, 79]. It seems that the estimated rms of the large-scale mode is very close to the result found in [40]. Therefore, adding the higher order correction terms to the amplitude equations are not necessary.

Another important aspect of the amplitude equations [40] is the numerical simulations. This should be done in order to test whether they exhibit the Nikolaevskiy chaos or not. Simulations performed in [40] show similar behaviour to the Nikolaevskiy dynamics even for small r [52]. The latter investigated these equations closely by means of numerical computations of the complex amplitude and the large-scale mode. It was found that the simulations reveal the chaotic structure of these two modes. In particular, regarding the pattern amplitude we have a co-existence of spatiotemporal chaos and an amplitude-death state, where $|A|$ is approximately equal to zero in a thin region in the central domain. Correspondingly, the large-scale mode also shows a chaotic state but incorporated with a single-front state in the middle of this dynamical chaos. Analogous behaviour to the single-

front state is observed in the Nikolaevskiy equation close to the onset of instability. A further investigation was done in [47, 48] for small and large domains where statistical measures of the two states were calculated along with some important features. One of the significant results drawn from this study is that there is a random movement of the single-front and the amplitude-death state if the domain size is small. In addition, the structure of these two states strongly depends on the domain size.

1.3.3 Higher dimensional amplitude equations

All of the above research, which has been done regarding the Nikolaevskiy equation, is for the one-dimensional case. Regarding higher dimensions, Fujisaka *et al.* [22] extended the amplitude equations found in [40] to the two-dimensional case. These equations have an extra higher-order viscosity term, which is important for stabilising the high-wavenumber modes in the simulations. In these equations the bifurcation parameter is scaled out, and thus they are computationally less expensive than the two-dimensional Nikolaevskiy equation. Numerical calculations in the two-dimensional system show that the solution of these equations remains finite. According to [22], the scaling used in the one-dimensional case is also valid for the two-dimensional case.

1.3.4 The damped Nikolaevskiy equation

Another way to study the dynamics of the solution of the Nikolaevskiy equation is to add an extra free parameter. This will be beneficial in that we can control this parameter and reduce it to reach the Nikolaevskiy chaos. Therefore, we can study the transition from regular stable solutions to spatiotemporal chaos occurring at onset as we reduce the extra parameter. Adding terms which cause the neutral mode to be linearly damped will achieve this goal.

In [14] damping terms were added to (1.2) and a detailed study for different degrees of damping was conducted. The transition from ordered stable rolls to chaos at onset was observed from numerical simulations as the damping was reduced to zero. By studying the stability of rolls analytically and numerically, the result revealed that strong damping reduces the Nikolaevskiy equation to a modified Ginzburg-Landau equation, which describes the dynamics of the solution. This leads to the existence of an Eckhaus-like [18, 28] stability region. On the other hand, weak damping destabilizes the rolls. This means that there is a critical value of damping, above which stable rolls exist for a fixed value of r. The last roll solutions losing stability, as damping is reduced, lie in a small cusp close to the marginal stability curve.

Different damping terms were added to the Nikolaevskiy equation in [70]. In this study a single generic dispersion relation was found for the stability of rolls for different scaling ranges and explanation of crossing over between them. The damping terms considered in [14, 70] give equivalent results. This is because by rescaling the two versions of the damped Nikolaevskiy equations we can find the corresponding result in both studies. Note that the aforementioned cusp of stability was not discovered in [70].

1.3.5 The dispersive Nikolaevskiy equation

The original Nikolaevskiy model [45] consists of odd and even spatial derivatives. As mentioned earlier, most of the existing studies consider only the even derivatives up to the sixth order. As we already know, adding extra terms to the Nikolaevskiy equation gives the opportunity to study the influence on the solution as we vary the coefficients and progressively reduce them to reach the Nikolaevskiy chaos. In addition to this, it is expected that these extra terms will lead to the existence of travelling wave solutions, due to the broken reflection symmetry. Therefore, similarly to the Kuramoto-Sivashinsky equation [31], if dispersion is strong we expect stable travelling wave solutions.

Beresnev and Nikolaevskiy [6] reinstated some odd derivatives and concluded that dispersion either destabilises the rolls or does not have any effect on the solution. This result is not accurate and needs to be reconsidered since it is based on insufficient numerical calculations and ambiguous evidence. We will see later that dispersion has a strong influence on the solution, in fact it stabilises the rolls. In [39] some of the odd derivatives were taken into account. The stability of travelling wave patterns resulting from the oscillatory finite-wavelength instability, after adding a dispersive term, was investigated. This was done by reducing the dispersive Nikolaevskiy equation to coupled generalised Ginzburg-Landau equations for the amplitude of travelling waves and the large-scale mode. These equations consist of the correct terms with some wrong coefficients and some extra terms, which should have been balanced out. Therefore, as with the non-dispersive Nikolaevskiy equation, these equations are not asymptotically self-consistent. As a consequence, the stability range of the travelling wave solutions is not accurate.

Numerical simulations of the dispersive Nikolaevskiy equation show the change of the chaotic state of the Nikolaevskiy equation to the periodic structure as the dispersion increases [34]. The conclusion which can be drawn is that there exists a threshold value of the dispersion coefficient, depending on r, above which stable travelling wave solutions exist [34].

1.3.6 Exact solutions of the Nikolaevskiy equation

The Nikolaevskiy equation admits exact travelling wave solutions [34]. The numerical simulation of the perturbed exact solution shows that throughout the simulation this solution retains its shape; and thus is stable. Although there is an exact stable solution of (1.2), it is of limited value and cannot describe the Nikolaevskiy chaos. In the numerical simulations we have spatiotemporal chaos (see figure 1.3) and this cannot be described by the exact travelling wave solutions mentioned. Therefore, this kind of solution is not considered in our study.

1.3.7 Applications

The Nikolaevskiy equation is a widely studied PDE due to its rich dynamical properties and physical applications. It was originally proposed for modelling longitudinal seismic waves in viscoelastic media [45]; afterwards researchers have shown an increased interest in applications of this equation. One of the applications is that the Nikolaevskiy equation is considered as a simple model for finite-wavenumber pattern formation coupled to a neutral mode arising from continuous symmetry (Galilean symmetry) [40, 72]. Significant research has been devoted to applying the Nikolaevskiy equation to many physical phenomena. Some examples of these applications include electroconvection [2, 26, 29, 49, 50, 60, 69], reaction-diffusion systems [23, 58, 61, 63, 64], transverse instabilities of travelling fronts for chemical reactions [14], laser ablation [1] and acoustic stimulation of oil wells [44]. In this subsection, a brief discussion of some of these physical models will be presented.

The soft-mode turbulent behaviour of the Nikolaevskiy equation and electroconvection of homeotropically aligned nematic liquid crystals are similar [2, 29, 60, 69]. In electroconvection in liquid crystals the system undergoes supercritical bifurcation. Moreover, amplitude equations and experiments show that the coupling of finite-wavelength patterns with a Goldstone mode leads to a direct transition to a chaotic state (soft-mode turbulence). This result was found in a 2-dimensional model [26, 50] and in 3-dimensional systems [49]. Furthermore, some experimental results were performed by [29, 60].

The Nikolaevskiy equation is also relevant to another physical phenomenon where it is considered as a phase equation for reaction-diffusion systems [23]. Tanaka [61, 63] derived the Nikolaevskiy equation from a certain class of oscillatory reaction-diffusion systems. This was achieved by considering a nonlocal Ginzburg-Landau equation [64] and a phase reduction technique [35]. This nonlocal Ginzburg-Landau phase equation for reaction-diffusion systems [58, 64] is considered qualitatively similar to the Nikolaevskiy equation in terms of the dispersion relation.

1.4 Aims

This thesis has the aim of assessing the influence of dispersion on solutions of the Nikolaevskiy equation. Prior studies regarding the dispersive Nikolaevskiy equation only considered the effect of adding one dispersive term. Moreover, the numerical calculations either produce conflicting conclusions or not enough to generate general results. Furthermore, the secondary stability of travelling wave solutions calculated analytically is not an accurate result. Due to this lack of investigation of the dispersive Nikolaevskiy equation, we aim to study this equation closely. First, we shall reinstate two of the dispersive terms to the Nikolaevskiy equation (1.2). Then we shall study the influence of dispersion on the dynamics of travelling wave solutions for different degrees of dispersion. This will be done in order to observe the transition to the Nikolaevskiy chaos as dispersion is reduced. The research consists of the secondary stability plots of travelling wave solutions computed numerically. These plots will give a general idea of what to expect in the asymptotic results. This study will also include the theoretical effort to study the stability of travelling wave solutions within the framework of reduced self-consistent amplitude equations, which will be done by using a weakly nonlinear analysis. In addition to this, we shall perform numerical simulations of the dispersive Nikolaevskiy equation. These results have been published in Physical Review E in 2010 [54].

The amplitude equations of the Nikolaevskiy equation were derived in [40] and closely investigated by [47, 48, 52]. Moreover, the numerical simulations of these equations manifest some interesting behaviour. This motivates two separate investigations regarding these equations. First, we consider a generalised form of the amplitude equations and investigate it numerically. This form consists of the same amplitude equations found in [40] with a general coefficient for the diffusion term in the first equation. The original coefficient of the diffusion term is 4, and this is related to the ratio of curvatures of the dispersion relation curve near the finite-wavelength and long-wavelength modes. Thus these generalised amplitude equations correspond to a system of pattern formation with the same symmetries as the Nikolaevskiy equation and a dispersion relation that is similar but does not necessarily have the same ratio of curvatures. The second investigation considers adding dispersion to the Nikolaevskiy equation and deriving the amplitude equations. Dispersion will result in the appearance of an advection term. Therefore, we analyse numerically the influence of dispersion on these equations and compare the result with the original amplitude equations.

A system coupling a Swift-Hohenberg equation and a Burgers' equation describing the interaction of finite-wavelength and large-scale modes will be introduced. These coupled equations have similar symmetries to the Nikolaevskiy equation. Due to the similarity of

these coupled equations to the Nikolaevskiy equation, we are interested in investigating whether the symmetries will lead to the same features of the solution or not. This research will include a systematic study of the secondary stability of wave solutions by means of analytical and numerical computations along with numerical simulations.

1.5 Thesis structure

This thesis is organised into six chapters. First, we present in chapter 2 a description of the Nikolaevskiy equation with no dispersion, where we introduce the main properties of the equation already given in the literature. This includes the dispersion relation, the secondary stability of roll solutions and the amplitude equations. In addition to this, the power spectrum will be studied and compared to that of the Kuramoto-Sivashinsky equation. Chapter 3 is devoted to studying systems similar to the Nikolaevskiy equation in terms of the stability of wave solutions and amplitude equations. Indeed, the amplitude equations (generalised version) will be closely examined through numerical computations. Dispersion will be added to the Nikolaevskiy equation in chapter 4, then the effect will be investigated in detail by means of analytical and numerical results. This is done for different magnitudes of dispersion. In addition to this, the dispersive Nikolaevskiy equation is reduced to similar amplitude equations for the non-dispersive case with an extra advection term and the effect of this term on the amplitude equations is analysed numerically. A coupled system of PDEs similar to the Nikolaevskiy equation is introduced in chapter 5. A detailed study of the secondary stability of roll solutions calculated analytically and numerically will be given and compared to the Nikolaevskiy equation. The last chapter (chapter 6) summarises the findings of this thesis and discusses some of the unanswered questions. In the appendix, we present an overview of the numerical methods used throughout this thesis. These are the Fourier spectral, exponential time differencing and exponential time differencing Runge-Kutta methods. In addition to this, we present three of the numerical codes used in this thesis. Specifically, these codes consist of the numerical solution of the Nikolaevskiy equation with dispersion, the numerical solution of the amplitude equations and the numerical calculation of the secondary stability of rolls for the Nikolaevskiy equation with dispersion.

Chapter 2

The Nikolaevskiy equation with no dispersion

2.1 Introduction

Before we proceed with our investigation of the Nikolaevskiy equation with dispersion we shall introduce more detailed background information concerning this equation with no dispersion, which provides significant aspects and properties of the solution. The results presented here are a review of previous work carried out regarding the Nikolaevskiy equation.

The Nikolaevskiy equation is written in the form

$$\frac{\partial u}{\partial t} = -\frac{\partial^2}{\partial x^2}\left[ru - \left(1 + \frac{\partial^2}{\partial x^2}\right)^2 u\right] - u\frac{\partial u}{\partial x}. \tag{2.1}$$

We impose spatial periodicity in the numerical simulations presented later. As mentioned in the previous chapter, the Nikolaevskiy equation possesses the Galilean, space translation, time translation and reflection symmetries.

In the following sections we shall begin by introducing the dispersion relation and the stability of the zero solution (§2.2). We will then go on to calculate the stationary periodic solutions along with their stability analysis in §2.3. Afterwards, we reduce the Nikolaevskiy equation to coupled amplitude equations describing the behaviour of the solution near the onset of instability in §2.4. We end our investigation, in §2.5, by setting out an example of numerical simulation of the Nikolaevskiy equation as well as computing numerically the power spectrum of (2.1) for different values of the parameter r. A final discussion will be given at the end of this chapter (§2.6).

2.2 Dispersion relation

The first thing we need to do, in order to study the properties and behaviour of solutions of the Nikolaevskiy equation, is to linearise around the stationary state $u \equiv 0$. This yields

$$\frac{\partial u}{\partial t} = -\frac{\partial^2}{\partial x^2}\left[ru - \left(1 + \frac{\partial^2}{\partial x^2}\right)^2 u\right].$$

Considering the evolution of the Fourier modes $e^{\mathrm{i}kx+\lambda t}$, implies the dispersion relation

$$\lambda = k^2\left[r - \left(1 - k^2\right)^2\right].$$

Figure 2.1 represents the growth rate λ of the linear modes for the Nikolaevskiy equation, where $r = 1$, 0.5, 0.2, 0.1, 0.05, 0.01 and -0.05 (solid curves from top to bottom). The dashed curve is the dispersion relation of the Kuramoto-Sivashinsky equation (1.5) for $r = 1$, for comparison. If $r < 0$, the growth rate is linearly damped for all modes and hence all initial perturbations decay. On the other hand, if $r > 0$ a band of unstable wave numbers, satisfying

$$\sqrt{1 - \sqrt{r}} < k < \sqrt{1 + \sqrt{r}},$$

appears in addition to a neutrally stable mode near $k = 0$. We will see later that this weakly damped mode plays a significant role in the dynamics of the solution because it couples nonlinearly with the modes in the vicinity of $k = 1$. Moreover, this mode will result in the appearance of a large-scale mode in the weakly nonlinear analysis.

We also notice that when r is small, the wavenumbers of the pattern and large-scale modes are well separated, in contrast with the case when r is large. The latter case gives a linear dispersion relation reminiscent of that for the Kuramoto-Sivashinsky equation [52, 62]. This result is also confirmed by the numerical calculations of the full nonlinear equation presented in §2.5.2 in terms of the power spectrum.

It is of particular interest to analyse the solution to the Nikolaevskiy equation just beyond the onset of pattern formation and describe the interaction of the pattern and large-scale modes. Therefore, we introduce the expression

$$r = \epsilon^2,$$

where $\epsilon \ll 1$. This implies that the existing band of instability around $k = 1$ has the width of order ϵ and the maximum growth rate is of order ϵ^2. This suggests the slow space and time scales $X = \epsilon x$ and $T = \epsilon^2 t$ in the weakly nonlinear regime, which we will use to analyse the stability of roll solutions in the next section.

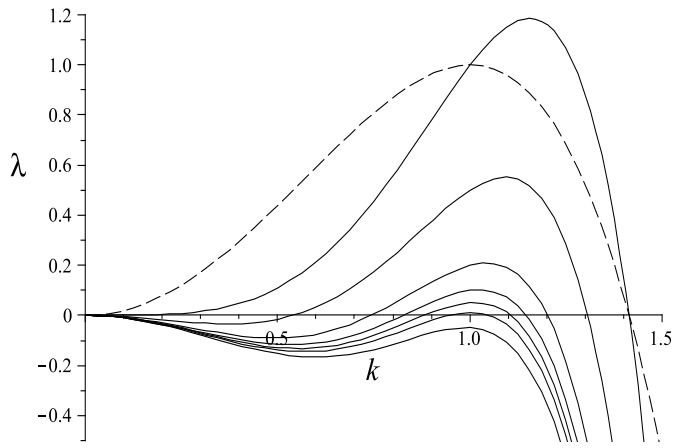

Figure 2.1: Dispersion relation $\lambda(k)$ of the Nikolaevskiy equation, where the values of r (solid curves from top to bottom) are: 1, 0.5, 0.2, 0.1, 0.05, 0.01 and -0.05. The dashed curve corresponds to the Kuramoto-Sivashinsky equation (1.5) for $r = 1$.

2.3 Stationary periodic solutions and their stability

This section will give an account of calculating the stationary periodic solutions (sometimes we refer to these by the term "rolls") of (2.1) and their stability. In particular, we review the work done by [40, 72] and present it within the framework of weakly nonlinear analysis as in [40].

2.3.1 Roll solutions

To find the roll solutions, we construct a weakly nonlinear expansion of u as follows:

$$u = \epsilon u_1 + \epsilon^2 u_2 + \epsilon^3 u_3 + \epsilon^4 u_4 + \cdots . \tag{2.2}$$

The appropriate rescaling of the time t is $T = \epsilon^2 t$ (since T is related to the maximum growth rate, which is of $O(\epsilon^2)$). This will result in replacing the partial derivative $\frac{\partial}{\partial t}$ by $\epsilon^2 \frac{\partial}{\partial T}$. Here $r = \epsilon^2$.

For solutions with wavenumber $k = 1+\epsilon q$, taken from the unstable band of the dispersion relation, we set $u_1 = A(T)e^{\mathrm{i}(1+\epsilon q)x} + c.c.$ Note that the $c.c.$ denotes the complex conjugate of the previous term and A is a complex amplitude of the pattern with finite-wavelength modes. From substituting (2.2) in (2.1), we find that all terms of $O(\epsilon)$ are balanced.

At $O(\epsilon^2)$ the resulting equation is

$$-\frac{\partial^2}{\partial x^2}\left(1 + \frac{\partial^2}{\partial x^2}\right)^2 u_2 + \mathrm{i}A^2 e^{2\mathrm{i}(1+\epsilon q)x} + c.c. = 0.$$

This yields $u_2 = -\frac{\mathrm{i}}{36}A^2 e^{2\mathrm{i}(1+\epsilon q)x} + c.c.$ Terms proportional to $e^{\pm\mathrm{i}(1+\epsilon q)x}$ do not appear in u_2 because any such term is absorbed in u_1.

Now we evaluate the coefficients of ϵ^3, which are given by

$$-\frac{\partial^2}{\partial x^2}\left(1+\frac{\partial^2}{\partial x^2}\right)^2 u_3 + \left(-1+4q^2+\frac{|A|^2}{36}+\frac{\partial}{\partial T}\right)Ae^{\mathrm{i}(1+\epsilon q)x} + c.c.$$
$$+\left(-\frac{19}{3}\mathrm{i}qA^2e^{2\mathrm{i}(1+\epsilon q)x}+\frac{1}{12}A^3e^{3\mathrm{i}(1+\epsilon q)x}\right)+c.c.=0.$$

Due to the presence of forcing terms proportional to $e^{\pm\mathrm{i}(1+\epsilon q)x}$, we need to impose a solvability condition in order to avoid the occurrence of secular terms in the solution u_3. Therefore, the coefficients of $e^{\mathrm{i}(1+\epsilon q)x}$ should vanish and thus we obtain the amplitude equation

$$\frac{dA}{dT}=A\left(1-4q^2-\frac{|A|^2}{36}\right). \tag{2.3}$$

It is apparent that this equation represents a *supercritical* pitchfork bifurcation because of the negative coefficient of $|A|^2$. Moreover, the steady states are $A=0$, and $A=\pm 6\sqrt{1-4q^2}$. This means that rolls have the real amplitude

$$a_0=6\sqrt{1-4q^2},$$

and so they exist for $q^2<1/4$ [40, 72].

It is worth noting that the linear part of the amplitude equation (2.3) can be deduced directly from the growth rate $\lambda=k^2\left[r-\left(1-k^2\right)^2\right]$ by simply replacing r by ϵ^2 and k by $1+\epsilon q$, where the slow temporal scale is $T=\epsilon^2 t$.

2.3.2 Stability of roll solutions

Having calculated the roll solutions, we next analyse their stability by adding perturbations. Thus we introduce the weakly nonlinear expansion [40]

$$u=\epsilon[a_0+a(X,T)]e^{\mathrm{i}(1+\epsilon q)x}+c.c.+\epsilon f(X,T)+\cdots.$$

Here f is a large-scale mode resulting from the neutral mode near $k=0$. For algebraic consistency, we choose $a=b+\mathrm{i}c$, with separate scalings for b and c. Then by considering coefficients of successive powers of $O(\epsilon)$ and linearising, we obtain from solvability conditions three amplitude equations. Because these equations are linear, we can arbitrarily set $b=O(1)$. Accordingly, by considering the orders of c and f in the weakly nonlinear expansion, we can then choose $c=O(\epsilon^{-1/4})$ and $f=O(\epsilon^{1/4})$. Moreover, the space and time variables are replaced with the consistent slow space and time scales $X=\epsilon^{3/4}x$ and $T=\epsilon^{3/2}t$. These particular scales are chosen to balance important terms appearing in the following amplitude equations. After several algebraic steps, the resulting linear amplitude equations [40] are

$$\begin{aligned}\frac{\partial c}{\partial T} &= 4\frac{\partial^2 c}{\partial X^2}-a_0 f,\\ \frac{\partial f}{\partial T} &= \frac{\partial^2 f}{\partial X^2}-2a_0\frac{\partial b}{\partial X},\\ \frac{\partial b}{\partial T} &= 4\frac{\partial^2 b}{\partial X^2}-8q\frac{\partial c}{\partial X}.\end{aligned}$$

Proceeding with the stability analysis of rolls, we write the previous equations as follows:

$$\begin{aligned}\left(\frac{\partial}{\partial T}-4\frac{\partial^2}{\partial X^2}\right)c &= -a_0 f,\\ \left(\frac{\partial}{\partial T}-\frac{\partial^2}{\partial X^2}\right)f &= -2a_0\frac{\partial b}{\partial X},\\ \left(\frac{\partial}{\partial T}-4\frac{\partial^2}{\partial X^2}\right)b &= -8q\frac{\partial c}{\partial X},\end{aligned}$$

Then we combine them into the following:

$$\left(\frac{\partial}{\partial T}-\frac{\partial^2}{\partial X^2}\right)\left(\frac{\partial}{\partial T}-4\frac{\partial^2}{\partial X^2}\right)^2 c = -16qa_0^2\frac{\partial^2 c}{\partial X^2}.$$

After substituting $c=\bar{c}e^{\mathrm{i}LX+\sigma T}$ in the previous equation, we obtain the dispersion relation

$$\sigma^3+9\sigma^2L^2+24\sigma L^4+16L^6-16qa_0^2L^2=0. \tag{2.4}$$

Note that, unlike L, q has an odd power and thus we expect different behaviours for positive and negative q.

We begin by considering the two limiting cases, of small and large L. If L is small, then $\sigma^3+9\sigma^2L^2+24\sigma L^4-16qa_0^2L^2\approx 0$. Thus $\sigma^3\sim 16a_0^2qL^2$, and to leading order in L: $\sigma=\sigma_{2/3}L^{2/3}$ and hence $\sigma_{2/3}^3=16a_0^2q$. This means that if $0<q<1/2$, we have a positive real eigenvalue (stationary instability). On the other hand, if $-1/2<q<0$, we have a complex conjugate pair of eigenvalues with positive real parts (oscillatory instability). Thus we conclude that all rolls are unstable in the limit of small L.

Now if L is large, then $\sigma^3+9\sigma^2L^2+24\sigma L^4+16L^6\approx 0$. This implies $\sigma\approx -L^2$ or $-4L^2$ (twice). Thus all rolls are stable to large-L disturbances. After concluding that rolls are unstable, now we consider general L for completeness regarding the stability analysis of rolls (monotonic and oscillatory instability boundaries).

To calculate the monotonic instability boundary for stationary periodic solutions, we put $\sigma=0$ in (2.4), which implies

$$L^4=a_0^2q.$$

Consequently, if $0<q<1/2$, the instability is stationary and there is a band of unstable modes having $0<L<L_c=(a_0^2q)^{1/4}$.

Regarding the oscillatory instability boundary for rolls, we set $\sigma=\mathrm{i}\Omega$ in (2.4). Then we obtain from comparing the real and imaginary parts

$$\begin{aligned}\Omega^3-24\Omega L^4 &= 0,\\ \Omega^2-\frac{16}{9}L^4+\frac{16}{9}a_0^2q &= 0.\end{aligned}$$

Combining these equations to eliminate Ω implies

$$L^4=-\frac{2a_0^2q}{25}.$$

Hence if $-1/2 < q < 0$, rolls undergo Hopf bifurcation if $L = L_0 = \left(-\frac{2a_0^2 q}{25}\right)^{1/4}$ and we have a band of unstable disturbances, satisfying $0 < L < L_0$.

To summarise, all small-amplitude stationary periodic solutions of the Nikolaevskiy equation are unstable [40, 72]. Indeed, this result also applies to rolls having wavenumber close to the marginal stability curve or close to the critical value [14, 70]. In addition to this, the growth rate of the instability of rolls is of order $\epsilon^{3/2}$, which is faster than that of the original rolls. This is shown in the numerical simulation of the Nikolaevskiy equation in figure 1.3, where rolls are slowly growing and then suddenly become unstable.

2.4 Amplitude equations

This section is devoted to reducing the Nikolaevskiy equation to coupled amplitude equations, which describe the solution near the onset of pattern formation [40]. We already expect an equation for the large-scale mode among these equations, due to the Galilean invariance [12]. It is worth mentioning that the scaling used to derive these equations was controversial. Moreover, several attempts were made before the correct scaling was discovered in [40]. In particular, different scalings based on inaccurate numerical calculations were suggested in [32, 71] in addition to inconsistent amplitude equations [39], which produce a wrong result regarding the stability of rolls. Here we introduce the self-consistent amplitude equations presented in [40] as well as numerical justification for the unusual scaling used to derive these equations [40, 62].

First, we introduce the slow time scale $T = \epsilon^2 t$ along with the slow space scale $X = \epsilon x$. The relative scalings of X and T are responsible for the appearance of the diffusion term in the amplitude equations. The coupling term in the amplitude equation for the large-scale mode will appear if u is of order $\epsilon^{3/2}$. Therefore, we introduce the expansion

$$u = \epsilon^{3/2} A(X,T) e^{\mathrm{i}x} + c.c. + \epsilon^2 u_2 + \epsilon^{5/2} u_3 + \epsilon^3 u_4 + \cdots . \tag{2.5}$$

At $O(\epsilon^2)$, a solvability condition implies that $u_2 = f(X,T)$. Here f is an arbitrary large-scale function, chosen at this particular order, so that the leading coupling term appears in the amplitude equation for A.

After equating coefficients of successive powers of $O(\epsilon^{1/2})$ and from solvability conditions, the governing amplitude equations are

$$\frac{\partial A}{\partial T} = A + 4\frac{\partial^2 A}{\partial X^2} - \mathrm{i}fA, \tag{2.6}$$

$$\frac{\partial f}{\partial T} = \frac{\partial^2 f}{\partial X^2} - \frac{\partial |A|^2}{\partial X}. \tag{2.7}$$

Note that the bifurcation parameter r does not appear in these amplitude equations. On the other hand, regarding the Nikolaevskiy equation r cannot be scaled out. Thus it is easier to study these amplitude equations rather than the Nikolaevskiy equation, which is numerically challenging when r is small.

From these equations we can conclude that the amplitude of the solution is scaled as $r^{3/4}$, which is different from the usual Ginzburg-Landau scaling where the amplitude of the solution is scaled as $r^{1/2}$. Due to this anomalous scaling, numerical computations should be carried out to find the range in r where this scaling is valid. In particular, the scaling should be tested against the rms of the solution of (2.1). Numerical computations achieved in [40] demonstrate that the rms of u is proportional to $r^{3/4}$ for $0.01 < r < 0.1$. Another study confirms that this scaling is also valid in a wider range in r: $0.001 < r < 0.1$ [62].

The amplitude equations (2.6) and (2.7) were closely investigated by [47, 79], where it was concluded that the amplitude equations can be improved by adding extra r-dependent terms to them. This observation is based on extracting the rms of A and f from numerical simulations of the full Nikolaevskiy equation for $10^{-5} \leq r \leq 0.04$. The result shows that the scaling of the complex amplitude is consistent with [40], presented here. On the other hand, the large-scale mode f is scaled as $r^{7/8}$, which is very close to the scaling used in [40]. Therefore, according to [47, 79], the modified amplitude equations provide a better representation of the Nikolaevskiy equation.

In summary, we have reduced the Nikolaevskiy equation to self-consistent amplitude equations [40]. In addition, if $r > 0.1$, the above amplitude equations are no longer valid for describing the behaviour of the solution of (2.1). As we have mentioned earlier, when $r > 0.1$ the Nikolaevskiy chaos resembles that of the Kuramoto-Sivashinsky equation in which the long-wavelength instability is dominant.

2.5 Numerical calculations

This part is dedicated to introducing a numerical simulation of the Nikolaevskiy equation showing the spatiotemporal chaos of the solution for a small value of the control parameter r. In addition to this, we calculate the time-averaged power spectrum for several values of r and compare the result to the Kuramoto-Sivashinsky equation. In particular, we discuss when the power spectrum of the two equations is similar.

2.5.1 Numerical simulation

This subsection is concerned with presenting a typical example of a numerical simulation of the Nikolaevskiy equation. In the numerical code, used to generate figure 2.2, we employ

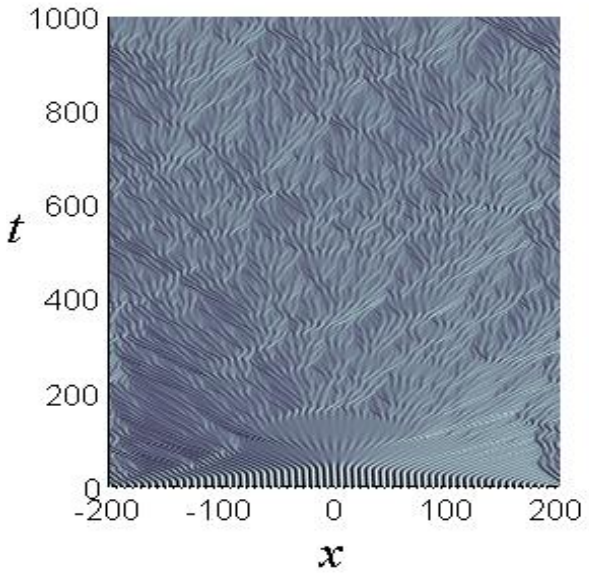

Figure 2.2: Numerical simulation of (2.1) with $r = 0.15$ exhibiting the evolution of a spatiotemporal chaotic state.

a Fourier pseudo-spectral scheme [21, 67] with a second-order exponential time differencing method [13], the *Matlab* code is given in appendix B. The initial data are a small amplitude cosine wave (see (2.2)) with wavenumber 1:

$$u = 12\epsilon\sqrt{1-4q^2}\cos x,$$

plus small random noise ($q = 0$). The parameter values are as follows: $r = 0.15$, the time step is 0.01, the number of Fourier modes is 512, the domain size is $l = 50\pi/\epsilon$ and the maximum time of the simulation is $150/r$. Note that the domain size and the maximum time are related to the slow space and time scales given in §2.3.1 also the number of Fourier modes is enough to produce an accurate solution. As shown in figure 2.2, we have initially the formation of a regular pattern which suddenly becomes unstable and is replaced with a spatiotemporal chaotic state. Indeed, the pattern becomes unstable on a shorter time scale than its formation, which is consistent with the analysis in §2.3.

2.5.2 Power spectrum

In this subsection we are interested in another aspect of characterising the Nikolaevskiy chaos: the time-averaged power spectrum $s(k) = \langle|\hat{u}_k|^2\rangle$ [34, 47, 62, 79]. Here $\hat{u}_k$ denotes the spatial Fourier transform of u_k in (2.1) and $\langle.\rangle$ denotes the long-time average. We begin by calculating the power spectrum for different values of r after initial transients. This will be achieved by using the same numerical code as in figure 2.2, where the initial condition is a small amplitude cosine wave plus small random noise. Moreover, the number of grid points is 2048 and the time step is $0.02/r$. Furthermore, the domain size is $l = \dfrac{51.2\pi}{\epsilon}$ and

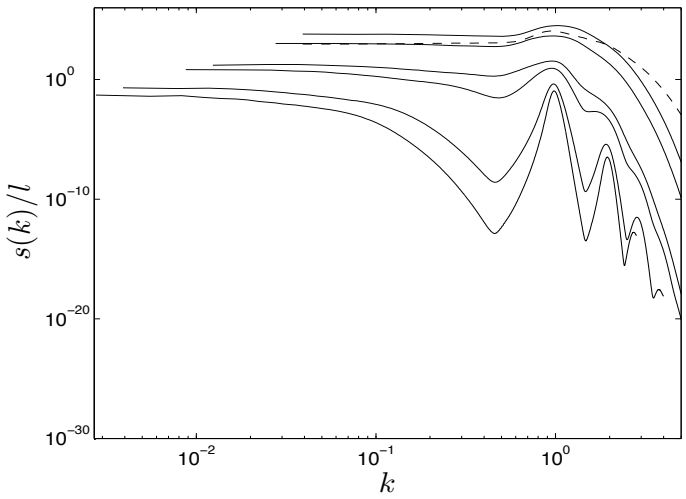

Figure 2.3: The log-log plot of the time-averaged power spectrum of the Nikolaevskiy equation as a function of the wavenumber k and different values of r (solid curves). The curves from top to bottom correspond to the following values of r: 1, 0.5, 0.1, 0.05, 0.01 and 0.005, where $l = \dfrac{51.2\pi}{\epsilon}$. The dashed curve is the power spectrum of the Kuramoto-Sivashinsky equation (1.5).

the simulation is performed over a time period of $20000/r$, which are related to the slow space and time scales X and T (all choices are similar to [47, 79]). We note that the domain size is large enough to give a universal form for $s(k)/l$ independent of the value of l [62]. In addition to this, since the number of Fourier modes in the unstable band is $\dfrac{\epsilon l}{2\pi}$, then by choosing the domain size $l = \dfrac{51.2\pi}{\epsilon}$ we guarantee that the number of Fourier modes will remain the same for any value of r [47].

In figure 2.3, $s(k)/l$ is plotted for various values of r, specifically, the solid curves from top to bottom correspond to the following values of r: 1, 0.5, 0.1, 0.05, 0.01 and 0.005. The dashed curve is the power spectrum of the Kuramoto-Sivashinsky equation (1.5) for $r = 1$, for comparison. Regarding the Nikolaevskiy equation, the graph exhibits the dependence of the power spectrum on r. Specifically, when r is small there is a distinct gap between the two modes $k = 0$ and $k = 1$. This shows that there is a significant scale separation between these two modes and the interaction between them leads to the Nikolaevskiy chaos. However, when r is large ($r > 0.1$), the peaks broaden and merge and the dominant modes occur near $k = 1$. As shown in the figure, this case is qualitatively similar to the Kuramoto-Sivashinsky equation [62, 78], where chaos arises from the dominant unstable long-wavelength modes.

It can be concluded that just beyond the onset of instability of the zero solution the interaction of the neutral and finite-wavelength modes is strong; and this leads to the Nikolaevskiy chaos.

2.6 Discussion

To summarise this chapter, it can be concluded that close to the onset of instability of spatially periodic solutions, the Nikolaevskiy equation exhibits an interesting type of spatiotemporal chaos. This unusual case, different from most pattern forming systems, is due to the presence of a large-scale mode. In addition to this, there is a strong scale separation between the long-wavelength and finite-wavelength instabilities. This leads to exceptional scalings of the pattern and large-scale modes. Further investigation regarding the Nikolaevskiy equation will be carried out in the following chapters, where we shall examine the amplitude equations and add dispersion.

Chapter 3

The generalised amplitude equations

3.1 Introduction

In this chapter we shall generalise the results regarding the Nikolaevskiy equation in terms of the stability of rolls and amplitude equations. In particular, the results are applicable to any system having a similar dispersion relation to that of the Nikolaevskiy equation and with the same symmetries.

Regarding the Nikolaevskiy equation, the ratio of curvatures of the dispersion curve near $k = 0$ and $k = 1$ is 4 (see the dashed line in figure 1.1). This is because the second derivative of the dispersion relation is

$$\lambda''(k) = 2(r-1) + 24k^2 - 30k^4,$$

and therefore, for $r = 0$, the curvatures at $k = 0$ and $k = 1$ are -2 and -8, respectively. We shall consider a general equation that has the same symmetries as the Nikolaevskiy equation with a similar dispersion relation; but that does not necessarily have the same ratio of curvatures near $k = 0$ and $k = 1$. Therefore, to study the stability of rolls for this system, we need to replace 4 by a general positive number, namely n. This analysis will be presented in §3.2. It is worth mentioning that an example of such a system is given in chapter 5, and the results introduced here are applicable to it.

Afterwards, in §3.3, we study the amplitude equations which were derived by Matthews and Cox [40] to describe the Nikolaevskiy chaos:

$$\begin{aligned} \frac{\partial A}{\partial T} &= A + 4\frac{\partial^2 A}{\partial X^2} - \mathrm{i}fA, \\ \frac{\partial f}{\partial T} &= \frac{\partial^2 f}{\partial X^2} - \frac{\partial |A|^2}{\partial X}, \end{aligned}$$

where $X \in [0, l]$ with periodic boundary conditions (here l is different from the previous chapter). We shall study these amplitude equations numerically with general n instead of 4.

For the special case $n = 4$, these equations were studied for a relatively small system size l, which is the only free parameter, by [52]. Then they were closely analysed by [47, 48] for different values of l. Therefore, we introduce briefly the results in §3.3.1, where we show the strong l-dependence of the behaviour and dynamics of these amplitude equations.

Also in §3.3.2, we perform numerical simulations for a generalised version of the amplitude equations with n instead of 4. This will be done for different values of n and fixed l. We will describe how the numerical results of the amplitude equations depend on n.

Finally, the conclusions drawn from this study are given at the end of the chapter in §3.4.

3.2 Stability of rolls

In this section we shall analyse the stability of rolls for systems similar to the Nikolaevskiy equation. Before we do this, we first recall the result for the Nikolaevskiy equation. As described in §2.3.2, we add perturbations $(a(X,T)e^{\mathrm{i}(1+\epsilon q)x}+\text{c.c.})$ to the rolls $(a_0 e^{\mathrm{i}(1+\epsilon q)x}+\text{c.c.})$, both of order ϵ; and replace a by $b + \mathrm{i}c$ for algebraic consistency. Since we are interested in analysing the stability of rolls we can derive linear amplitude equations. Consequently, we arbitrarily set $b = O(1)$, and thus $c = O(\epsilon^{-1/4})$, $f = O(\epsilon^{1/4})$ and replace the space and time variables with the consistent slow space and time scales: $X = \epsilon^{3/4}x$ and $T = \epsilon^{3/2}t$. Then we apply a weakly nonlinear analysis to obtain the following linear amplitude equations:

$$\begin{aligned}
\frac{\partial c}{\partial T} &= 4\frac{\partial^2 c}{\partial X^2} - a_0 f, \\
\frac{\partial f}{\partial T} &= \frac{\partial^2 f}{\partial X^2} - 2a_0\frac{\partial b}{\partial X}, \\
\frac{\partial b}{\partial T} &= 4\left(\frac{\partial^2 b}{\partial X^2} - 2q\frac{\partial c}{\partial X}\right).
\end{aligned}$$

Here $a_0 = 6(1-4q^2)^{1/2}$ and $r = \epsilon^2$. For details regarding the derivation of these equations, see §2.3.2.

Now we generalise the amplitude equations by replacing 4 by n $(n > 0)$ as follows:

$$\begin{aligned}
\frac{\partial c}{\partial T} &= n\frac{\partial^2 c}{\partial X^2} - a_0 f, \\
\frac{\partial f}{\partial T} &= \frac{\partial^2 f}{\partial X^2} - 2a_0\frac{\partial b}{\partial X}, \\
\frac{\partial b}{\partial T} &= n\left(\frac{\partial^2 b}{\partial X^2} - 2q\frac{\partial c}{\partial X}\right).
\end{aligned}$$

Here $a_0 = 6(1-nq^2)^{1/2}$, and therefore rolls exist if $q^2 < 1/n$.

Having generalised these equations, we next study the stability of rolls. We already know that the result for the Nikolaevskiy equation is that all rolls at onset are unstable [40, 72]; we determine below whether this conclusion remains true for general values of n or not.

To analyse the stability of rolls, we combine the generalised amplitude equations into the following:

$$\left(\frac{\partial}{\partial T}-\frac{\partial^2}{\partial X^2}\right)\left(\frac{\partial}{\partial T}-n\frac{\partial^2}{\partial X^2}\right)^2 c=-4na_0^2q\frac{\partial^2 c}{\partial X^2}.$$

After substituting $c=\bar{c}e^{\mathrm{i}LX+\sigma T}$ in the previous equation, we then obtain the following dispersion relation:

$$\sigma^3+(2n+1)\sigma^2L^2+n(n+2)\sigma L^4+n^2L^6-4na_0^2qL^2=0. \tag{3.1}$$

Since the power of q is odd, we expect different behaviours for positive and negative q and this is not the case with L (even powers).

First, we consider small-L disturbances, therefore we have $\sigma^3+(2n+1)\sigma^2L^2+n(n+2)\sigma L^4-4na_0^2qL^2\approx 0$ which implies $\sigma^3\sim 4na_0^2qL^2$. Therefore, to leading order in L we get $\sigma=\sigma_{2/3}L^{2/3}$ and hence $\sigma_{2/3}^3=4na_0^2q$. If $0<q<1/\sqrt{n}$, we get a positive real eigenvalue (stationary instability). On the other hand, if $-1/\sqrt{n}<q<0$, we get a complex conjugate pair of eigenvalues with positive real parts (oscillatory instability). This implies that all rolls are unstable to small-L disturbances provided that $a_0^2q\neq 0$; and the growth rate of instability increases as n becomes large.

Regarding the case of large L, we have $\sigma^3+(2n+1)\sigma^2L^2+n(n+2)\sigma L^4+n^2L^6\approx 0$; and therefore $\sigma\approx -L^2$ or $-nL^2$ (twice). Thus we clearly have stability of rolls for large-L disturbances.

Having established our main result, which is that all rolls remain unstable for general values of n, we next provide more details of the instability for general L. Firstly, we calculate the monotonic instability boundary by substituting $\sigma=0$ in (3.1):

$$L^4=\frac{4a_0^2q}{n}.$$

This shows that if $0<q<1/\sqrt{n}$, then we have a stationary bifurcation if $L=L_c=\left(\frac{4a_0^2q}{n}\right)^{1/4}$ and there is a band of unstable disturbances having $0<L<L_c$.

Secondly, we calculate the oscillatory instability boundary by substituting $\sigma=\mathrm{i}\Omega$ in (3.1); and from comparing the real and imaginary parts we get

$$\begin{aligned}\Omega^3-n(n+2)\Omega L^4 &= 0,\\ \Omega^2-\frac{n^2}{2n+1}L^4+\frac{4n}{2n+1}a_0^2q &= 0.\end{aligned}$$

In order to eliminate Ω we combine these equations as follows:

$$L^4=-\frac{2a_0^2q}{(n+1)^2}.$$

Therefore, if $-1/\sqrt{n}<q<0$ we have oscillatory instability with Hopf bifurcation if

$$L=L_c=\left(-\frac{2a_0^2q}{(n+1)^2}\right)^{1/4}.$$

Moreover, there is a band of unstable wavenumbers: $0 < L < L_c$.

In conclusion, systems similar to the Nikolaevskiy equation will have the same property that rolls are unstable at onset [40, 72]. In view of this conclusion, it is important to emphasise that it is only valid if $a_0^2 q$ is not small; since if $a_0^2 q$ is small, then from (3.1) we get stable rolls. Thus if q or a_0^2 are small, the analysis needs to be closely investigated as done later in §5.8. Unlike the Nikolaevskiy equation, there might be similar systems having a thin region of stability around $k = 1$ as with the system given in chapter 5 or near the marginal stability curve, for example the damped Nikolaevskiy equation [14].

3.3 Amplitude equations

In this section we are going to present a general version of the amplitude equations in [40] (presented in §2.4). These equations are

$$\frac{\partial A}{\partial T} = A + n\frac{\partial^2 A}{\partial X^2} - \mathrm{i}fA, \tag{3.2}$$

$$\frac{\partial f}{\partial T} = \frac{\partial^2 f}{\partial X^2} - \frac{\partial |A|^2}{\partial X}. \tag{3.3}$$

In these equations we have replaced the coefficient of the diffusion term (in the first equation) by n ($n = 4$ for the Nikolaevskiy equation).

In the following subsections we introduce some of the significant behaviour exhibited by the amplitude equations (3.2) and (3.3) for two cases: first for the special case $n = 4$ and then for general n, by means of numerical simulations. The amplitude equations of the Nikolaevskiy equation were studied in [47, 48, 52], which show universal dynamical features in A and f that are highly dependent on the domain size. A brief description of these results is given in §3.3.1. The amplitude equations with general n have not previously been explored. Therefore, we consider this case for different values of n in §3.3.2.

3.3.1 Special case $n = 4$

In this subsection we shall numerically integrate (3.2) and (3.3) for $n = 4$ (as the amplitude equations of the Nikolaevskiy equation) in a finite system $0 < X < l$ with periodic boundary conditions. In addition, we give a brief overview of the results given in [47, 48, 52]. In the numerical code we use a pseudo-spectral scheme (for spatial discretisation) [21, 67] and an exponential time differencing fourth-order Runge-Kutta method (for time stepping) [13, 30]. The simulations are carried out over a long time (up to $T = 10000$–100000) and the long-time averages of $|A|^2$ and f are calculated after initial transients. For details refer to appendix C.

First we begin by simulating (3.2) and (3.3) with random initial conditions ($A = 0$ and $f = 0$ both plus small random noise of order 0.01) as given in figure 3.1 and $l = 150$.

The temporal evolution of $|A|$ in figure 3.1(a) (upper figure) shows that after a while the simulation settles into a thin region in the central domain where $|A|$ is approximately equal to zero (amplitude-death state). Moreover, there is a spatiotemporal chaos in the other parts of the domain (see figure 3.1(b), where $|A|$ (solid curve) is plotted at the end of the simulation). This is also exhibited in the time average $\langle |A|^2 \rangle$ in figure 3.1(c), where it is calculated after 5000 time units in order to capture the amplitude-death state. On the other hand, regarding f the numerical simulation in figure 3.1(a) (lower figure) settles into a state where f decreases linearly in the middle of the domain (single-front state) and is chaotic in the other parts (see the dashed curve in figure 3.1(b)). The single-front state of f is illustrated in the time average $\langle f \rangle$ in figure 3.1(c), which is calculated after 5000 time units.

It can be concluded from the previous simulation that there is an amplitude-death state of A incorporated with a single-front state of f; however, it takes some time to settle into these states. Moreover, the time averages $\langle |A|^2 \rangle$ and $\langle f \rangle$ should be calculated after the fronts are in the middle of the domain in order to capture their profiles. Therefore, in the following simulations, we shall change the initial condition for f to be a sine wave, which locates the domain in the neighbourhood of $X = l/2$. Namely, we choose the initial conditions $A = 0$ and $f = -10 \sin(2\pi(X - l/2)/l)$ (both plus small random noise of order 0.01) as in [52]. These initial conditions are a suitable choice since they capture the fronts soon after the beginning of the simulation and locate them in the middle of the domain, which is an advantage for calculating the time average.

We have seen in the simulation of (3.2) and (3.3) that there is a coexistence of an amplitude-death state and a single-front state for A and f, respectively (see figure 3.1). The position of these two structures fluctuates slightly due to spatiotemporal chaos [47, 48, 52]. Although the temporal movement of the front is shown in the simulation of (3.2) and (3.3), it was not taken into account in [52]. On the other hand, the numerical simulations performed in [47, 48] considered tracking the front and it was concluded that the displacement of the front is strong for small domains and is almost stationary for large domains. Since we use relatively small domain sizes in our numerical simulations, we need to shift A and f for averaging purposes so that the front centre (with $f = 0$) lies at the middle of the domain in order to capture the profiles of the long-time averages of $|A|^2$ and f. This will be done by determining the displacement of the front and aligning it so that it is in the middle of the spatial domain [47, 48]. Specifically, we consider the region close to the middle of the domain (five grid points from the right and left of the middle of the domain) and calculate where f is immediately above and below zero. Afterwards, by shifting the grid points, we position the front so that this region, where f crosses zero, is in the centre of the domain. Figure 3.2 shows the front displacement about $X = l/2$ during the simulation of (3.2) and

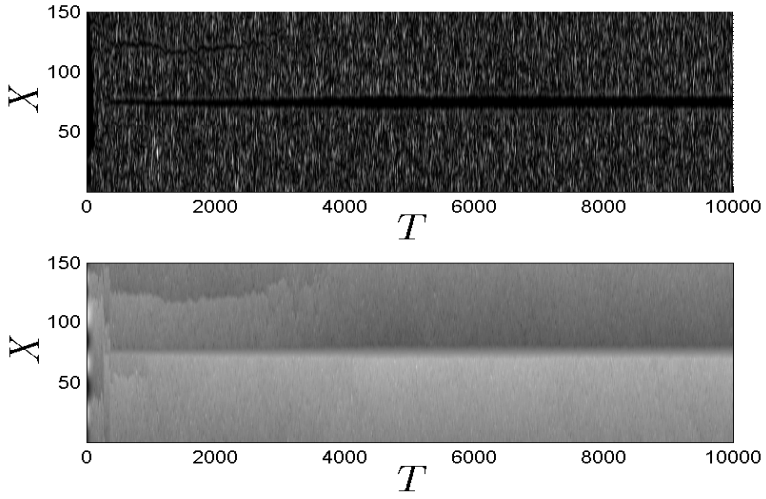

(a)

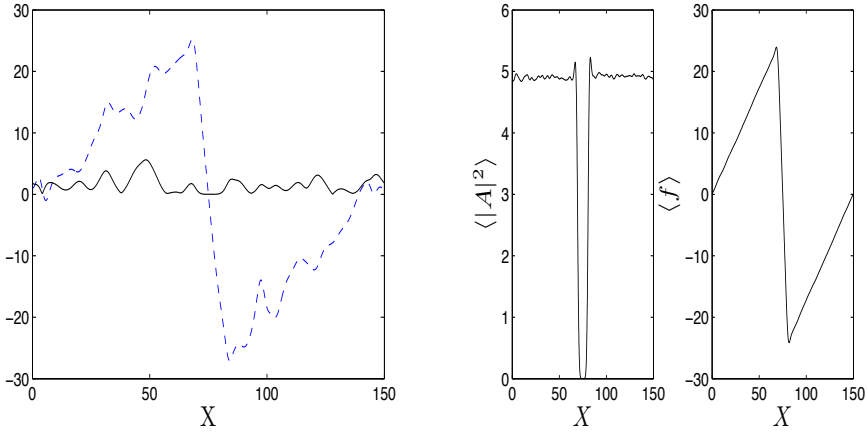

(b) (c)

Figure 3.1: Numerical simulations of (3.2) and (3.3), where $l = 150$, $n = 4$ and random initial conditions. The temporal evolutions of $|A|$ and f are shown in grey scale plots in (a) (from top to bottom) while $|A|$ (solid curve) and f (dashed curve) are plotted in (b) at the end of the simulation. (c) exhibits the time averages: $\langle |A|^2 \rangle$ and $\langle f \rangle$.

(3.3), where $n = 4$ and $l = 150$. As exhibited in the figure, the front is not stationary and the shifting with time is strong. Note that in the numerical simulations we shall position the front in the middle of the domain; and therefore $\langle . \rangle$ denotes the long-time front-tracking average; and we will refer to it by the term "time average". Also note that we aligned the fronts in the middle of the domain in figure 3.1.

After setting the suitable initial conditions and taking into account the displacement of the front, we now numerically simulate (3.2) and (3.3) for $n = 4$ and $l = 150$ to observe the properties of the solution. In figure 3.3, the temporal evolutions of $|A|$ and f are plotted in (a) (from top to bottom) while $|A|$ (solid curve) and f (dashed curve) are plotted in

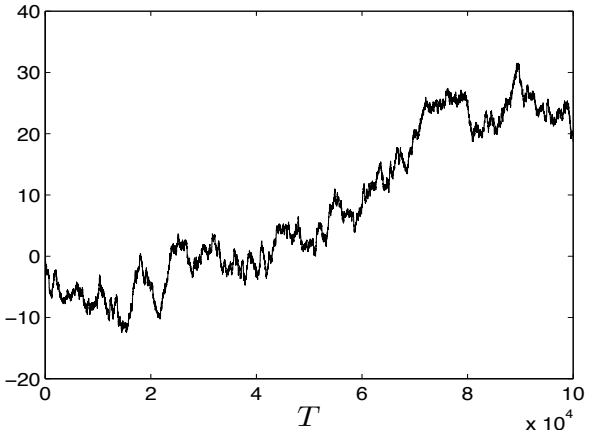

Figure 3.2: The front displacement about $X = l/2$ during the simulations of (3.2) and (3.3), where $l = 150$ and $n = 4$ (see the text for details).

(b) at the end of the simulation. Figure 3.3 (c) exhibits the time-averaged profiles $\langle |A|^2 \rangle$ and $\langle f \rangle$. As shown in the simulation of $|A|$ (the solid curve in figure 3.3(b)), there is a spatiotemporal chaotic state incorporated with a small region of an amplitude-death state in the central domain where $|A|$ vanishes. This is also shown in the time average $\langle |A|^2 \rangle$, where it is approximately equal to zero for a small range in the centre of the domain and the chaotic state occurs when $\langle |A|^2 \rangle \approx 5$. On the other hand, the simulation of f in figure 3.3(b) (dashed curve) also exhibits spatiotemporal chaos with a single-front state in the central domain where f decreases linearly. The time average $\langle f \rangle$ has a negative sharp slope ($\langle f_X \rangle \approx -3.6$) in the central domain and the maximum of $\langle f \rangle$ is approximately 24.24 (see figure 3.3(c)). Moreover, in the chaotic state of f, the corresponding $\langle f \rangle$ has a positive slope ($\langle f_X \rangle \approx 0.35$).

We shall denote the slope of the front within the chaotic regions by $\langle f_X \rangle = m_1$ and the slope of the front in the middle of the domain by $\langle f_X \rangle = -m_2$. Note that the two lines on the right and left in figure 3.3(c) have approximately the same slope and we shall consider m_1 to be the slope of the line on the left hand side.

To examine the robustness of the coexistence of the two fronts for A and f, we perform some simulations with different domain sizes. This will be done in order to find out whether the amplitude-death and single-front structures will still appear in the numerical simulations. We choose the domain sizes 100 and 200 as given in figures 3.4(a) and (b), respectively. In the simulations we obtain the same behaviour for A and f as with domain size $l = 150$ (same initial conditions), where the chaotic state of $\langle |A|^2 \rangle$ fluctuates about 5 and the maximum of $\langle f \rangle / l$ is approximately the same for $l = 100$, $l = 150$ and $l = 200$. It can be concluded that the two fronts of A and f appearing in the simulations are robust in all domains.

The coexistence of spatiotemporal chaos and amplitude-death state is also found in the

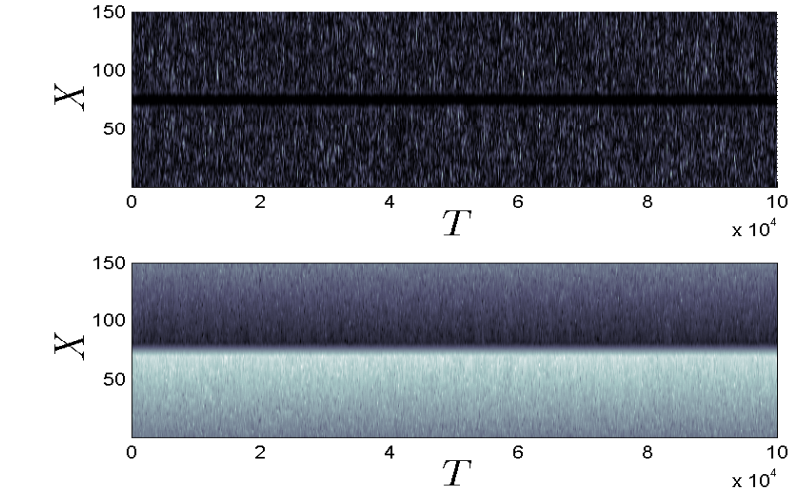

(a)

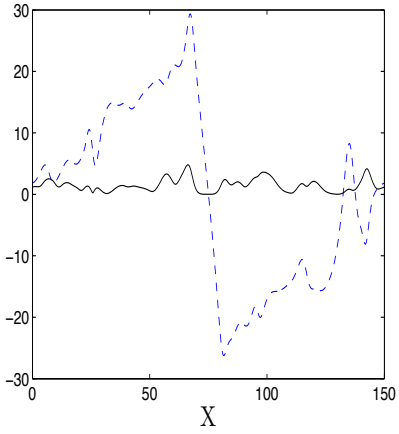

(b)

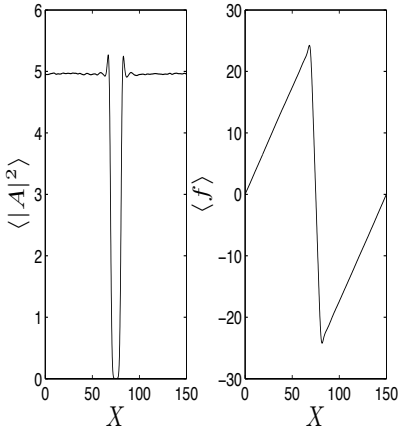

(c)

Figure 3.3: Numerical simulations of (3.2) and (3.3), where $l = 150$ and $n = 4$. The initial conditions are $A = 0$ and $f = -10\sin(2\pi(X - l/2)/l)$, both plus random noise. The temporal evolutions of $|A|$ and f are shown in grey scale plots in (a) (from top to bottom) while $|A|$ (solid curve) and f (dashed curve) are plotted in (b) at the end of the simulation. (c) exhibits the time averages: $\langle|A|^2\rangle$ and $\langle f\rangle$.

Nikolaevskiy equation itself near the onset of instability [52]. In figure 3.5 we calculated the time average of the solution of the Nikolaevskiy equation between the times 3500 and 4500, where $l = 150\pi$, $r = 0.01$ and the initial condition is $u = -10\epsilon^2\sin(2\pi(x - l/2)/l)$ with small perturbations. This particular initial condition is taken from the asymptotic expansion of u (see (2.5)):

$$u \sim \epsilon^{3/2}A(X,T)e^{ix} + c.c. + \epsilon^2 f(X,T),$$

where $r = \epsilon^2$ and $A = 0$ and $f = -10\sin(2\pi(X - l/2)/l)$ (the same as in the numerical simulations of (3.2) and (3.3)). In this figure we notice that the global structure of $\langle u\rangle$ is

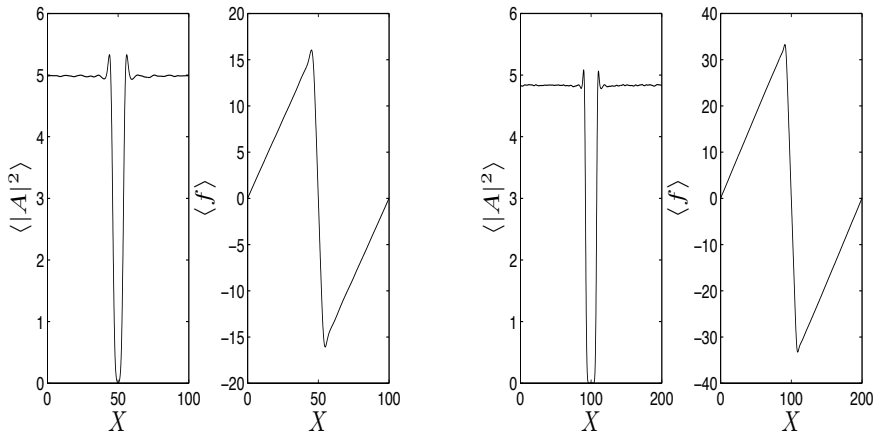

Figure 3.4: The time averages $\langle |A|^2 \rangle$ and $\langle f \rangle$ calculated for $n = 4$ and (a) $l = 100$ and (b) $l = 200$. The initial conditions are $A = 0$ and $f = -10 \sin(2\pi(X - l/2)/l)$ (both plus small random noise of order 0.01).

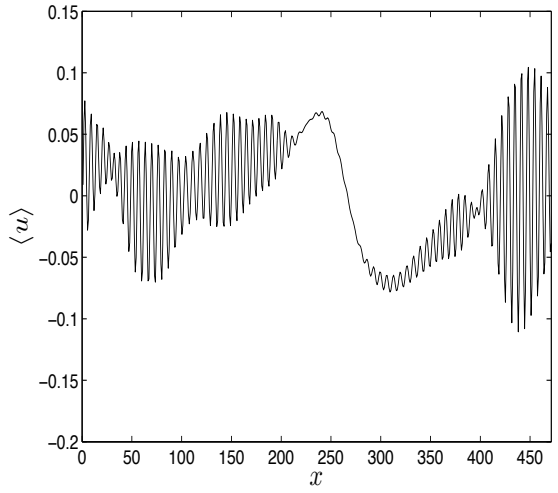

Figure 3.5: The time average of the solution of the Nikolaevskiy equation calculated between the times 3500 and 4500 for $l = 150\pi$ and $r = 0.01$.

reminiscent of $\langle f \rangle$. In particular, in some regions $\langle u \rangle$ has a steep negative slope, where there are no small-scale oscillations (A is very small) and in other domains, $\langle u \rangle$ has a positive slope. This is shown in figure 3.5 in the neighbourhood of $x = 275$. Note that the time average of u is evaluated without tracking the front since it is calculated for a relatively short time.

The amplitude equations of the Nikolaevskiy equation were closely examined by [47, 48] for different domain sizes. In particular, they considered three different separate domain sizes. In the first case of small domains, $l \lesssim 220$, it was concluded from this study that the mid-front slope of $\langle f \rangle$ is independent of l and the slope in the chaotic region increases slowly

with l. In addition, the maximum value of $\langle f\rangle/l$ is almost fixed, and the front translates over a long time. In addition to this, regarding A, as l is increased the size of the amplitude-death regions remains approximately the same with $\langle|A|^2\rangle \approx 5$ in the chaotic domains.

For intermediate domains, $l \lesssim 560$, regarding the time average $\langle f\rangle$, the front becomes wider and less steep as l is increased and the slope in the chaotic region continues to increase. The drifting of the front becomes weaker with increasing l. The amplitude of chaotic fluctuations of A and f decrease. Finally, the amplitude-death state of $\langle|A|^2\rangle$ becomes wider.

In large domains, $l \gtrsim 560$, the front is stationary and the maximum value of $\langle f\rangle$ and the slope of the chaotic regions saturate at fixed values and the front profile expands as we increase l. Moreover, the front slope decays with l. The amplitude-death state of $\langle|A|^2\rangle$ grows in width with l while the amplitude of fluctuations decays.

Throughout this subsection we considered the domain sizes 100, 150 and 200, which are considered "small" domains ($l \lesssim 220$) according to [47, 48]. For comparison, the results in [47, 48] were calculated for longer times. Despite this, our results seem to be similar.

In the simulations given in the next subsection, we shall change the value of n and fix l, and then repeat the simulations for a different value of l.

3.3.2 General n

In this subsection we shall again numerically integrate (3.2) and (3.3) but for different values of n in a finite domain as given in appendix C. The initial conditions are fixed as before: $A = 0$ and $f = -10\sin(2\pi(X - l/2)/l)$ (both plus small random noise of order 0.01). This is because if we choose different initial conditions it might take a longer time until the two fronts of A and f are in the middle of the domain. The time averages $\langle|A|^2\rangle$ and $\langle f\rangle$ are calculated with $T = 50000$–100000, after initial transients. As above, for averaging purposes, the profiles are shifted at each time step so that the front is at the centre of the spatial domain. The simulations will be performed for two values of the domain sizes (150 and 200) and n will range from 1 to 10.

After repeating the simulations of (3.2) and (3.3) for different values of n ranging from 1 to 10 in a domain length of 150, we have plotted the time averages $\langle f\rangle$ and $\langle|A|^2\rangle$ in figure 3.6. In the numerical simulations for $n = 1$ and $n = 2$, the amplitude-death and single-front structures of A and f (respectively) do not appear, although it seems that there is an initial formation of them (see figures 3.6(a) and (b)). If we increase n to 3, the amplitude-death state for A and the single-front state for f can be seen through the time averages as shown in figure 3.6(c). Similarly, if we choose other values of n, the global structures of A and f are still present (see figures 3.6(d)–(j)). As we increase n, the amplitude-death state of A

widens and the amplitude of fluctuations decreases.

Regarding f, we have collected data from figure 3.6 as shown in figure 3.8 ("$*$"). The data collected are m_1 and m_2, which are the slope of the front within the active region and the slope of the front in the middle of the domain, respectively (see figures 3.8(a) and (b)). In addition to this, we have also calculated the maximum value of $\langle f \rangle / l$ as shown in figure 3.8(c). As n increases from 3 to 10, the changes in m_1, m_2 and $max(\langle f \rangle / l)$ are exhibited in these figures; and we clearly have two regimes separated by $n \approx 5$. For $n < 5$, the slope m_1 of the active region increases as a function of n and the slope of the middle domain m_2 decreases. The latter will result in making the front wider and less steep. Regarding the maximum value of $\langle f \rangle / l$, it increases with n. Figure 3.9(a) presents the differences between the time averages $\langle f \rangle$ for $n = 3$ (solid curve) and $n = 5$ (dashed curve). As n increases from 3 to 5, $max(\langle f \rangle)$ increases and the middle of the front widens slightly to the left. Moreover, the slope of the two lines on the left and right increases.

On the other hand, if $n > 5$, m_2 decreases with increasing n and similarly to the previous case as we increase n the time-averaged profile $\langle f \rangle$ (in the middle of the domain) widens and becomes less steep (see figure 3.9(b)). The slope m_1 and the maximum value of $\langle f \rangle / l$ also decrease as functions of n. Figure 3.9 exhibits the differences between two profiles of $\langle f \rangle$ for $n = 5$ (solid curve) and $n = 9$ (dashed curve). As shown in the figure, when n changes from 5 to 9 the profile of $\langle f \rangle$ becomes smaller and the middle part widens slightly to the left. Furthermore, the slope of the two lines on the right and left changes (decreases).

We have repeated the simulations for the same values of n with a different domain size, namely $l = 200$ as exhibited in figure 3.7. The data collected from these figures are shown in figure 3.8 ("$\circ$"). The result is close to the previous case ($l = 150$) except that we have two regimes for $n < 4.5$ and $n > 4.5$.

To summarise, regarding the generalised amplitude equations, we observed universal features in the numerical simulations for a wide range of n for a relatively small domain size. These features are the amplitude-death and the single-front states for A and f, respectively. The behaviour and the dynamics of these two fronts are strongly influenced by n.

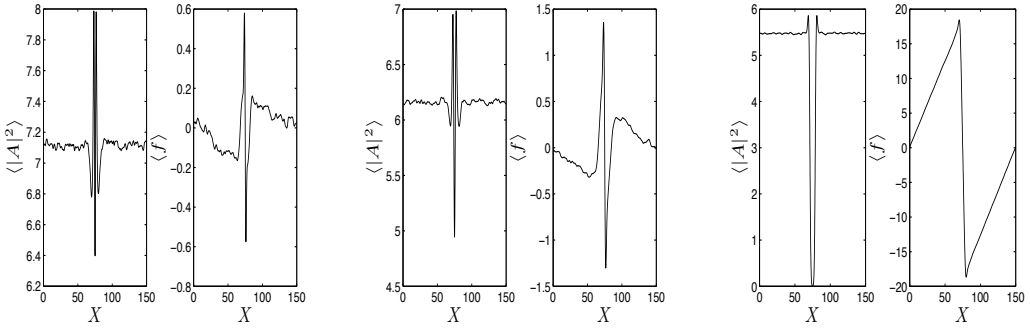

(a) $n = 1$ (b) $n = 2$ (c) $n = 3$

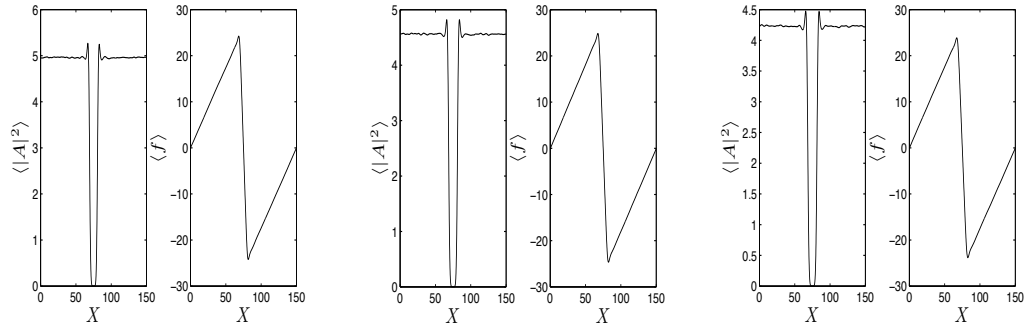

(d) $n = 4$ (e) $n = 5$ (f) $n = 6$

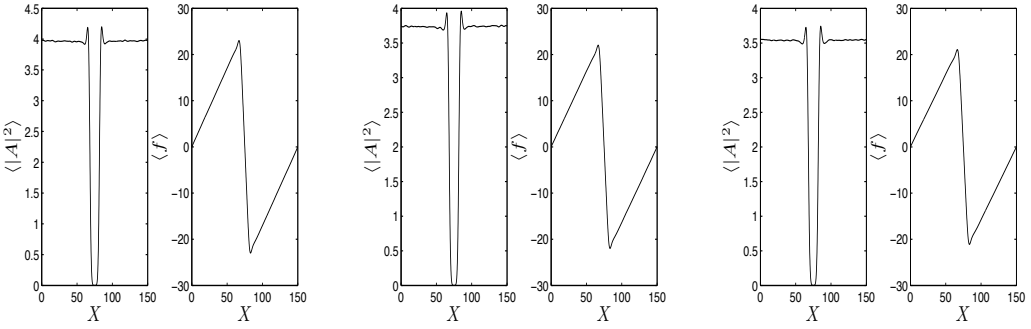

(g) $n = 7$ (h) $n = 8$ (i) $n = 9$

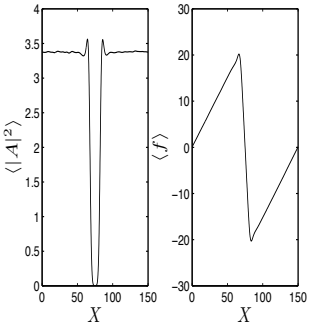

(j) $n = 10$

Figure 3.6: Plots of the time-averaged profiles: $\langle f \rangle$ and $\langle |A|^2 \rangle$ of (3.2) and (3.3) for different values of n as indicated under each graph, where $l = 150$.

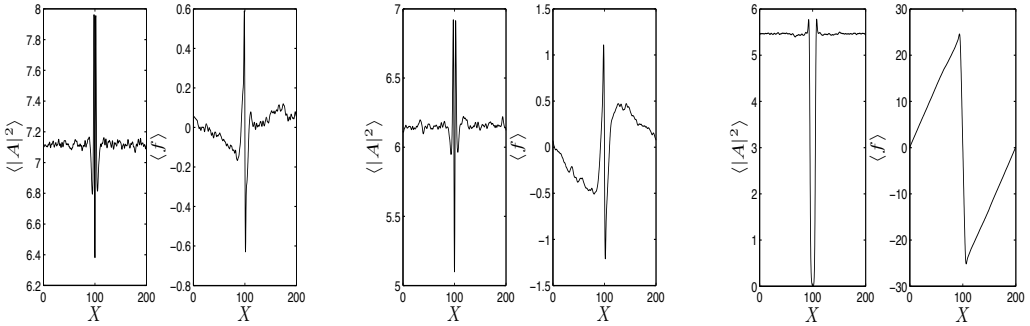

(a) $n = 1$ (b) $n = 2$ (c) $n = 3$

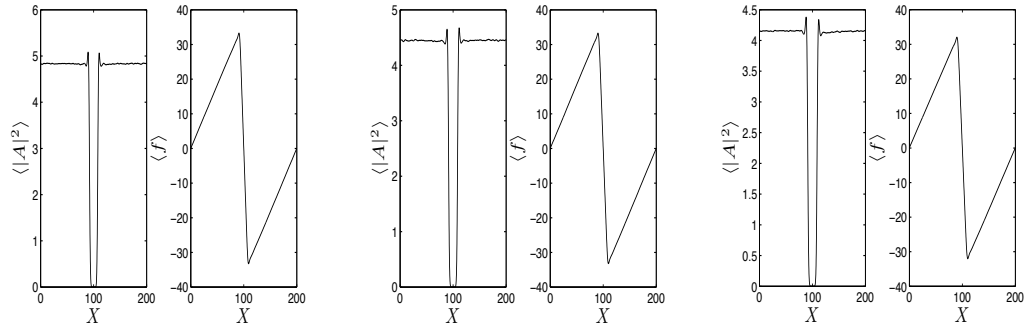

(d) $n = 4$ (e) $n = 5$ (f) $n = 6$

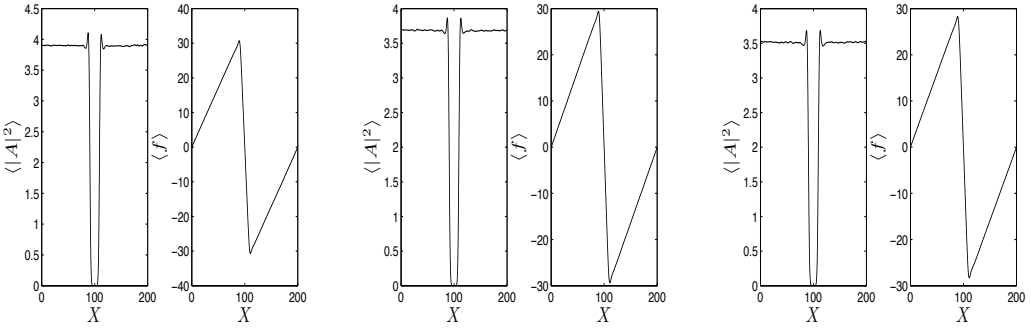

(g) $n = 7$ (h) $n = 8$ (i) $n = 9$

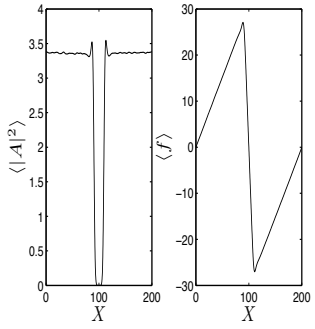

(j) $n = 10$

Figure 3.7: Plots of the time-averaged profiles: $\langle f \rangle$ and $\langle |A|^2 \rangle$ of (3.2) and (3.3) for different values of n as indicated under each graph, where $l = 200$.

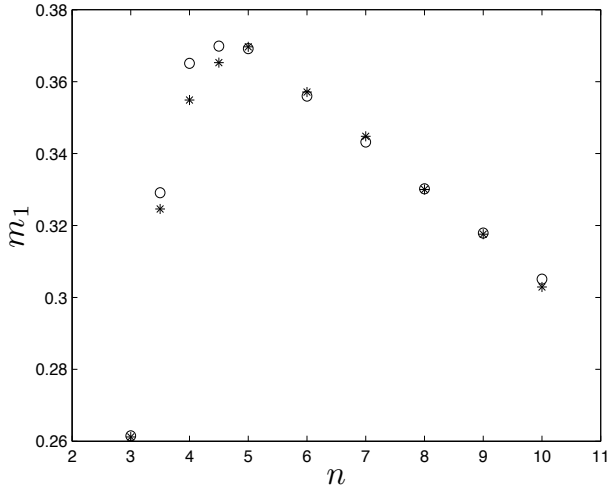

(a)

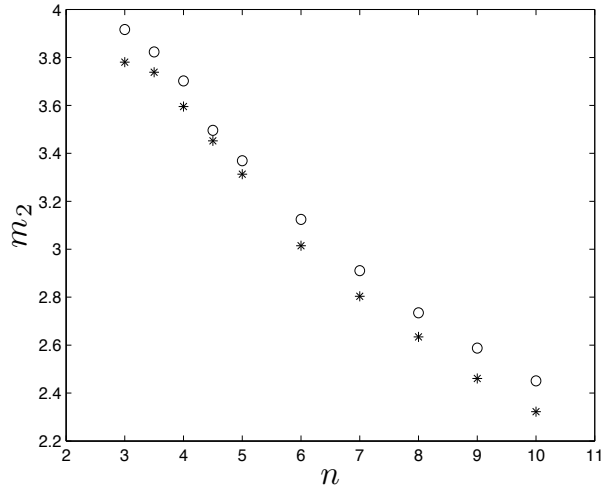

(b)

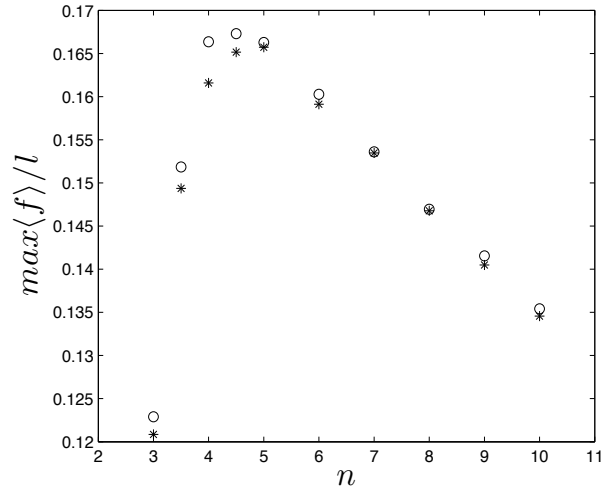

(c)

Figure 3.8: The slopes (a) m_1 and (b) m_2 plotted against different values of n and (c) the maximum value of $\langle f\rangle/l$ plotted against n for $l = 150$ (“$*$”) and $l = 200$ (“$\circ$”).

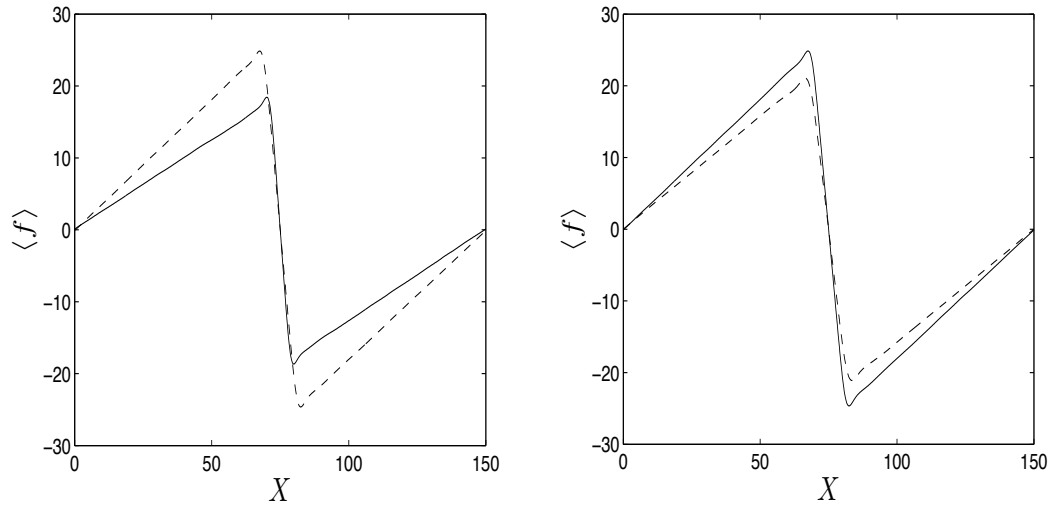

Figure 3.9: Plot of the time average $\langle f \rangle$ for two values of n: (a) $n = 3$ (solid curve) and $n = 5$ (dashed curve) and (b) $n = 5$ (solid curve) and $n = 9$ (dashed curve), where $l = 150$.

3.4 Discussion

In this chapter we studied a system, similar to the Nikolaevskiy equation, with coupling between finite-wavelength instability and a large-scale mode and with the same symmetries. We considered two different aspects: the stability of rolls and the amplitude equations. These two results are applicable to this system by including a positive parameter n, which takes the value $n = 4$ in the Nikolaevskiy equation. It was found that all roll solutions are unstable at onset for all values of n provided that the wavenumber is not close to the marginal stability curve nor close to the critical wavenumber.

Regarding the amplitude equations, a state of amplitude-death and single-front is found to arise in the numerical simulations for a wide range of n. This is similar to the case of the amplitude equations of the Nikolaevskiy equation ($n = 4$). For relatively small system sizes, this state is strongly influenced by the coefficient of the diffusion term in the first amplitude equation (n). It seems that if n is small the amplitude-death and single-front structures are not clear; however, as we increase n they become more distinguishable. In addition, the statistical measures of these structures depend on the values of n.

Chapter 4

The Nikolaevskiy equation with dispersion

4.1 Introduction

For the control parameter $r > 0$, numerical simulations of the Nikolaevskiy equation exhibit a sudden onset of complicated dynamics as shown in figure 1.3. In order to understand the behaviour of solutions of the Nikolaevskiy equation, extra terms will be introduced in this chapter, which will give us the opportunity of progressively decreasing them in order to reach the Nikolaevskiy chaos. The extra terms chosen are dispersive terms, which are precisely the third and fifth spatial derivatives.

The original Nikolaevskiy model [45] includes dispersive terms; however, the following studies either did not pay them attention or did not produce adequate results. One of the studies regarding dispersion was carried out by Kudryashov and Migita [34], where they found that adding dispersion leads to stable periodic waves by means of numerical simulations. In addition to this, the amplitude equations of the Nikolaevskiy equation with dispersion were presented in [39]. However, they are asymptotically inconsistent and do not produce accurate results regarding the stability of travelling wave solutions. Therefore, the research conducted regarding adding dispersion to the Nikolaevskiy equation is insufficient and needs a close investigation.

One of the key aspects of this chapter is to investigate the effect of adding dispersion to the Nikolaevskiy equation on the stability of rolls (which, due to the dispersive terms, take the form of travelling waves). This chapter will consist of systematic expansions and numerical computations. We shall vary the degree of dispersion to reach the circumstance in which the rolls are stable, and then reduce the dispersion to observe the chaotic state related to the non-dispersive equation.

Another point of interest is deriving the amplitude equations of the dispersive Nikolaevskiy equation describing slow modulations in space and time; and examining the influence of dispersion on these equations through numerical computations. The latter will be performed in a fixed domain size with various values of dispersion.

This chapter will be divided into nine main sections. In the next section (§4.2), the Nikolaevskiy equation with dispersion will be presented along with some significant features. Section 4.3 will be devoted to calculating the secondary stability of rolls numerically and presenting some plots for certain values of α and β. Then in the next three sections we will investigate the secondary stability of rolls analytically for different degrees of dispersion. In particular, §4.4 will include the derivation of the coupled amplitude equations, using a weakly nonlinear analysis, for the case of strong dispersion. Moreover, there will be numerical simulations of the governing amplitude equations. Afterwards, intermediate dispersion will be introduced in §4.5 and analysed because the previous section suggests different scaling for small values of the dispersion parameters. Section 4.6 then deals with weak dispersion and will be divided into two subsections, according to the wavenumber of the travelling waves: in one case the basic travelling waves have wavenumber close to the critical value and in the other close to the marginal stability curve. The amplitude equations characterising the behaviour of the solution regarding weak dispersion will be presented in §4.7 along with numerical simulations. In §4.8 the analytical results will be tested against numerical simulations of the Nikolaevskiy equation with dispersion. Finally, an overview of the findings will be given at the end of this chapter in §4.9. Note that the terms "travelling wave" and "roll" will be used interchangeably in this chapter.

4.2 The Nikolaevskiy equation with dispersion

The Nikolaevskiy equation with dispersion is written as

$$\frac{\partial u}{\partial t}+u\frac{\partial u}{\partial x}=-\frac{\partial^2}{\partial x^2}\left[r-\left(1+\frac{\partial^2}{\partial x^2}\right)^2\right]u+\alpha\frac{\partial^3 u}{\partial x^3}+\beta\frac{\partial^5 u}{\partial x^5}, \tag{4.1}$$

where α and β are the dispersion coefficients. This equation is similar to the original model proposed by Nikolaevskiy [45] , with spatial derivatives up to the sixth order. In the numerical simulations we shall impose spatial periodicity. Similarly to the non-dispersive Nikolaevskiy equation, (4.1) has Galilean symmetry: $x\mapsto x+Vt$, $u\mapsto u+V$ (V is a constant). This means that the spatial average of u, which is $\langle u\rangle=\dfrac{1}{l}\displaystyle\int_0^l u dx$, may be set to zero (as in chapter 1). In contrast, the reflection symmetry: $x\mapsto -x$, $u\mapsto -u$ is no longer valid because of the presence of the dispersive terms. However, we have the symmetry: $x\mapsto -x$, $u\mapsto -u$, $\alpha\mapsto -\alpha$, $\beta\mapsto -\beta$, thus we need to consider only $\beta\geq 0$ or $\alpha\geq 0$. In this chapter we shall

consider the case $\beta \geq 0$.

The starting point for the theoretical analysis of (4.1) is to linearise around the steady state $u \equiv 0$, then add spatially periodic perturbations $e^{\mathrm{i}kx+\lambda t}$, which implies the dispersion relation

$$\lambda = k^2\left[r - \left(1-k^2\right)^2\right] + \mathrm{i}k^3\left(k^2\beta - \alpha\right) = \lambda_r + \mathrm{i}\lambda_i.$$

Therefore, the perturbations are in the form of travelling waves with phase speed

$$c = -\frac{\lambda_i}{k} = k^2(\alpha - k^2\beta),$$

and group velocity

$$v = -\frac{\partial\lambda_i}{\partial k} = k^2(3\alpha - 5\beta k^2).$$

The stability of the zero solution is determined by the sign of the real part of λ, and thus we have the same growth rate as the non-dispersive Nikolaevskiy equation (see figure 1.1). For $r > 0$, there exists a band of unstable (growing) wavenumbers in the vicinity of $k = 1$ and a weakly damped large-scale mode near $k = 0$. The latter will result in the appearance of a large-scale mode in the weakly nonlinear regime, which will significantly affect the dynamics of the solution. We are interested in studying the stability of travelling wave solutions just beyond the onset of finite-wavelength instability. Therefore, we introduce the expression

$$r = \epsilon^2 r_2 \quad (\epsilon \ll 1).$$

Note that r_2 is added to allow potential supercritical and subcritical bifurcations (depending on the sign of r_2).

Before proceeding with deriving the governing amplitude equations, which indicate the stability of travelling waves, we first calculate the secondary stability plots. This will be done in order to ascertain the main features of the stability of rolls.

4.3 Secondary stability of travelling waves calculated numerically

In the next two subsections there will first be an explanation of the method for calculating the stability of travelling wave solutions numerically. Afterwards, the stability diagrams will be found for fixed values of α and β.

4.3.1 Numerical method

To calculate the secondary stability of rolls for a fixed value of the parameters, we first compute the travelling roll solution $\bar{u}(x,t) = f(z)$, where $z = x - \bar{c}t$ and $\bar{c}$ is the speed of

the waves. Then we substitute in (4.1), which yields

$$\bar{c}\frac{df}{dz} + (1-r)\frac{d^2f}{dz^2} + 2\frac{d^4f}{dz^4} + \frac{d^6f}{dz^6} + \alpha\frac{d^3f}{dz^3} + \beta\frac{d^5f}{dz^5} - f\frac{df}{dz} = 0. \tag{4.2}$$

This equation is a formula for the phase speed $\bar{c}$ and f. If we imagine that f is known, to find $\bar{c}$, multiply (4.2) by $\dfrac{df}{dz}$ and integrate from 0 to $l = \frac{2\pi}{k}$ with respect to z. This implies

$$\int_0^l \left[\bar{c}\left(\frac{df}{dz}\right)^2 + (1-r)\frac{df}{dz}\frac{d^2f}{dz^2} + 2\frac{df}{dz}\frac{d^4f}{dz^4} + \frac{df}{dz}\frac{d^6f}{dz^6} + \alpha\frac{df}{dz}\frac{d^3f}{dz^3} + \beta\frac{df}{dz}\frac{d^5f}{dz^5}\right] dz$$
$$- \int_0^l f\left(\frac{df}{dz}\right)^2 dz = 0. \tag{4.3}$$

This equation can be simplified by using integration by parts. First, we find the second term

$$\int_0^l \frac{df}{dz}\frac{d^2f}{dz^2}dz = \frac{1}{2}\left[\left(\frac{df}{dz}\right)^2\right]_0^l = 0.$$

This is because f is periodic and thus it follows that $f'(0) = f'(l)$. Now we calculate the third term:

$$\begin{aligned}
\int_0^l \frac{df}{dz}\frac{d^4f}{dz^4}dz &= \left[\frac{df}{dz}\frac{d^3f}{dz^3}\right]_0^l - \int_0^l \frac{d^2f}{dz^2}\frac{d^3f}{dz^3}dz \\
&= -\int_0^l \frac{d^2f}{dz^2}\frac{d^3f}{dz^3}dz \\
&= -\left[\left(\frac{d^2f}{dz^2}\right)^2\right]_0^l + \int_0^l \frac{d^2f}{dz^2}\frac{d^3f}{dz^3}dz \\
&= \int_0^l \frac{d^2f}{dz^2}\frac{d^3f}{dz^3}dz \\
&= -\int_0^l \frac{df}{dz}\frac{d^4f}{dz^4}dz.
\end{aligned}$$

This implies $\displaystyle\int_0^l \frac{df}{dz}\frac{d^4f}{dz^4}dz = 0$; and similarly, $\displaystyle\int_0^l \frac{df}{dz}\frac{d^6f}{dz^6}dz = 0$. Also we have $\displaystyle\int_0^l \alpha\frac{df}{dz}\frac{d^3f}{dz^3}dz = -\int_0^l \alpha\left(\frac{d^2f}{dz^2}\right)^2$ and $\displaystyle\int_0^l \beta\frac{df}{dz}\frac{d^5f}{dz^5}dz = \int_0^l \beta\left(\frac{d^3f}{dz^3}\right)^2 dz$. Accordingly, after applying integration by parts, (4.3) can be reduced to

$$\int_0^l \left[\bar{c}\left(\frac{df}{dz}\right)^2 - \alpha\left(\frac{d^2f}{dz^2}\right)^2 + \beta\left(\frac{d^3f}{dz^3}\right)^2 - f\left(\frac{df}{dz}\right)^2\right] dz = 0.$$

Thus if $f(z)$ is known, the corresponding speed $\bar{c}$ may be found from

$$\bar{c} = \frac{\int_0^l \left[\alpha(\frac{d^2f}{dz^2})^2 - \beta(\frac{d^3f}{dz^3})^2 + f(\frac{df}{dz})^2\right] dz}{\int_0^l (\frac{df}{dz})^2 dz}. \tag{4.4}$$

After finding the formula for the phase speed, we now calculate the roll solution $\bar{u}$. First, we obtain a numerical approximation to $f(z)$ by using the truncated Fourier series

$$\bar{u} = f(z) = \sum_{-N/2+1}^{N/2} \bar{u}_n e^{\mathrm{i}nkz}.$$

Equation (4.2) can be rewritten as

$$\mathcal{L}f + \mathcal{N}(f) = 0,$$

where the linear terms are

$$\mathcal{L}f = \bar{c}\frac{df}{dz} + (1-r)\frac{d^2f}{dz^2} + 2\frac{d^4f}{dz^4} + \frac{d^6f}{dz^6} + \alpha\frac{d^3f}{dz^3} + \beta\frac{d^5f}{dz^5},$$

and the nonlinear term is $\mathcal{N}(f) = -f\dfrac{df}{dz} = -\dfrac{1}{2}\dfrac{d}{dz}(f^2)$. The linear terms are easily found in spectral space

$$\mathcal{L}f(z) = \sum_{-N/2+1}^{N/2} \mathcal{L}(nk)\bar{u}_n e^{\mathrm{i}nkz},$$

where

$$\mathcal{L}(nk) = \mathrm{i}\bar{c}nk + n^2k^2\left[r - (1-n^2k^2)^2\right] - \mathrm{i}\alpha n^3k^3 + \mathrm{i}\beta n^5k^5.$$

On the other hand, the quadratic term is calculated using a pseudo-spectral scheme by transforming first to physical space and then carrying out the multiplication before transforming back to spectral space. Given the Fourier coefficients $\bar{u}_n$ we denote by $\bar{v}_n$ the corresponding coefficients of the nonlinear term so that

$$\mathcal{N}(f) = \sum_{-N/2+1}^{N/2} \bar{v}_n e^{\mathrm{i}nkz}.$$

The coupled equations of the unknowns are thus

$$\mathcal{L}(nk)\bar{u}_n + \bar{v}_n = 0 \qquad \text{for } n = -N/2+1, \cdots, N/2,$$

and $\bar{c}$ is given in (4.4). The travelling wave solution is invariant under translation, so to provide a unique solution we may also fix the phase of $f(z)$; we do so by setting $\Im\bar{u}_1 = 0$. By using the *fsolve* tool in *Matlab* we can approximate the values of $\bar{u}_n$.

After calculating the roll solutions, we determine their stability by adding a perturbation $\tilde{u}(x,t)$, and therefore from (4.1) we obtain

$$\begin{aligned}\frac{\partial}{\partial t}(\bar{u}+\tilde{u}) &= -\frac{\partial^2}{\partial x^2}\left[r - \left(1+\frac{\partial^2}{\partial x^2}\right)^2\right](\bar{u}+\tilde{u}) + \alpha\frac{\partial^3}{\partial x^3}(\bar{u}+\tilde{u}) + \beta\frac{\partial^5}{\partial x^5}(\bar{u}+\tilde{u}) - \bar{u}\frac{\partial\bar{u}}{\partial x} \\ &\quad -\bar{u}\frac{\partial\tilde{u}}{\partial x} - \tilde{u}\frac{\partial\bar{u}}{\partial x} - \tilde{u}\frac{\partial\tilde{u}}{\partial x}.\end{aligned}$$

Since $\bar{u}$ is a solution of (4.1), then

$$\frac{\partial\tilde{u}}{\partial t} = -\frac{\partial^2}{\partial x^2}\left[r - \left(1+\frac{\partial^2}{\partial x^2}\right)^2\right]\tilde{u} + \alpha\frac{\partial^3\tilde{u}}{\partial x^3} + \beta\frac{\partial^5\tilde{u}}{\partial x^5} - \bar{u}\frac{\partial\tilde{u}}{\partial x} - \tilde{u}\frac{\partial\bar{u}}{\partial x} - \tilde{u}\frac{\partial\tilde{u}}{\partial x}. \tag{4.5}$$

We ignore the term $\tilde{u}\frac{\partial\tilde{u}}{\partial x}$ because we linearise in $\tilde{u}$. Since this equation is separable, then $\tilde{u}$ can be written as $e^{\sigma t}U(x)$. Moreover, $\tilde{u}$ is $2\pi/k$-periodic in x and thus $\tilde{u}$ takes the form

$$\tilde{u} = e^{\sigma t + \mathrm{i}pz}\sum_{-N/2+1}^{N/2} v_n e^{\mathrm{i}nkz},$$

where we may restrict attention to perturbations with wavenumber in the range $-k/2 \leq p \leq k/2$, because if p is outside this interval we obtain the same perturbation by a shift of index in the sum. Substituting the Fourier series of $\tilde{u}$ and $\bar{u}$ in (4.5) and dividing by $e^{\sigma t+\mathrm{i}pz}$ gives

$$\sum_{-N/2+1}^{N/2}(\sigma-\mathrm{i}\bar{c}K_n)v_n e^{\mathrm{i}nkz} = \sum_{-N/2+1}^{N/2}\mathcal{L}(nk+p)v_n e^{\mathrm{i}nkz} - \sum_{-N/2+1}^{N/2}\bar{u}_n e^{\mathrm{i}nkz}\sum_{-N/2+1}^{N/2}\mathrm{i}K_m v_m e^{\mathrm{i}mkz} - \sum_{-N/2+1}^{N/2}v_n e^{\mathrm{i}nkz}\sum_{-N/2+1}^{N/2}\mathrm{i}mk\bar{u}_m e^{\mathrm{i}mkz},$$

where $\mathcal{L}(nk+p) = K_n^2[r-(1-K_n^2)^2] - \mathrm{i}\alpha K_n^3 + \mathrm{i}\beta K_n^5$ and $K_n = p+nk$. The last two sums can be rearranged as follows:

$$\sum_{-N/2+1}^{N/2}(\sigma-\mathrm{i}\bar{c}K_n)v_n e^{\mathrm{i}nkz} = \sum_{-N/2+1}^{N/2}\mathcal{L}(nk+p)v_n e^{\mathrm{i}nkz} - \sum_{-N/2+1}^{N/2}e^{\mathrm{i}nkz}\sum_{m}\mathrm{i}K_m v_m\bar{u}_{n-m} - \sum_{-N/2+1}^{N/2}e^{\mathrm{i}nkz}\sum_{m}\mathrm{i}mkv_{n-m}\bar{u}_m.$$

Here m ranges over an appropriate set of values determined by n and subsequently $max(-N/2+1, n-N/2) \leq m \leq min(N/2, n+N/2-1)$. Equating the coefficients of $e^{\mathrm{i}nkz}$ for $-N/2+1 \leq n \leq N/2$ gives

$$(\sigma-\mathrm{i}\bar{c}K_n)v_n = \mathcal{L}(nk+p)v_n - \sum_{m}\mathrm{i}K_m v_m\bar{u}_{n-m} - \sum_{m}\mathrm{i}mkv_{n-m}\bar{u}_m.$$

These equations can be rewritten as the eigenvalue problem

$$\sigma v_n = \sum_{m} a_{nm}v_m.$$

The eigenvalues of this system are computed numerically, for a large number of samples of p taken from $[-k/2, k/2]$, and we determine the largest real part among all eigenvalues. This value will identify whether the original travelling waves are stable or unstable. Note that the numerical code of this scheme is given in appendix D.

In the next subsection we provide some stability graphs based on the above method.

4.3.2 Secondary stability graphs

We shall begin by finding the stability plots in the (k, r) plane. This will be done by fixing α and β, then for a fixed value of r we take samples in k between $\sqrt{1-\sqrt{r}}$ and $\sqrt{1+\sqrt{r}}$ (i.e. inside the marginal curve). We begin by choosing small positive values of r up to 0.9. This is because if $r \geq 0.9$, then the dispersion relation of the Nikolaevskiy equation is qualitatively similar to the Kuramoto-Sivashinsky equation (see figure 4.1). On the other hand, if $r < 0$ all travelling waves are linearly stable (see figure 1.1). Now we use the *Matlab* code, as in

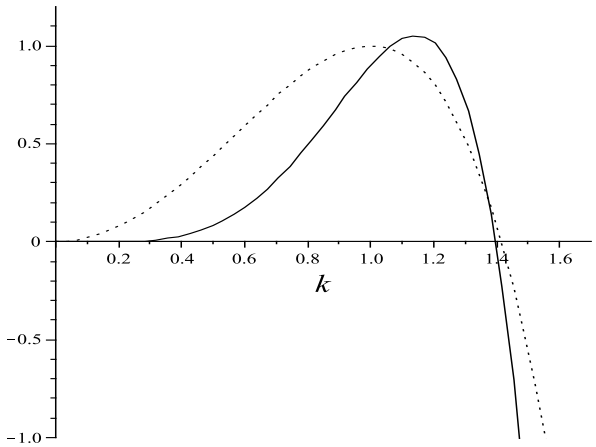

Figure 4.1: The real part of the dispersion relation of the Nikolaevskiy equation with dispersion where $r = 0.9$ (solid line). The dotted line is the dispersion relation of the Kuramoto-Sivashinsky equation (1.5) for $r = 0.9$.

appendix D, to calculate the maximum real part of the growth rates of the disturbances to the rolls. If this value is negative, then the rolls are stable. Accordingly, the stability region for travelling waves is found. Note that the number of samples in k and p is sufficient to not miss any small region of stability. We usually take 200 samples of k in the relevant interval. Then for each k we usually take 300 samples in p (perturbation wavenumber), where $-k/2 \leq p \leq k/2$. Note that in some instances we had to increase the number of samples for k or p; for example, for very small values of r we increased the number of samples in p. The number of Fourier modes is $N = 16$. Table 4.1 shows the modulus of the seven Fourier modes of the roll solution of (4.1) for $N = 16$ and $\alpha = 40$, $\beta = 5$, $r = 0.9$ and $k = 1$. As shown in the table, after the fifth Fourier mode the other modes are very small. After checking several examples, we found that the number of Fourier modes chosen here is sufficient.

In the next part we shall generate a series of plots for different parameter values in order to explore the characteristics of the stability region of rolls. The rationale for our choice of parameter values will be explained at the end of §4.4 after the analytical work.

The first case considered in finding the stability diagrams is setting $\beta = 0$ and changing α. Note that (4.1) is invariant under $(\alpha, u, x) \mapsto (-\alpha, -u, -x)$ when $\beta = 0$, so we need to consider only $\alpha \geq 0$. If α is small ($\alpha = 1/2$), the stable region in (k, r) space seems to be a narrow strip with an upper bound (see figure 4.2(a)). For $r > 0.0078$, all travelling wave solutions are unstable. If α becomes large ($\alpha = 2$), this strip becomes larger and wider such that for $r > 0.22$ all rolls are unstable as exhibited in figure 4.2(b). For larger values of α ($\alpha = 5$), the stable region becomes wider, the upper bound disappears and a symmetrical Eckhaus-like stability region is present for $r < 0.0002$ (see figure 4.2(c)). Figure 4.2 illustrates the three different stability regions, where the stable region lies within the

$\lvert\bar{u}_1\rvert = 1.6121 \times 10^{1}$
$\lvert\bar{u}_2\rvert = 2.5517 \times 10^{0}$
$\lvert\bar{u}_3\rvert = 2.0076 \times 10^{-1}$
$\lvert\bar{u}_4\rvert = 4.0102 \times 10^{-3}$
$\lvert\bar{u}_5\rvert = 1.5213 \times 10^{-4}$
$\lvert\bar{u}_6\rvert = 3.5265 \times 10^{-6}$
$\lvert\bar{u}_7\rvert = 6.1425 \times 10^{-8}$

Table 4.1: The modulus of the seven Fourier modes of the roll solution of (4.1) for $\alpha = 40$, $\beta = 5$, $r = 0.9$ and $k = 1$.

dashed curves. In this figure we notice that an Eckhaus-like stability region is apparent (for small r) only for large values of α because it is hard to find it numerically for small α. Moreover, the shrinkage of the stable region as we decrease α is consistent with the fact that for the non-dispersive Nikolaevskiy equations all roll solutions are unstable [14, 40, 70, 72].

Now we set instead $\alpha = 0$ and vary β as displayed in figure 4.3. Similarly to the previous case, we need to consider only $\beta \geq 0$. For $\beta = 2$, the travelling waves are stable for small values of r. Moreover, the stable region is narrow and ends at $r \approx 0.065$, because all rolls are unstable if $r > 0.065$, see figure 4.3(a). If β is larger, namely $\beta = 10$, the stable region ends at $r \approx 0.09$ and another stable region appears at $r \approx 0.6$ and continues at least as far as 0.9 as exhibited in figures 4.3(b) and (c). Similar comments apply for a larger value of β ($\beta = 20$) but here an Eckhaus-like stability region is present at the bottom of the curve (see figures 4.3(d) and (e)). Note that again this Eckhaus-like stability region cannot be found numerically for small β.

Now fix $\alpha = 2$ and take $\beta = 0$, $\beta = 3/4$ and $\beta = 2$, as shown in figure 4.4 for $\beta = 0$ and $\beta = 2$. When $\beta = 0$ the stable region is a narrow strip bounded from above where rolls are unstable if $r > 0.22$ (figure 4.4(a)). This stable region disappears if instead we choose $\beta = 3/4$. If $\beta = 2$, the stable region is present but it is wider and shorter than in the case $\beta = 0$ where stable rolls exist if $r < 0.0029$ (figure 4.4(b)).

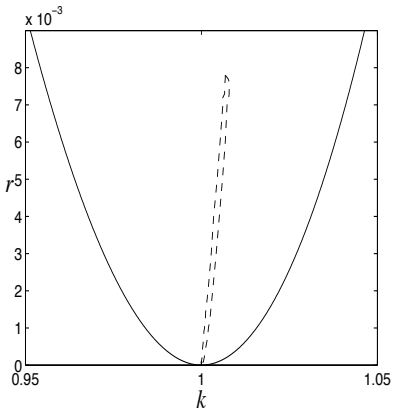

(a) $\alpha = 1/2$ and $\beta = 0$.

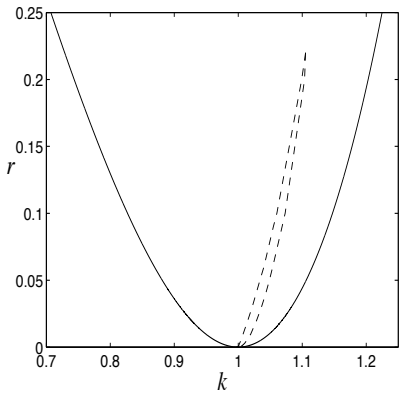

(b) $\alpha = 2$ and $\beta = 0$.

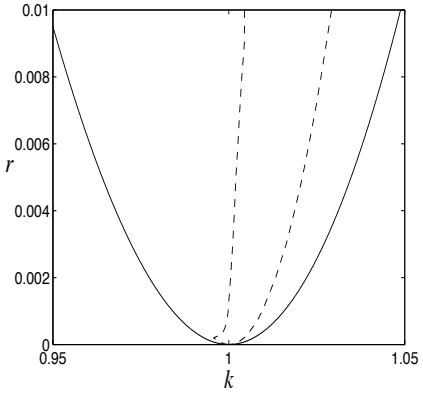

(c) $\alpha = 5$ and $\beta = 0$.

Figure 4.2: The secondary stability of travelling wave solutions of (4.1) calculated numerically for (a) $\alpha = 1/2$, (b) $\alpha = 2$ and (c) $\alpha = 5$, where $\beta = 0$. The stable region lies inside the dashed curves and the marginal curve is given by $r = (1-k^2)^2$. Note that the stable region in (c) continues at least up to $r = 0.9$ and an Eckhaus-like stability region is visible for small r.

Now we set $\beta = 10$ and take $\alpha = 0$, $\alpha = 22$ and $\alpha = 40$. If $\alpha = 0$, then the stable region occupies two independent areas as displayed in figure 4.5(a). Specifically, the lower stable region is bounded from above by $r \approx 0.22$ and the upper stable region is bounded from below by $r \approx 0.294$. When $\alpha = 22$ there is no stable region. If $\alpha = 40$, then two stable regions are present and the lower of the two has an Eckhaus-like stability region for $r < 0.001$ (see figures 4.5(b) and (c)).

Examples of complicated stability regions arise when we set $\alpha = 40$ and vary β as shown in figure 4.6. For $\beta = 5$, an Eckhaus-like stability region is valid for $r < 0.001$ (see figure 4.6(a)). Moreover, the stable region continues at least as far as $r = 0.9$. As β becomes large ($\beta = 5.5$) the stable region splits into several parts (see figure 4.6(b)). When $\beta = 6$ we have instability for very small values of r ($r < 0.039$) and the stable region splits into as many as

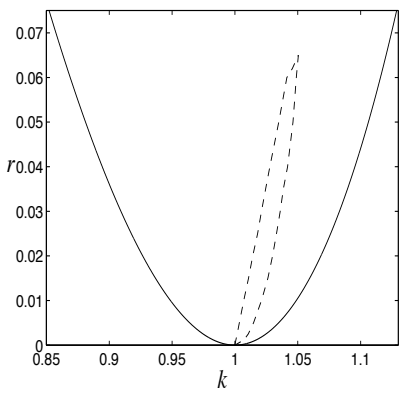

(a) $\alpha = 0$ and $\beta = 2$.

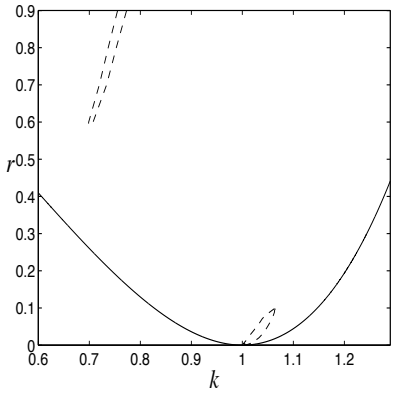

(b) $\alpha = 0$ and $\beta = 10$.

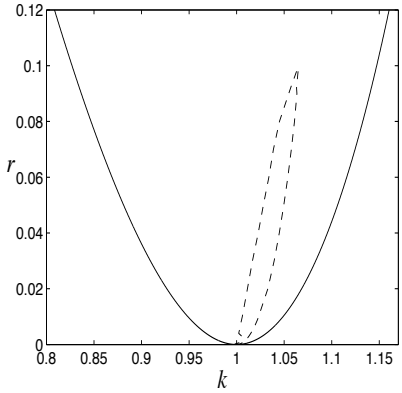

(c) $\alpha = 0$ and $\beta = 10$.

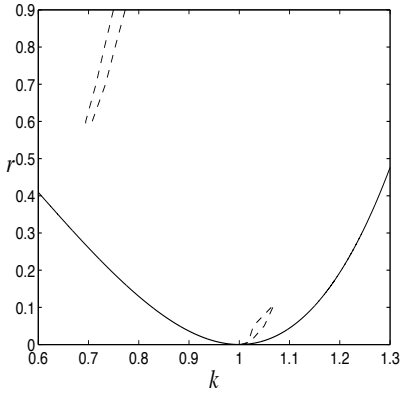

(d) $\alpha = 0$ and $\beta = 20$.

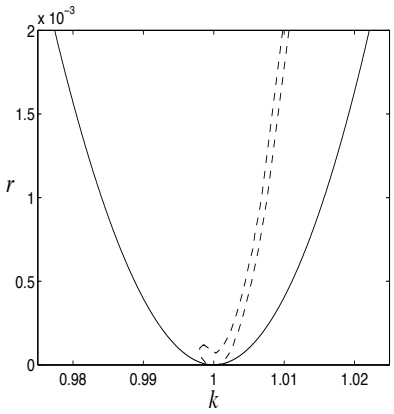

(e) $\alpha = 0$ and $\beta = 20$.

Figure 4.3: The secondary stability of travelling wave solutions of (4.1) calculated numerically for (a) $\beta = 2$, (b) $\beta = 10$ and (d) $\beta = 20$, where $\alpha = 0$. The stable region lies inside the dashed curves and the marginal curve is given by $r = (1-k^2)^2$. Note that (c) is a close up of (b) and similarly (e) is a close up of (d).

five parts in a horizontal cross-section (see figure 4.6(c)). Finally, if $\beta = 10$ the stable region covers two parts as exhibited in figure 4.6(d).

In the previous calculations, r and k are the free system parameters and α and β are

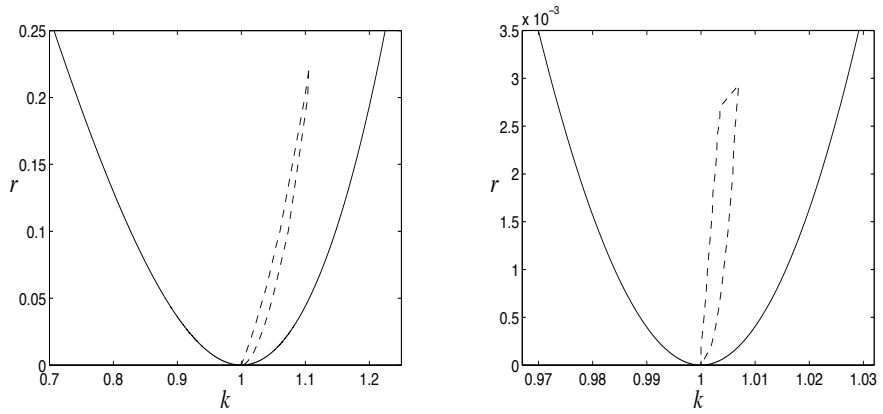

(a) $\alpha = 2$ and $\beta = 0$. (b) $\alpha = 2$ and $\beta = 2$.

Figure 4.4: The secondary stability of travelling waves of (4.1) calculated numerically for (a) $\beta = 0$ and (b) $\beta = 2$, where $\alpha = 2$. The stable region lies inside the dashed curves and the marginal curve is given by $r = (1 - k^2)^2$.

fixed. Accordingly, the stable region was found in the (k, r) plane. Next, we are interested in calculating the stability graphs in the (k, α) plane for fixed r and β and the (k, β) plane for fixed r and α. This is done in order to examine the effect of dispersion on the stability of rolls for a fixed r.

The first graph we present is for fixed $r = 0.01$ and $\beta = 0$. This choice of r implies that rolls exist if $0.9487 < k < 1.0488$. We already know that for $\alpha = 0$ there are no stable travelling wave solutions (non-dispersive Nikolaevskiy equation). Moreover, as α increases we obtain for small r an Eckhaus-like stability region. These predictions agree with figure 4.7(a), where the stable region exists for $\alpha > 0.563$. On the other hand, if we take $r = 0.1$, then rolls exist for $0.8269 < k < 1.1473$ and the stable region exists for $\alpha > 1.515$ (see figure 4.7(b)). It can be concluded from these two graphs that when we increase r, the critical value for α, to allow stable travelling wave solutions, increases.

Now if $\alpha = 40$ and $r = 0.1$, then rolls exist for $0.8269 < k < 1.1473$. From figure 4.6 when $r = 0.1$, we expect that for small values of β there is one stable region and afterwards it splits into several parts for larger β. This result is exhibited in figure 4.7(c), where the structure of the stability region changes for large values of β.

After presenting several numerical stability graphs, for fixed values of the dispersion coefficients, we conclude that it is possible to observe an Eckhaus-like stability region near the bottom of the marginal curve. In addition to this, various choices for dispersion manifest different topologies where the secondary stability regions can be complicated. We are unable to draw any significant general conclusions about the form of the secondary stability plots, limiting ourselves to some specific examples. In the sections that follow we shall consider

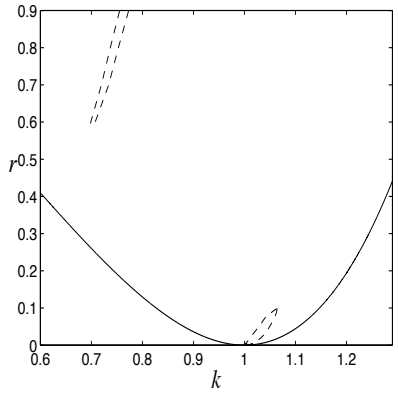

(a) $\alpha = 0$ and $\beta = 10$.

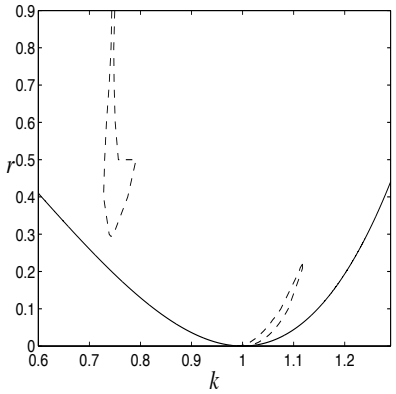

(b) $\alpha = 40$ and $\beta = 10$.

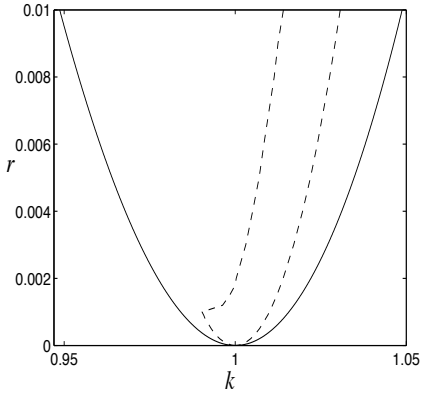

(c) $\alpha = 40$ and $\beta = 10$.

Figure 4.5: The secondary stability of travelling waves of (4.1) calculated numerically for (a) $\alpha = 0$ and (b) $\alpha = 40$, where $\beta = 10$. The stable region lies inside the dashed curves and the marginal curve is given by $r = (1 - k^2)^2$. Note that (b) is the same as (c) but with higher values of r.

investigating some cases of the previous results by means of asymptotic expansions.

4.4 Strong dispersion: $\alpha, \beta = O(1)$

In this section and the following two sections we shall investigate analytically the effect, on the stability of travelling waves, of adding dispersion to the Nikolaevskiy equation. We already expect that dispersion stabilises the spatially periodic solution as demonstrated in §4.3 by means of numerical calculations. The most straightforward circumstance in which to analyse the secondary stability of the travelling wave solutions arises when the dispersion parameters α and β are each $O(1)$. To differentiate it from later sections, we shall characterise this case as *strong dispersion*.

We begin by applying a weakly nonlinear regime on (4.1), thus we introduce the appro-

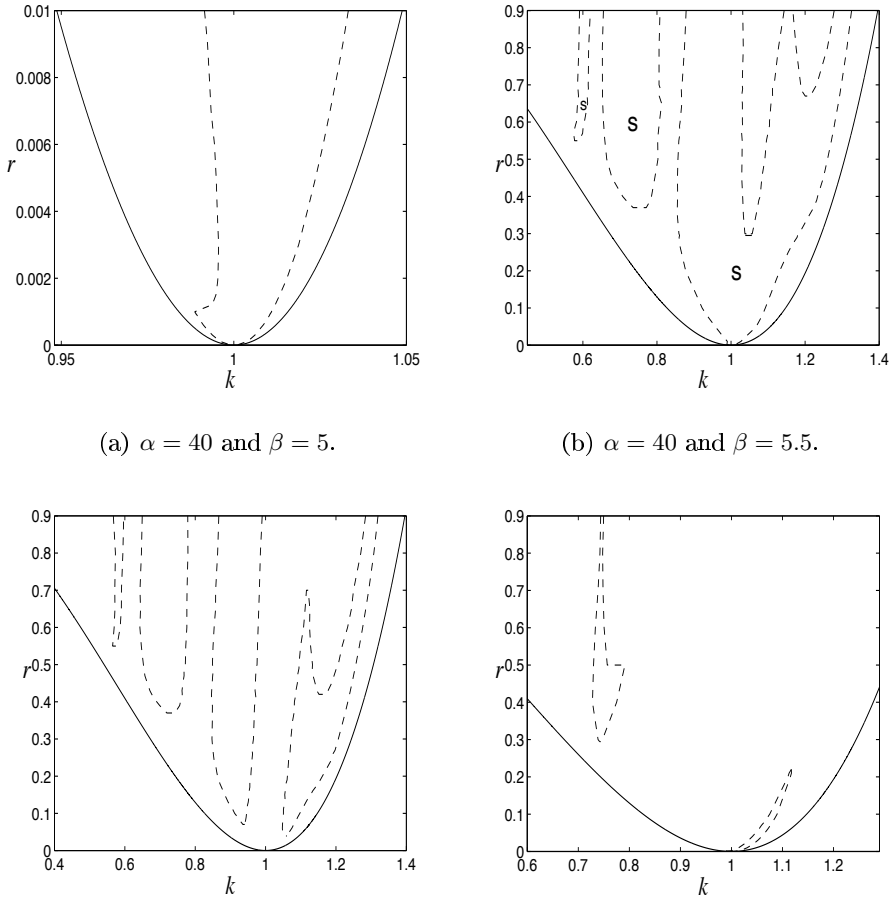

(a) $\alpha = 40$ and $\beta = 5$.

(b) $\alpha = 40$ and $\beta = 5.5$.

(c) $\alpha = 40$ and $\beta = 6$.

(d) $\alpha = 40$ and $\beta = 10$.

Figure 4.6: The secondary stability of travelling wave solutions of (4.1) calculated numerically for (a) $\beta = 5$, (b) $\beta = 5.5$, (c) $\beta = 6$ and (d) $\beta = 10$, where $\alpha = 40$. The stable region lies inside the dashed curves and the marginal curve is given by $r = (1 - k^2)^2$. Note that the stable region in (a) continues at least up to $r = 0.9$. To clarify the stability regions in (b) we indicate them by "s".

priate expansion for u

$$u = \epsilon u_1 + \epsilon^2 u_2 + \epsilon^3 u_3 + \epsilon^4 u_4 + \cdots , \tag{4.6}$$

with $r = \epsilon^2 r_2$, $X = \epsilon x$, $T = \epsilon^2 t$ and $\tau = \epsilon t$. The large time scale T is related to the growth rate λ_r and therefore near the wavenumber $k = 1$, T should have the same order as r. The specific order of the large space scale X is necessary in order to balance diffusion terms appearing later in the amplitude equations. Finally, τ is related to the $O(1)$ group velocity, which explains why it has the same order as X.

From substituting (4.6) in (4.1) with the above scaling and considering successive orders in ϵ, it turns out that at $O(\epsilon)$ $u_1 = A(X, T, \tau)e^{\mathrm{i}(x-ct)} + c.c$, where A is a slowly varying complex amplitude and the phase speed of the waves is $c = \alpha - \beta$. Proceeding to the next

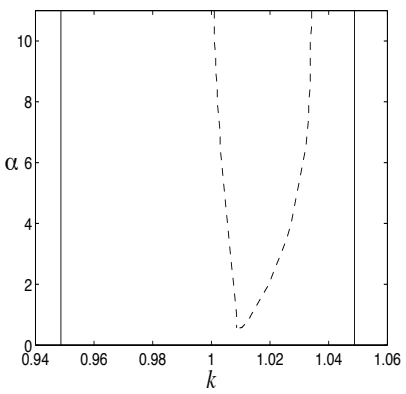

(a) $r = 0.01$ and $\beta = 0$.

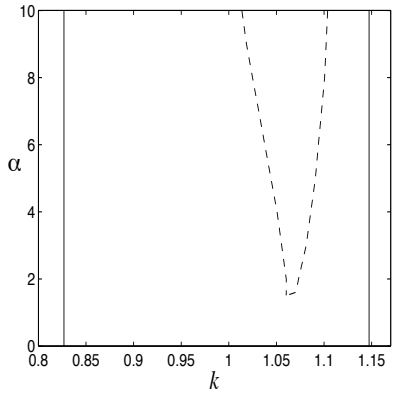

(b) $r = 0.1$ and $\beta = 0$.

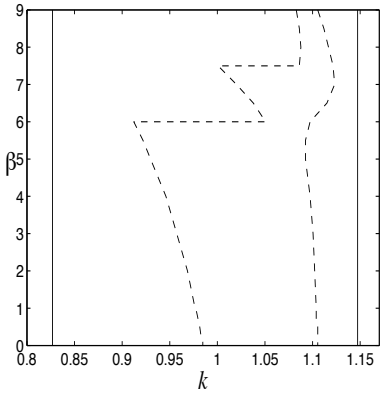

(c) $\alpha = 40$ and $r = 0.1$.

Figure 4.7: The secondary stability of rolls of (4.1) calculated numerically for fixed r and β or α as indicated under each figure. The stable region lies inside the dashed curves and the two vertical lines indicate the existence region of rolls.

order, the coefficient of $e^{\mathrm{i}(x-ct)}$ yields

$$\frac{\partial A}{\partial \tau} + (3\alpha - 5\beta)\frac{\partial A}{\partial X} = 0.$$

In order to satisfy this solvability condition we need to choose $A = A(T, \xi)$ where $\xi = X - v\tau$ is a coordinate moving at the group velocity of the waves ($v = 3\alpha - 5\beta$). According to the new scaling we have

$$u_2 = -\frac{\mathrm{i}A^2}{36(1 + \mathrm{i}(\alpha - 5\beta)/6)} e^{2\mathrm{i}(x-ct)} + c.c + f(X, T, \tau).$$

f stands for a slow varying real function chosen to appear at this order to balance terms arising at $O(\epsilon^3)$.

After straightforward calculations, the corresponding amplitude equations which come from solvability conditions are

$$\begin{aligned}\frac{\partial A}{\partial T} &= \left[r_2 - \frac{1-\mathrm{i}(\alpha-5\beta)/6}{36+(\alpha-5\beta)^2}|A|^2\right]A + [4+\mathrm{i}(3\alpha-10\beta)]\frac{\partial^2 A}{\partial \xi^2} - \mathrm{i}fA,\\ \frac{\partial f}{\partial \tau} &= -\frac{\partial |A|^2}{\partial \xi}.\end{aligned}$$

The second amplitude equation suggests, since $A = A(T,\xi)$, the natural choice of $f = f(T,\xi)$. Therefore, $-v\frac{\partial f}{\partial \xi} = -\frac{\partial |A|^2}{\partial \xi}$ and hence $vf = |A|^2 + K(T)$, for some as yet unknown $K(T)$. Thus from the asymptotic expansion of u and since $\langle u\rangle = 0$, we have $\langle f\rangle = 0$. This implies $f = \frac{-\langle |A|^2\rangle + |A|^2}{v}$; by substituting this in the governing equation we obtain the nonlocal Ginzburg-Landau equation

$$\frac{\partial A}{\partial T} = \left[r_2 - \frac{1-\mathrm{i}(\alpha-5\beta)/6}{36+(\alpha-5\beta)^2}|A|^2 + \mathrm{i}\frac{\langle |A|^2\rangle - |A|^2}{v}\right]A + [4+\mathrm{i}(3\alpha-10\beta)]\frac{\partial^2 A}{\partial \xi^2}. \tag{4.7}$$

From this equation, by substituting $A = a_0 e^{\mathrm{i}q\xi}$, the amplitude of rolls is given by

$$a_0 = 6\left(r_2 - 4q^2\right)^{1/2}\left(1 + \tfrac{1}{36}(\alpha-5\beta)^2\right)^{1/2}. \tag{4.8}$$

It is worth mentioning that $f = \frac{-\langle |A|^2\rangle + |A|^2}{v}$ imposes the constraint that v should not be zero. Therefore, the scaling used in this section breaks down when v is small; in particular, this is the case when α and β are both small.

Now we simplify (4.7) by substituting $\hat{A} = \sqrt{\frac{a_1}{r_2}}A$, $\hat{T} = r_2 T$ and $\hat{\xi} = \frac{\sqrt{r_2}}{2}\xi$, where $a_1 = \frac{1}{36+(5\beta-\alpha)^2}$. This implies the complex Ginzburg-Landau equation (CGLE) but with an additional term involving $(\langle |A|^2\rangle - |A|^2)A$ as follows:

$$\frac{\partial A}{\partial T} = A + \mathrm{i}d(\langle |A|^2\rangle - |A|^2)A + (1+\mathrm{i}a)\frac{\partial^2 A}{\partial \xi^2} - (1+\mathrm{i}b)|A|^2 A, \tag{4.9}$$

where

$$\begin{aligned} a &= \frac{3\alpha-10\beta}{4},\\ b &= \frac{5\beta-\alpha}{6},\\ d &= \frac{36+(5\beta-\alpha)^2}{v}.\end{aligned}$$

Note that for simplicity, we have dropped the hats on the variables in this equation.

Similar equations to (4.9), including a nonlocal nonlinear term, were also derived and analysed for electrical and magnetic systems [17, 20], reaction diffusion systems [58, 64], dissipative systems [33] and convection in a rotating cylindrical annulus [46]. In electrical and magnetic systems, the nonlocal CGLE was analysed in terms of the stability of spatially periodic solutions and the result shows that there are Eckhaus and modified Eckhaus stability regions for periodic solutions [20]. In addition to this, in reaction diffusion systems, the stability analysis of plane-wave solutions of the nonlocal CGLE revealed new types of

instability different from the conventional CGLE [64]. In dissipative systems the analysis shows that there are stable travelling and standing waves for the nonlocal CGLE [33].

Due to the similarity of (4.9) to the CGLE, it possesses the same plane-wave solutions [3, 75, 76], which have the form $A = Qe^{\mathrm{i}(\omega T+q\xi)}$. Here the real amplitude satisfies $Q^2 = 1-q^2$ and $\omega = q^2(b-a)-b$. To study the stability of the plane-wave solution we put $A = [1+n(T,\xi)]Qe^{\mathrm{i}(\omega T+q\xi)}$ and linearise in the perturbation n, which yields

$$\frac{\partial n}{\partial T} = (1+\mathrm{i}a)\left(\frac{\partial^2 n}{\partial \xi^2}+2\mathrm{i}q\frac{\partial n}{\partial \xi}\right) - (1+\mathrm{i}b)Q^2(n^*+n) + \mathrm{i}dQ^2\left(\langle n+n^*\rangle - (n^*+n)\right).$$

Now upon setting $n(T,\xi) = R(T)e^{\mathrm{i}L\xi} + S^*(T)e^{-\mathrm{i}L\xi}$ and equating the coefficients of $e^{\mathrm{i}L\xi}$ and $e^{-\mathrm{i}L\xi}$; we have respectively

$$\frac{\partial R}{\partial T} = -(1+\mathrm{i}a)L(LR+2qR) - (1+\mathrm{i}b)Q^2(R+S) - \mathrm{i}dQ^2(R+S),$$

$$\frac{\partial S}{\partial T} = -(1-\mathrm{i}a)L(LS-2qS) - (1-\mathrm{i}b)Q^2(R+S) + \mathrm{i}dQ^2(R+S).$$

After putting $R = \bar{R}e^{\lambda T}$ and $S = \bar{S}e^{\lambda T}$ two equations are obtained, and in order to have a nontrivial solution the determinant of the matrix of the coefficients of R and S should be zero. This gives an eigenvalue problem for λ. We analyse it by seeking long-wavelength instabilities; expanding in powers of the perturbation wavenumber L gives

$$\lambda = -2\mathrm{i}q(a-b-d)L + L^2Q^{-2}\left(-1-a(b+d)+q^2\left[3+2(b+d)^2+a(b+d)\right]\right) + O(L^3).$$

It is apparent from this equation that the solution has long-wavelength oscillatory instability if

$$q^2\left(3+2(b+d)^2+a(b+d)\right) > 1+a(b+d),$$

and since

$$1+a(b+d) < 3+2(b+d)^2+a(b+d),$$

then the stability is determined by the following cases:

i. If $1+a(b+d) > 0$, then $3+2(b+d)^2+a(b+d) > 0$. Thus we have stability for a band of wavenumbers satisfying

$$0 \le q^2 < q_c^2 \equiv \frac{1+a(b+d)}{3+2(b+d)^2+a(b+d)} < 1. \tag{4.10}$$

ii. If $1+a(b+d) < 0$, then we have instability for any $0 \le q^2 < 1$.

. Choosing $a = b = d = 0$ recovers the usual GLE for A; and correspondingly (i) illustrates the Eckhaus stability ($q^2 < 1/3$) [18, 28, 74].

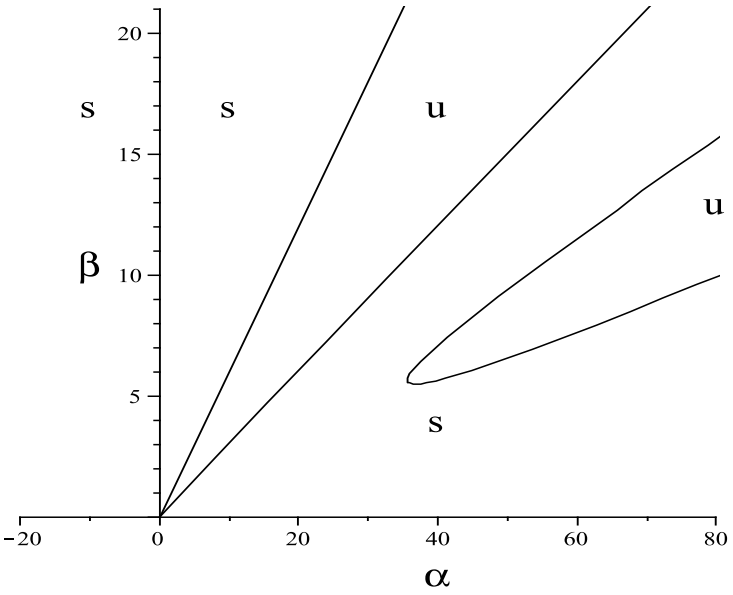

Figure 4.8: Diagram showing the sign of $1 + a(b + d)$ in (α, β) parameter space. Regions with "s" correspond to stable plane waves with wavenumber given by (4.10). The other regions with "u" mean that all plane waves are unstable.

From conditions (i) and (ii) it is concluded that the stability of the solution to (4.9) is determined by the sign of $1 + a(b + d)$. Using this fact we next determine where, in (α, β) parameter space, cases (i) or (ii) apply. Figure 4.8 captures the graph of β against α for the solution of the equation $1 + a(b + d) = 0$. When crossing each of the curves, the sign of $1 + a(b + d)$ changes. The notations "s" and "u" represent when $1 + a(b + d)$ is positive and negative, respectively. Therefore, the region with the "s" sign corresponds to the existence of stable wave solutions with wavenumber satisfying (4.10). On the other hand, the region with the "u" sign corresponds to unstable waves. Because (4.1) has reflection symmetry with respect to x, u, α and β, only the upper half of the graph is presented.

Now that we have predicted the stability of the plane-wave solutions, we present some simulations of the initial value problem for (4.9). The numerical scheme used is pseudo-spectral for spatial discretisation [21, 67] combined with a second-order exponential time differencing method for time integration [13], a similar *Matlab* code is given in [75]. The domain size is $l = 64\pi$ and the initial condition is a travelling wave with wavenumber $q = \frac{2n\pi}{l}$ (n is the number of waves in the box) plus random noise. Our first choice is $\alpha = 10$, $\beta = 2.6$ and $q = 0.875$ (case (i)). These travelling waves are predicted to be unstable. In figure 4.9(a) a transient behaviour followed by a state close to stable plane waves with a different wavenumber is present. The second choice is the same as the previous one but with $q = 0.3125$ waves (case (i) with stability). Figure 4.9(b) illustrates the stability of these waves. The final choice is $\alpha = 8.4$, $\beta = 2.6$ and $q = 0.625$ waves (case (ii)). The simulation shown in figure 4.9(c) exhibits the evolution of a chaotic state where the simulation never

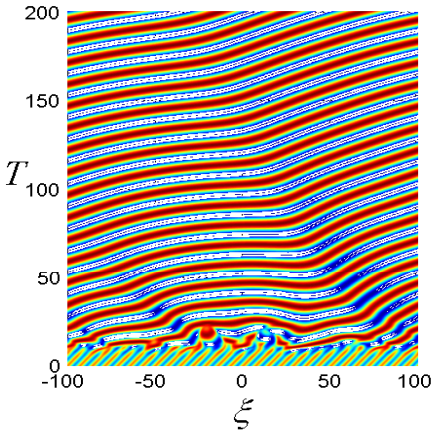

(a) $\alpha = 10$, $\beta = 2.6$ and $q = 0.875$.

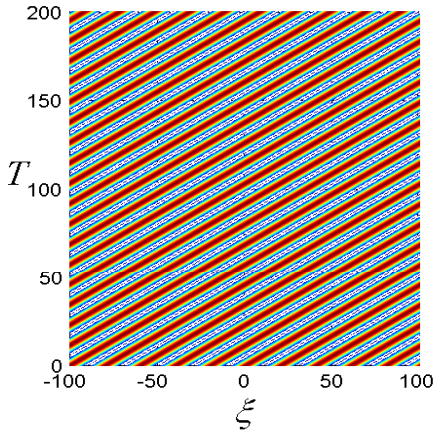

(b) $\alpha = 10$, $\beta = 2.6$ and $q = 0.3125$.

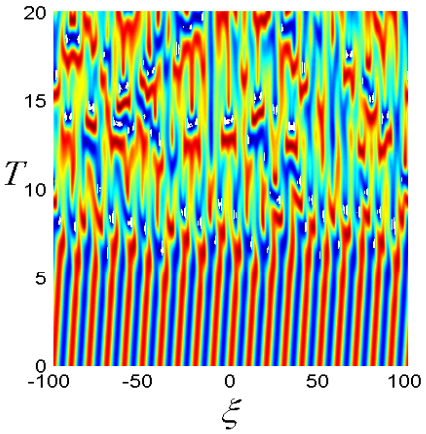

(c) $\alpha = 8.4$, $\beta = 2.6$ and $q = 0.625$.

Figure 4.9: Space-time numerical simulations of the amplitude equation (4.9) where the real value of A is plotted as a function of ξ and T. The values of α, β and the wavenumber of the initial condition (plane wave plus small-amplitude random noise) are given under each figure.

settles down, and is persistently time dependent. The numerical simulations produced results which corroborate the findings of the previous theoretical approach.

Now we go back to figure 4.8 where the stability analysis for travelling wave solutions is summarised. This figure illustrates the existence of stable roll solutions for appropriate fixed values of α and β (not both zero) in the limit $r \to 0$. This result is consistent with the secondary stability plots found in §4.3. As far as the strong dispersion is concerned, the analysis corresponds to the lower part of the stability plots; for example, when $\alpha = 5$ and $\beta = 0$ figure 4.2(c) exhibits an Eckhaus-like stability region for small r. This is already predicted from the analysis given in this section, since α and β lie in the stable region in figure 4.8. Another example of such agreement of the analysis with the secondary stability plots arises when $\alpha = 40$ and $\beta = 6$. As shown in figure 4.6(c), for small r there are no

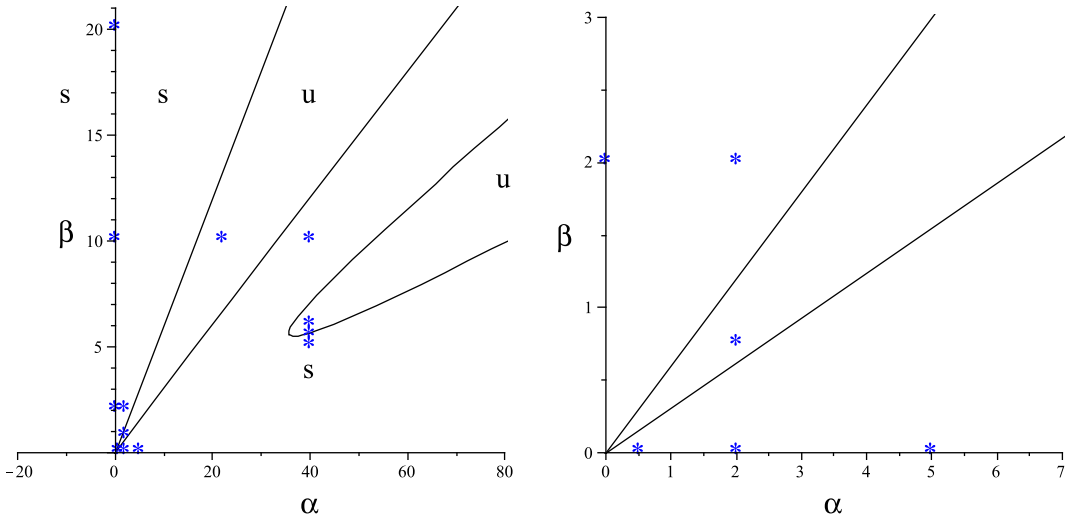

(a) (b)

Figure 4.10: Same as figure 4.8. The secondary stability pictures in §4.3 are generated according to these values of α and β indicated by "$*$". These values were chosen in order to show trends for $\alpha = 0$, $\beta = 0$ and along a cross section through each of the regions marked "u". (b) is a close up of (a).

stable travelling wave solutions. This is also confirmed by the stability analysis illustrated in figure 4.8, where α and β are taken from the unstable region. The values of α and β chosen for the secondary stability plots in §4.3 are given in figure 4.10, for the sake of comparison between the stability plots and the asymptotic analysis. By comparing the two analyses, we found that they are consistent in the limit of small r.

This section leads to the conclusion that a band of stable wavenumbers can exist for appropriate large α and β. However, this analysis breaks down when v is small (α and β are both small). In addition, the analysis predicts that stable rolls persist down to α, $\beta = 0$. This conflicts with the fact that for $\alpha = \beta = 0$ all roll solutions are unstable at onset; and therefore this contradiction for small α and β needs to be resolved. This motivates an investigation of intermediate dispersion with $\alpha, \beta = O(\epsilon^{3/4})$ in the next section.

4.5 Intermediate dispersion: $\alpha, \beta = O(\epsilon^{3/4})$

The previous analysis shows that stable travelling wave solutions can exist if α and β are of $O(1)$. For small α and β, different scaling must be considered. Namely, we adapt the scaling first used in [72] for the non-dispersive case and then extended in [14] for the damped Nikolaevskiy equation. Therefore, set $X = \epsilon^{3/4}x$, $T = \epsilon^{3/2}t$, $\tau = \epsilon^{3/4}t$, $\alpha = \epsilon^{3/4}\hat{\alpha}$ and $\beta = \epsilon^{3/4}\hat{\beta}$. The ultimate justification for having chosen the scaling for α and β follows from balancing extra terms (generated by dispersion) with the leading-order terms appearing in the

amplitude equations in [14]. This scaling is discovered after several experiments. Regarding τ, it is related to $\hat{c} = \hat{\alpha} - \hat{\beta}$ and therefore it should have the same order as α and β. The scalings of X and T were chosen to balance diffusion with advection terms in the following amplitude equations.

Applying a weakly nonlinear analysis on (4.1) gives

$$u = \epsilon[a_0 + \epsilon^{1/2}a(X,T)]e^{\mathrm{i}M} + c.c. + \epsilon^{7/4}f(X,T) + \cdots,$$

where $M = (1+\epsilon q)x + \epsilon^{1/4}\psi(X,T) - \hat{c}\tau - \epsilon^{1/4}\hat{v}qT$, $\hat{v} = 3\hat{\alpha} - 5\hat{\beta}$ and $a_0 = 6\sqrt{r_2 - 4q^2}$ (travelling wave solutions exist if $r_2 > 4q^2$). $a(X,T)$ is the amplitude of disturbances to the pattern and $f(X,T)$ is a large-scale mode. Both a and f, at their particular orders, are necessary to balance terms appearing in the following amplitude equations. Here $(1+\epsilon q)x$ gives the spatial variation of the rolls. Moreover, $-\hat{c}\tau$ corresponds to the waves travelling with phase speed $c = \epsilon^{3/4}\hat{c}$. Also $-\epsilon^{1/4}\hat{v}qT$ represents the rescaled group velocity ($v = \epsilon^{3/4}\hat{v}$) of the envelope of the waves. Finally, the term $\epsilon^{1/4}\psi(X,T)$ is a phase that will evolve dynamically according to some amplitude equations that arise from solvability conditions.

After substituting the asymptotic expansion of u in (4.1), the amplitude equations will appear from solvability conditions at successive powers of $O(\epsilon^{1/4})$. These amplitude equations are

$$\begin{aligned}
\frac{\partial\psi}{\partial T} &= 4\frac{\partial^2\psi}{\partial X^2} - f - \hat{v}\frac{\partial\psi}{\partial X},\\
\frac{\partial f}{\partial T} &= \frac{\partial^2 f}{\partial X^2} - 2a_0\frac{\partial a}{\partial X},\\
\frac{\partial a}{\partial T} &= 4\frac{\partial^2 a}{\partial X^2} - 4a_0\left(\frac{\partial\psi}{\partial X}\right)^2 - 8a_0 q\frac{\partial\psi}{\partial X} - \hat{v}\frac{\partial a}{\partial X}.
\end{aligned}$$

Note that the α and β terms are represented in these equations only through the terms $\hat{v}\dfrac{\partial\psi}{\partial X}$ and $\hat{v}\dfrac{\partial a}{\partial X}$. These represent advection of the pattern envelope at the rescaled group velocity $\hat{v}$. In addition, the rescaled group velocity of the large-scale mode f is 0, and hence no corresponding term appears in the second equation.

In order to study the stability of the roll solutions, we reduce the above amplitude equations to a nonlinear phase equation. This is done first by writing these equations as follows:

$$\begin{aligned}
\left(\frac{\partial}{\partial T} - 4\frac{\partial^2}{\partial X^2} + \hat{v}\frac{\partial}{\partial X}\right)\psi &= -f,\\
\left(\frac{\partial}{\partial T} - \frac{\partial^2}{\partial X^2}\right)f &= -2a_0\frac{\partial a}{\partial X},\\
\left(\frac{\partial}{\partial T} - 4\frac{\partial^2}{\partial X^2} + \hat{v}\frac{\partial}{\partial X}\right)a &= -4a_0\left(\frac{\partial\psi}{\partial X}\right)^2 - 8a_0 q\frac{\partial\psi}{\partial X},
\end{aligned}$$

and then combining them into the following equation:

$$\left(\frac{\partial}{\partial T}-4\frac{\partial^2}{\partial X^2}+\hat{v}\frac{\partial}{\partial X}\right)^2\left(\frac{\partial}{\partial T}-\frac{\partial^2}{\partial X^2}\right)\psi=-16a_0^2\left(\frac{\partial\psi}{\partial X}+q\right)\frac{\partial^2\psi}{\partial X^2}. \tag{4.11}$$

Linearising this equation and putting $\psi=\bar{\psi}e^{\mathrm{i}LX+\sigma T}$ gives the dispersion relation

$$\sigma^3+9\sigma^2L^2+24\sigma L^4+16L^6-16a_0^2qL^2-\hat{v}^2\sigma L^2-\hat{v}^2L^4+\mathrm{i}\hat{v}(2\sigma^2L+10\sigma L^3+8L^5)=0. \tag{4.12}$$

Before studying the dispersion relation for general L, it is helpful to consider the two limiting cases, of small and large L. If L is small, then $\sigma^3\sim 16a_0^2qL^2$. Thus to leading-order in L, $\sigma=\sigma_{2/3}L^{2/3}$ with $\sigma_{2/3}^3=16a_0^2q$. This shows that all rolls are unstable if L is small. On the other hand, if L is very large, then we have $\sigma^3+9\sigma^2L^2+24\sigma L^4+16L^6\approx 0$. Thus $\sigma=\{-4L^2,-4L^2,-L^2\}$ which shows that for large-L disturbances, travelling waves are stable. It can be concluded that if $a_0^2q\neq 0$, then all roll solutions are unstable at onset. The rest of the section provides more details of the instability for general L.

In order to find the marginal stability boundary we set $\sigma=\mathrm{i}\Omega$ and substitute it in the dispersion relation (4.12). After comparing the real and the imaginary parts, the following is obtained:

$$\begin{aligned}\Omega^3-24\Omega L^4+\hat{v}^2\Omega L^2+2\hat{v}L\Omega^2-8\hat{v}L^5 &= 0,\\ \Omega^2-\frac{16}{9}L^4+\frac{16}{9}a_0^2q+\frac{\hat{v}^2}{9}L^2+\frac{10}{9}\hat{v}L\Omega &= 0.\end{aligned}$$

Eliminating Ω between these two equations gives

$$16a_0^6q^3-2500L^{12}+2100L^8a_0^2q+384L^4a_0^4q^2-200\hat{v}^2L^{10}-4\hat{v}^4L^8-44\hat{v}^2L^6a_0^2q+\hat{v}^2L^2a_0^4q^2=0. \tag{4.13}$$

In this equation L and $\hat{v}$ appear at even powers and thus we can restrict our attention to positive L and $\hat{v}$ with no loss of generality. Regarding q, both odd and even powers occur, hence different behaviours for positive and negative q are expected, which already applies to the non-dispersive case [72].

For the case of no dispersion [40, 72] (details in §2.3.2), there is monotonic instability of the waves if $0<q<\frac{\sqrt{r_2}}{2}$ with unstable modes satisfying $0<L<(a_0^2q)^{1/4}$. In addition, oscillatory instability of the rolls occurs when $-\frac{\sqrt{r_2}}{2}<q<0$ with unstable disturbances having $0<L<(-\frac{2}{25}a_0^2q)^{1/4}$.

It is convenient to rewrite (4.13) free from r_2 by substituting $a_0^2=36(r_2-4q^2)$, $q'=\frac{q}{\sqrt{r_2}}$, $L'=\frac{L}{r_2^{3/8}}$ and $v'=\frac{\hat{v}}{r_2^{3/8}}$. The resulting equation is

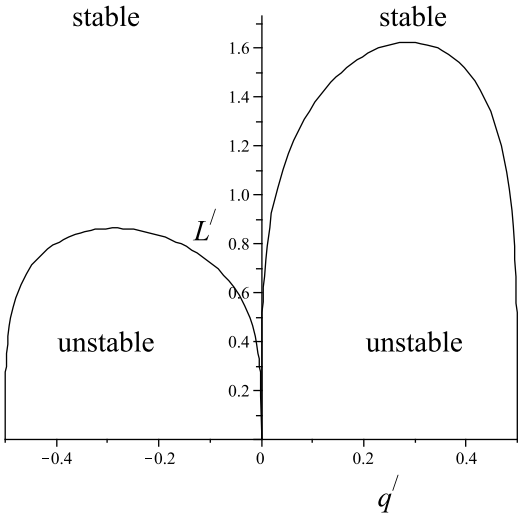

Figure 4.11: Predicted secondary stability boundaries of spatially periodic solutions of (4.11) with no dispersion. We have monotonic stability on the right and oscillatory on the left.

$$
\begin{aligned}
&- 50v'^2L'^{10} - v'^4L'^8 + 18900L'^8q' - 75600L'^8q'^3 + 124416L'^4q'^2 - 995328L'^4q'^4 \\
&+ 1990656L'^4q'^6 - 625L'^{12} - 396v'^2L'^6q' + 1584v'^2L'^6q'^3 + 324v'^2L'^2q'^2 \\
&- 2592v'^2L'^2q'^4 + 5184v'^2L'^2q'^6 + 186624q'^3 - 2239488q'^5 + 8957952q'^7 \\
&- 11943936q'^9 = 0. \qquad (4.14)
\end{aligned}
$$

Figures 4.11 and 4.12 illustrate the stability boundaries of travelling waves according to (4.14) with $v' = 0$ and $v' = 5$, respectively. The single curve in figure 4.11 ($0 < q < \frac{\sqrt{r_2}}{2}$) gives a single curve for $v' \neq 0$ in figure 4.12. On the other hand, the Hopf curve ($\sigma = \pm i\Omega$) for $v' = 0$ and $-\frac{\sqrt{r_2}}{2} < q < 0$ splits into two curves when $v' \neq 0$. Moreover, as v' increases, the gap between these two curves increases likewise. The lower of these two curves is not relevant for determining the stability boundary because as it is crossed, only one of the three eigenvalues (real part) changes its sign; it is only by crossing the upper curve that the solution gains stability.

The stability analysis of intermediate dispersion shows that all rolls are unstable provided that $a_0^2 q$ is not small. This means that if q or a_0^2 are small, then the scaling used here is no longer valid. This motivates two separate investigations for small q and a_0^2, which will be done in the next section.

4.6 Weak dispersion: $\alpha, \beta = O(\epsilon)$

In the next two subsections, the two cases $|q| \ll 1$ and $|a_0^2| \ll 1$ will be investigated. The first case represents the region particularly close to the critical wavenumber $k = 1$ and the

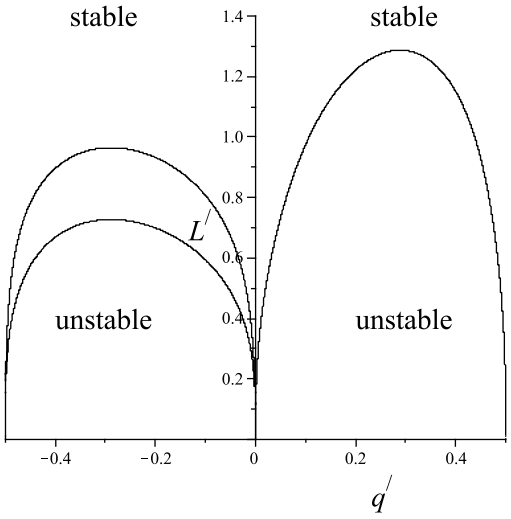

Figure 4.12: Same as figure 4.11 but with dispersion ($v' = 5$). The left hand side of the stability boundaries of (4.11) splits into two and the region below the upper boundary is unstable. Thus the lower curve is not relevant in determining the stability of travelling waves; it is shown here for completeness.

second is the region particularly close to the marginal stability curve.

4.6.1 Close to the critical wavenumber $k = 1$

As has already been emphasised, the analysis in the previous section breaks down in the limit $q \to 0$, where the wavenumber of the rolls is $1 + \epsilon q$. So in this subsection we seek to address the question of the stability of rolls with k even closer to 1, $k = 1 + \epsilon^2 q$. Then the distinguished balance occurs for smaller values of α and β, namely $\alpha = \epsilon\hat{\alpha}$ and $\beta = \epsilon\hat{\beta}$.

Upon setting $\hat{c} = \hat{\alpha} - \hat{\beta}$, $r = \epsilon^2 r_2$, $\hat{v} = 3\hat{\alpha} - 5\hat{\beta}$, $X = \epsilon x$, $T = \epsilon^2 t$ and $\tau = \epsilon t$ (same scaling employed by [14, 72] in the non-dispersive case) and also applying a weakly nonlinear analysis on (4.1), we have

$$u = \epsilon[6\sqrt{r_2} + \epsilon^2 a(X,T)]e^{\mathrm{i}M} + c.c. + \epsilon^3 f(X,T) + \cdots,$$

for $M = (1 + \epsilon^2 q)x + \epsilon\psi(X,T) - \hat{c}\tau + \epsilon(-\hat{v}q + \frac{r_2}{6}(\hat{\alpha} - 5\hat{\beta}))T$. The extra terms involving $\hat{\alpha}$ and $\hat{\beta}$ correspond to nonlinear effects of the finite roll amplitude on the speed of the rolls, which also arise from (4.7).

Finally, the amplitude equations are achieved at $O(\epsilon^4)$ and $O(\epsilon^5)$ by applying solvability conditions as follows:

$$\begin{aligned}
\frac{\partial\psi}{\partial T} &= 4\frac{\partial^2\psi}{\partial X^2} - f - \hat{v}\frac{\partial\psi}{\partial X},\\
\frac{\partial f}{\partial T} &= \frac{\partial^2 f}{\partial X^2} - 12r_2^{1/2}\frac{\partial a}{\partial X},\\
\frac{\partial a}{\partial T} &= 4\frac{\partial^2 a}{\partial X^2} - 24r_2^{1/2}\left(\frac{\partial\psi}{\partial X}\right)^2 - \hat{v}\frac{\partial a}{\partial X} - 6r_2^{1/2}\frac{\partial f}{\partial X} - 2r_2 a\\
&\quad +6r_2^{1/2}\left(-8q + \frac{22}{3}r_2 + 12\frac{\partial^2}{\partial X^2} + (10\hat{\beta} - 3\hat{\alpha})\frac{\partial}{\partial X}\right)\frac{\partial\psi}{\partial X}.
\end{aligned}$$

Unlike the previous case (in §4.5), in the third equation $\hat{\alpha}$ and $\hat{\beta}$ appear not only through the rescaled group velocity term $\hat{v}$, but also through the term $10\hat{\beta} - 3\hat{\alpha}$.

Combining these amplitude equations yields the phase equation

$$\begin{aligned}
&\left(\frac{\partial}{\partial T} - 4\frac{\partial^2}{\partial X^2} + \hat{v}\frac{\partial}{\partial X} + 2r_2\right)\left(\frac{\partial}{\partial T} - 4\frac{\partial^2}{\partial X^2} + \hat{v}\frac{\partial}{\partial X}\right)\left(\frac{\partial}{\partial T} - \frac{\partial^2}{\partial X^2}\right)\psi =\\
&-576r_2\frac{\partial\psi}{\partial X}\frac{\partial^2\psi}{\partial X^2} + 72r_2\left(\frac{22}{3}r_2 - 8q + 8\frac{\partial^2}{\partial X^2} + \frac{\partial}{\partial T} + 5\hat{\beta}\frac{\partial}{\partial X}\right)\frac{\partial^2\psi}{\partial X^2}. \qquad (4.15)
\end{aligned}$$

To answer the stability question, the previous equation is linearised and solutions proportional to $e^{\mathrm{i}LX+\sigma T}$ are found, which implies the dispersion relation

$$\begin{aligned}
&\sigma^3 + 9\sigma^2L^2 + 24\sigma L^4 + 16L^6 + 528r_2^2L^2 - 576r_2qL^2 + 82r_2\sigma L^2 - 568r_2L^4 + 2r_2\sigma^2 - \hat{v}^2\sigma L^2\\
&- L^4\hat{v}^2 + \mathrm{i}(2r_2\hat{v}\sigma L + 360r_2\hat{\beta}L^3 + 8\hat{v}L^5 + 10\hat{v}\sigma L^3 + 2\hat{v}\sigma^2 L + 2r_2\hat{v}L^3) = 0. \qquad (4.16)
\end{aligned}$$

In analysing (4.16), first large L is considered which gives the same result as in §4.5 where all eigenvalues have a negative real part. On the other hand, if L is small, we choose $\sigma = \sigma_1 L + \sigma_2 L^2 + \cdots$. Then substituting in (4.16) and equating the coefficients of L^2 and L^3, gives

$$\begin{aligned}
r_2\sigma_1^2 - 288r_2q + 264r_2^2 + \mathrm{i}r_2\hat{v}\sigma_1 &= 0,\\
\sigma_1^3 + 82r_2\sigma_1 + 4r_2\sigma_1\sigma_2 + 2\mathrm{i}r_2\hat{v}\sigma_2 + 2\mathrm{i}\hat{v}\sigma_1^2 - \hat{v}^2\sigma_1 + 2\mathrm{i}r_2\hat{v} + 360\mathrm{i}r_2\hat{\beta} &= 0.
\end{aligned}$$

Correspondingly, we obtain

$$\sigma_1 = \frac{1}{2}\left(-\mathrm{i}\hat{v} \pm \sqrt{-\hat{v}^2 + 1152q - 1056r_2}\right), \qquad (4.17)$$

$$\sigma_2 = \pm\frac{\frac{-72}{r_2}\mathrm{i}\hat{v}q + \frac{171}{2}\mathrm{i}\hat{v} - 180\mathrm{i}\hat{\beta}}{\sqrt{-\hat{v}^2 + 1152q - 1056r_2}} + \frac{91}{2} - \frac{72}{r_2}q. \qquad (4.18)$$

For the case of no dispersion, we have monotonic instability if $q \geq \frac{11}{12}r_2$. If $q < \frac{11}{12}r_2$, then σ_1 is purely imaginary in this case and thus σ_2 is the only applicable condition for stability. Thus if $q \leq \frac{91}{144}r_2$ rolls are unstable to an oscillatory instability. Figure 4.13 captures the stability boundaries of (4.15); and this recovers the result obtained by Tribelsky and Velarde [72].

To find the criterion for stability of (4.15) with dispersion, σ_1 is considered which shows that travelling wave solutions are unstable as long as $q \geq \frac{11}{12}r_2 + \frac{\hat{v}^2}{1152}$. The $\frac{\hat{v}^2}{1152}$ term indicates

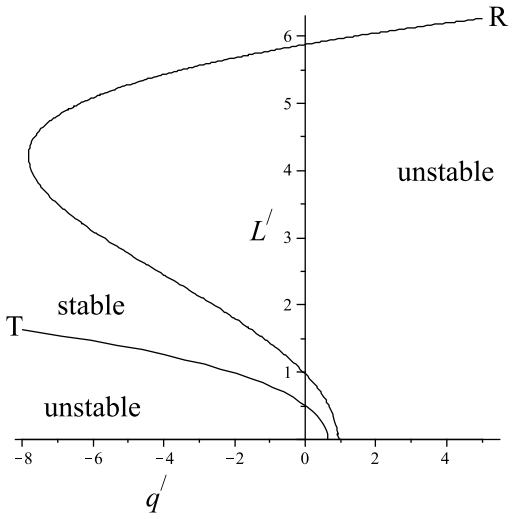

Figure 4.13: The stability boundaries of (4.15) for no dispersion, where the right hand side curve R is the monotonic instability and the left hand side curve T is the oscillatory instability. Also $q' = \frac{q}{r_2}$ and $L' = \frac{L}{\sqrt{r_2}}$.

that these rolls are stabilised towards the oscillatory instability by the presence of dispersion. Otherwise if $q < \frac{11}{12}r_2 + \frac{\hat{v}^2}{1152}$, then σ_1 is purely imaginary, and stability is determined by σ_2 given by (4.18); and in this case we have

$$\sigma_2 = \pm\frac{\frac{-72}{r_2}\hat{v}q + \frac{171}{2}\hat{v} - 180\hat{\beta}}{\sqrt{\hat{v}^2 - 1152q + 1056r_2}} + \frac{91}{2} - \frac{72}{r_2}q, \tag{4.19}$$

a consideration of which shows that these rolls are made more unstable to the long-wavelength oscillatory instability in the presence of dispersion.

Now we consider general values for L and find the oscillatory instability boundary, so we put $\sigma = \mathrm{i}\Omega$ in (4.16). Comparing the real and imaginary parts yields

$$\begin{aligned}
\Omega^3 - 82r_2\Omega L^2 - 24\Omega L^4 - 2r_2\hat{v}L^3 + 2\hat{v}\Omega^2 L + \hat{v}^2\Omega L^2 - 8\hat{v}L^5 - 360r_2\hat{\beta}L^3 &= 0,\\
9L^2\Omega^2 + 2r_2\Omega^2 - 16L^6 - 528r_2^2L^2 + 576r_2qL^2 + 568r_2L^4 + L^4\hat{v}^2 + 10\hat{v}\Omega L^3 + 2r_2\hat{v}L\Omega &= 0.
\end{aligned}$$

Combining these two equations gives

$$\begin{aligned}
&(-439200L^{10}r_2 - 8109542L^8r_2^2 - 21513415L^6r_2^3 + 45409950L^4r_2^4 - 18616052r_2^5L^2\\
&- 9303840r_2^5q + 13022208q^2r_2^4 - 437400r_2^4L^2\hat{\beta}^2 + 50922720r_2^4L^2q - 604800L^8qr_2\\
&- 13058496L^6qr_2^2 - 54473544L^4r_2^3q + 20000L^{12} - 3981312q^2r_2^2L^4 - 33965568q^2r_2^3L^2\\
&+ 2186184r_2^6 - 32400r_2^5\hat{\beta}^2 - 1968300L^4\hat{\beta}^2r_2^3 - 2952450r_2^2L^6\hat{\beta}^2 - 5971968r_2^3q^3)\\
&+ 45(9L^2 + 2r_2)r_2\hat{\beta}(342r_2^3 + 1259r_2^2L^2 - 288qr_2^2 - 864qr_2L^2 + 1004L^4r_2 + 240L^6)\hat{v}\\
&+ (19088L^8r_2 - 41094r_2^4L^2 - 11229r_2^3L^4 + 53280L^4r_2^2q + 12672L^6qr_2 + 60408r_2^3L^2q\\
&+ 5760r_2^4q + 1600L^{10} - 10368r_2^2L^2q^2 - 5240r_2^5 + 43850L^6r_2^2)\hat{v}^2\\
&- 45r_2\hat{\beta}L^2(r_2 + 4L^2)^2\hat{v}^3 + 2L^2(5r_2 + L^2)(r_2 + 4L^2)^2\hat{v}^4 = 0.
\end{aligned}$$

We eliminate r_2 from this equation by setting $q' = \frac{q}{r_2}$, $L' = \frac{L}{\sqrt{r_2}}$, $\alpha' = \frac{\hat{\alpha}}{\sqrt{r_2}}$, $\beta' = \frac{\hat{\beta}}{\sqrt{r_2}}$ and $v' = \frac{\hat{v}}{\sqrt{r_2}}$, which is more convenient for the subsequent analysis. This implies

$$
\begin{aligned}
&(-439200L'^{10} - 8109542L'^{8} - 21513415L'^{6} + 45409950L'^{4} - 18616052L'^{2} \\
&- 9303840q' + 13022208q'^{2} - 437400L'^{2}\beta'^{2} + 50922720L'^{2}q' - 604800L'^{8}q' \\
&- 13058496L'^{6}q' - 54473544L'^{4}q' + 20000L'^{12} - 3981312q'^{2}L'^{4} - 33965568q'^{2}L'^{2} \\
&+ 2186184 - 32400\beta'^{2} - 1968300L'^{4}\beta'^{2} - 2952450L'^{6}\beta'^{2} - 5971968q'^{3}) \\
&+ 45(9L'^{2} + 2)\beta'(342 + 1259L'^{2} - 288q' - 864q'L'^{2} + 1004L'^{4} + 240L'^{6})v' \\
&+ (19088L'^{8} - 41094L'^{2} - 11229L'^{4} + 53280L'^{4}q' + 12672L'^{6}q' + 60408L'^{2}q' + 5760q' \\
&+ 1600L'^{10} - 10368L'^{2}q'^{2} - 5240 + 43850L'^{6})v'^{2} \\
&- 45\beta'L'^{2}(1 + 4L'^{2})^{2}v'^{3} + 2L'^{2}(5 + L'^{2})(1 + 4L'^{2})^{2}v'^{4} = 0.
\end{aligned}
$$

Proceeding with the stability analysis for general-L' disturbances is rather intricate and therefore instead we consider special cases. First, we assume that $\beta' = 0$ and draw the stability boundaries in the (q', L') plane for different values of α' as displayed in figure 4.14. In order to understand the change in the stability boundaries as α' becomes large, we begin by investigating small α' (hence small v') in the $L' = 0$ limit. We already know from the aforementioned analysis, in particular (4.17), that the right-hand stability curve (labelled R) intersects the q'-axis at $q'_+ = \frac{11}{12} + \frac{v'^2}{1152}$. In addition, for small v' and from (4.19) the left-hand stability curves intersect the q'-axis at $\frac{91}{144} \pm \frac{5v'}{18\sqrt{82}} + O(v'^2)$. This shows that near the point $(\frac{91}{144}, 0)$ the left stability boundary T in figure 4.13 splits into two curves (see figure 4.14) and each moves in the opposite direction an amount proportional to α'. We shall label the furthest right of these curves, which intersects the q'-axis at $q'_- \sim \frac{91}{144} + \frac{5|v'|}{18\sqrt{82}}$, by T and ignore the far left curve (see figure 4.14). This is because by crossing the latter only one real part of the eigenvalues changes its sign and hence it does not affect the stability. With the increase in α', q'_- moves to the right more rapidly than q'_+. Eventually, for sufficiently large α', $q'_- = q'_+$ and thus all rolls become unstable in the limit $L' = 0$. On the other hand, if α' is large, $\sigma_2 \approx \pm(-72q' + \frac{171}{2}) + \frac{91}{2} - 72q'$ and hence q'_- halts at $\frac{131}{144}$. However, q'_+ continues to move to the right and this results in the appearance of a stability region in the limit $L' = 0$. In fact, for sufficiently large α', some rolls are stable to disturbances for all L'.

Figure 4.14 illustrates the stability boundaries for different values of α' with $\beta' = 0$. In this figure, when α' becomes large the right stability curve R moves to the right. Then at the value $\alpha'_c \approx 5.7$ a stable region appears (see figure 4.14(f)). Afterwards, for any value of α' greater than 5.7 the stable region becomes clearer. Therefore, the critical value above which stable rolls exist is $\alpha'_c \approx 5.7$. Since $\alpha = \alpha'\sqrt{r}$, then the stability condition reads $r < (\alpha/\alpha'_c)^2$. If we apply this result to $\alpha = 1/2$ and $\beta = 0$, we obtain stability of rolls for $r < 0.0077$. This

exhibits remarkably good agreement with the secondary stability plot given in figure 4.2(a), where the stable region is delimited from above by $r \approx 0.0078$.

If instead we set $\alpha' = 0$, a broadly similar result to the previous case is discovered, as shown in figure 4.15. It illustrates that for small β' there are no stable rolls and then they are stabilised for sufficiently large β'. As can be seen in figure 4.15, the two curves R and T intersect the q'-axis and then coalesce. Afterwards, they both lift off from the q'-axis as we increase β' and then reattach to the q'-axis when $\beta'_c \approx 5.0607$ as exhibited in figure 4.15(h). Therefore, $\beta' > 5.0607$ will result in the appearance of a stable region.

After calculating the critical values of dispersion for stability, in what follows we shall consider another special case. This case involves setting $\hat{\alpha} = 1$ and $\hat{\beta} = 0$ ($\alpha = \epsilon\hat{\alpha}$ and $\beta = \epsilon\hat{\beta}$) with small-$L$ disturbances. Then the stability of travelling wave solutions will be examined as r_2 is varied ($r = \epsilon^2 r_2$). This will be done in order to compare the analytical result with some of the secondary stability plots found in §4.3. It follows from (4.17) that rolls are unstable if $q \geq \frac{11}{12}r_2 + \frac{\hat{v}^2}{1152}$. If $q < \frac{11}{12}r_2 + \frac{\hat{v}^2}{1152}$, then σ_1 is purely imaginary and hence σ_2 must be considered. As far as (4.19) is concerned, if $q \leq 0$, then there is at least one positive value for σ_2; and hence instability. Similarly, taking $r_2 \geq \frac{144}{91}q$ gives instability. In addition to the previous conditions, the sign of σ_2 must be inspected to answer the stability question for rolls. Figure 4.16(a) illustrates the following graphs $q = \frac{11}{12}r_2 + \frac{\hat{v}^2}{1152}$ (solid line), $q = 0$, $q = \frac{91}{144}r_2$ (dashed line) and $\sigma_2 = 0$ (dotted lines). The areas under the solid line and above the dashed line are unstable (see figure 4.16(a)). Moreover, crossing the line $q = 0$ does not change the sign of the eigenvalues of σ and hence does not affect the stability. Therefore, it is apparent that the stable region lies between the dashed and solid lines. To find precisely this region, a small value for r_2 is fixed and the two graphs of σ_2 are plotted against q. It is found that the sign of the eigenvalues of σ_2 is negative for the range of q lying between the dotted lines in the upper and lower parts of the graph and between the dotted and the solid lines for a small range of intermediate values of r_2. For example, if $r_2 = 0.01$, figure 4.17 shows that both values of the two roots of σ_2 are negative approximately when $0.0087 \leq q \leq 0.0158$. This lies within the area between the dotted lines in the lower part of the graph in figure 4.16(a).

Although the solid and dotted lines in figure 4.16(a) appear almost parallel, for large r_2 they are not (see figure 4.16(b)). This is because they have the slopes $\frac{11}{12}$ and approximately $\frac{91}{144}$, respectively.

The previous analysis raises the question whether the stable region for rolls is infinite or not. In other words, what happens if r_2 is large. For this we consider large r_2 with $q = O(r_2)$, because figure 4.16(a) suggests that stable rolls lie in some region around a straight line in (q, r_2) parameter space. In this limit, from σ_1, we have instability if $q > \frac{11}{12}r_2$. Also σ_2 can

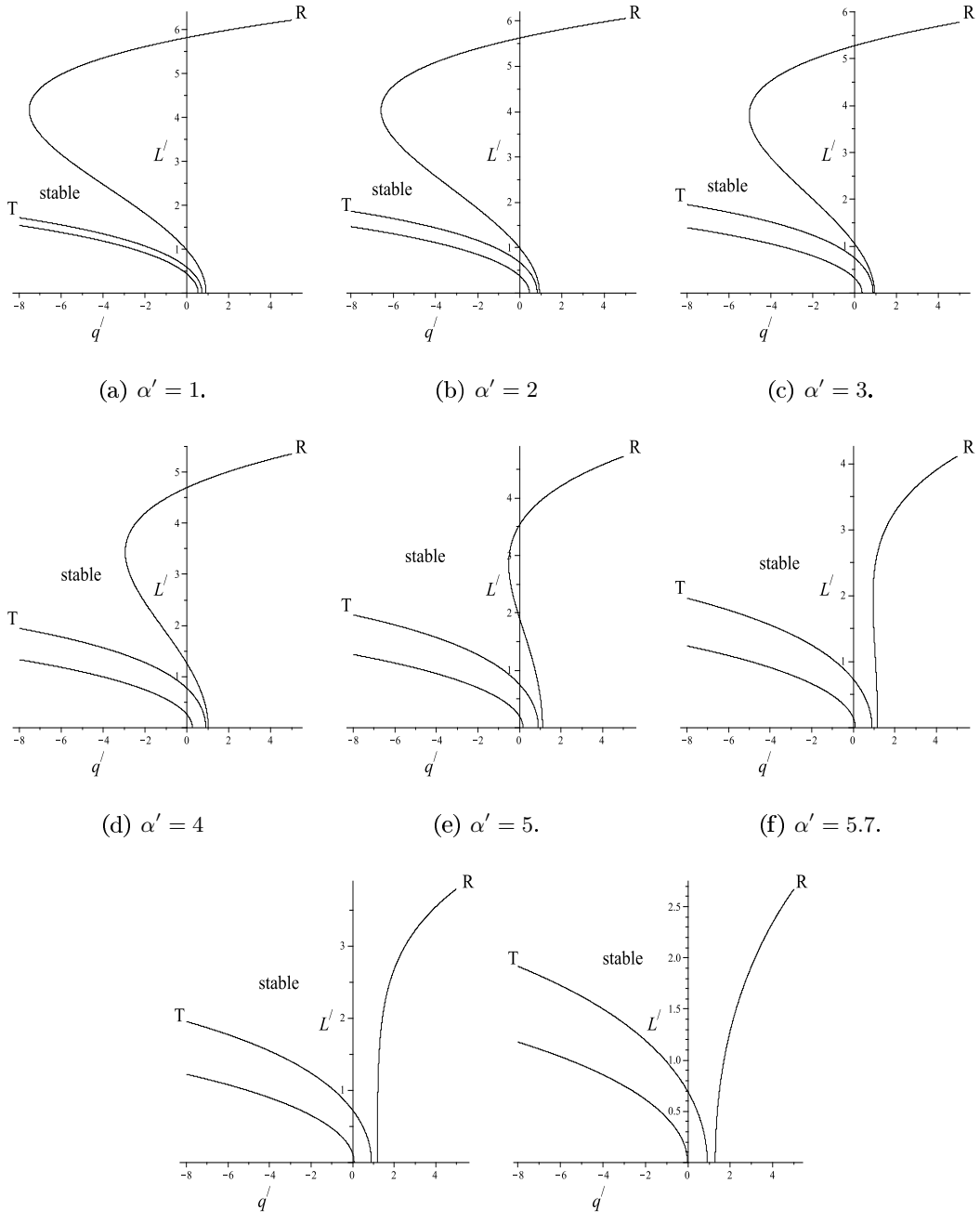

(a) $\alpha' = 1$. (b) $\alpha' = 2$ (c) $\alpha' = 3$.

(d) $\alpha' = 4$ (e) $\alpha' = 5$. (f) $\alpha' = 5.7$.

(g) $\alpha' = 6$ (h) $\alpha' = 7$.

Figure 4.14: The stability boundaries of travelling waves according to (4.15) for $\beta' = 0$ and different values for α' as shown below each figure. Note that the far left curve does not affect the stability but is included for completeness. See the text for more details.

be written as $\sigma_2 = \frac{91}{2} - \frac{72}{r_2}q + O(r_2^{-1/2})$. Thus the stability condition for large r_2 and small-L disturbances is given by

$$\frac{91}{144}r_2 < q < \frac{11}{12}r_2.$$

This implies that for small α and β ($O(\epsilon)$) there can be a narrow region of stable travelling waves in the vicinity of $k = 1$. In addition, there is no upper limit on the size of r_2, allowing

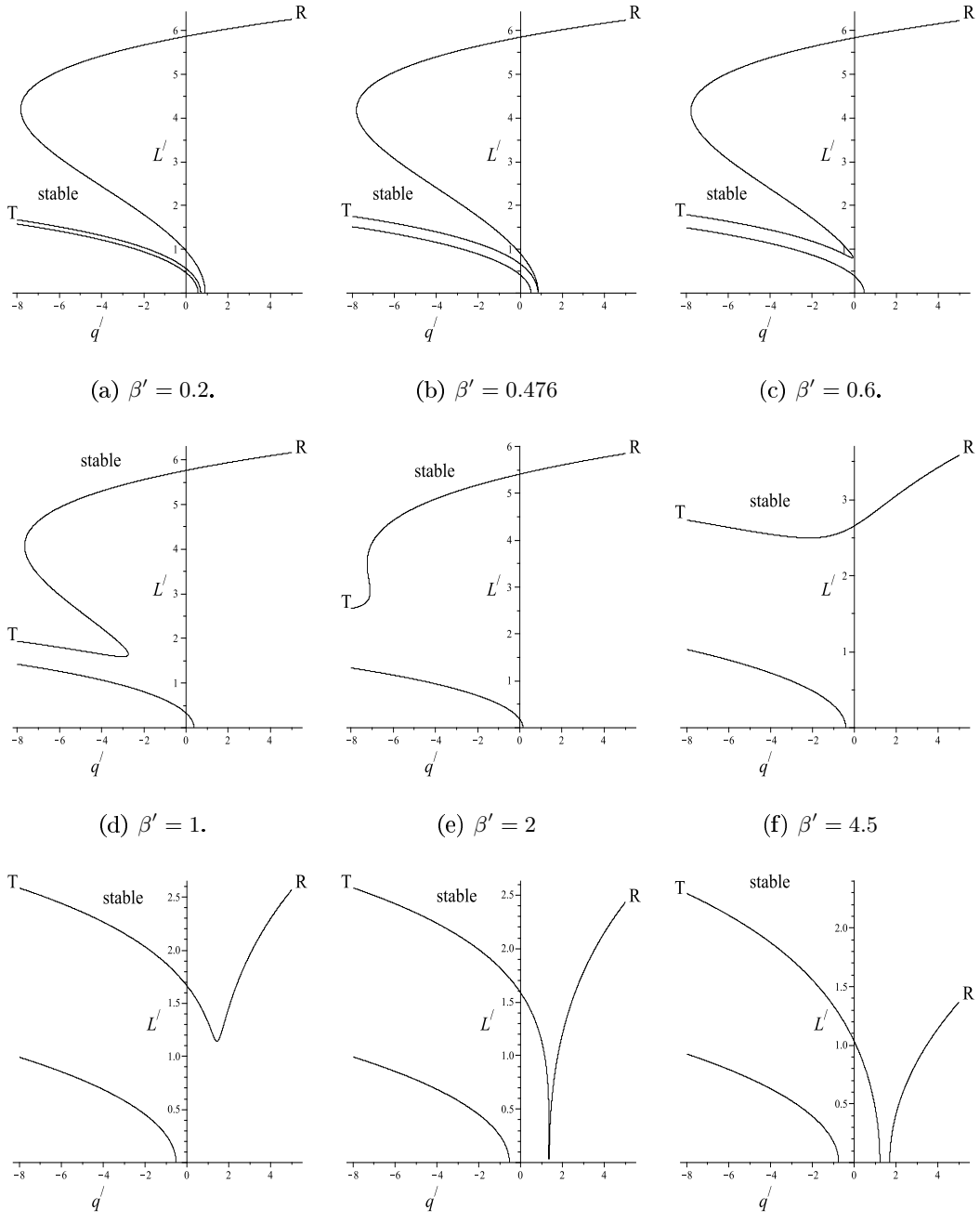

(a) $\beta' = 0.2$. (b) $\beta' = 0.476$ (c) $\beta' = 0.6$.

(d) $\beta' = 1$. (e) $\beta' = 2$ (f) $\beta' = 4.5$

(g) $\beta' = 5$. (h) $\beta' = 5.0607$. (i) $\beta' = 6$

Figure 4.15: Same as figure 4.14 but here instead $\alpha' = 0$ and the different values for β' are given below each figure.

stable rolls.

On the question of stability of travelling wave solutions, this study found that if the wavenumber is close to the critical value then stable rolls exist. To be more specific, we have considered each dispersive term separately and found that there is a critical value where the system is unstable if dispersion is less than this value. On the other hand, with dispersion above this value, rolls gain stability.

For weaker dispersion than the scaling used here, namely if α and β are of order ϵ^2,

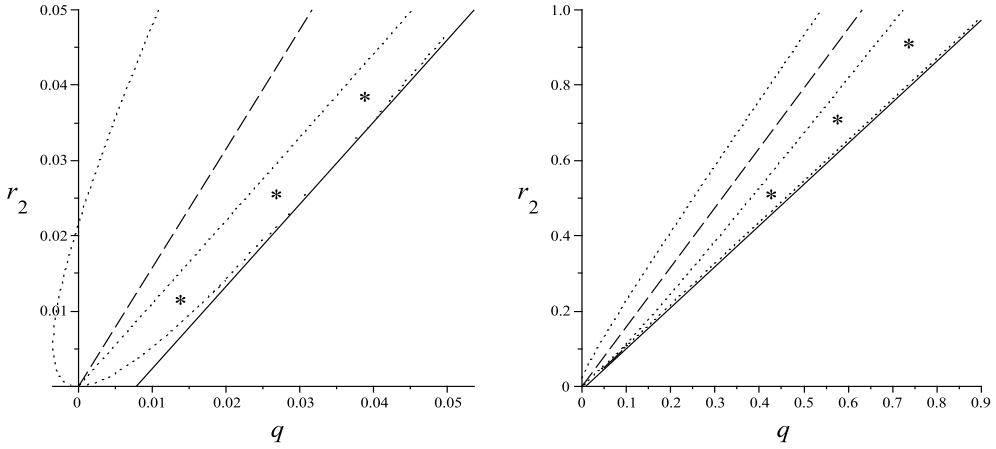

Figure 4.16: The graphs of $\sigma_2 = 0$ (dotted lines), $q = \frac{11}{12}r_2 + \frac{\hat{v}^2}{1152}$ (solid line) and $q = \frac{91}{144}r_2$ (dashed line). Travelling wave solutions are stable inside the region marked with asterisks; for details refer to the text. (b) is the same as (a) but with higher values of r_2.

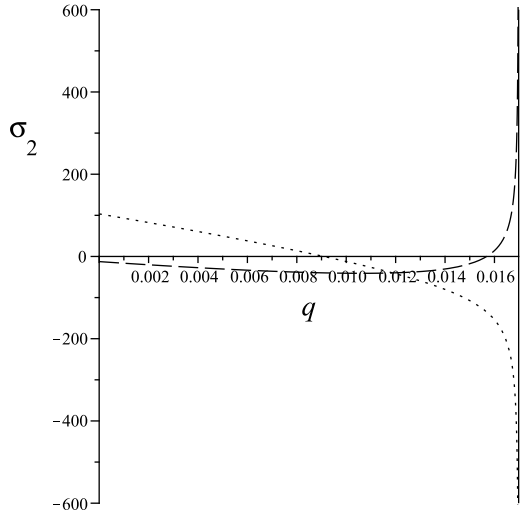

Figure 4.17: The two graphs of $\sigma_2 = 0$ (dotted and dashed lines) against q with $r_2 = 0.01$, where the solid line is the vertical asymptote of $\sigma_2 = 0$. The rolls are stable in the interval in q where both roots of σ_2 are negative.

we have calculated separately the amplitude equations and found that there is no effect of dispersion. This is because dispersive terms do not appear in the amplitude equation; and hence we have the same result as the Nikolaevskiy equation, which is that all rolls are unstable. The current findings add substantially to our understanding of the transition to the Nikolaevskiy chaos as the dispersion is reduced.

4.6.2 Close to the marginal curve

In this subsection we consider the second case in which the analysis in §4.5 breaks down: the region close to the marginal stability curve (by using the same scaling in [14] in the non-dispersive case). Correspondingly, the right and left marginal stability boundaries will be denoted by $k_m^+(\epsilon)$ and $k_m^-(\epsilon)$. For convenience, we set $r_2 = 1$, without losing generality. From substituting the expansion $k_m^\pm = k_0 + \epsilon k_1 + \epsilon^2 k_2 + \epsilon^3 k_3 + \cdots$ into the equation $k^2\left[\epsilon^2 - (1-k^2)^2\right] = 0$, we obtain $k_m^\pm = 1 \pm \frac{1}{2}\epsilon - \frac{1}{8}\epsilon^2 \pm \frac{1}{16}\epsilon^3 + \cdots$. We now choose the wavenumber $k = k_m^\pm \mp \epsilon^2\kappa$, which is very close to the marginal stability boundary.

Applying a weakly nonlinear analysis on (4.1) and using the same scaling as in §4.6.1, gives

$$u = \epsilon^{3/2}[\breve{a_0} + a(X,T)]e^{\mathrm{i}M} + c.c + \epsilon^2 f(X,T) + \cdots,$$

where $M = kx + \psi - \hat{c}\tau \mp \frac{1}{2}\hat{v}T$. The roll solution satisfies $\breve{a_0}^2 = 144\kappa$. After considerable algebra, we obtain the linear amplitude equations for perturbations to the travelling waves

$$\begin{aligned}
\frac{\partial\psi}{\partial T} &= 4\frac{\partial^2\psi}{\partial X^2} - f \pm \frac{4}{\breve{a_0}}\frac{\partial a}{\partial X} - \hat{v}\frac{\partial\psi}{\partial X},\\
\frac{\partial f}{\partial T} &= \frac{\partial^2 f}{\partial X^2} - 2\breve{a_0}\frac{\partial a}{\partial X},\\
\frac{\partial a}{\partial T} &= 4\frac{\partial^2 a}{\partial X^2} \mp 4\breve{a_0}\frac{\partial\psi}{\partial X} - \hat{v}\frac{\partial a}{\partial X}.
\end{aligned}$$

Combining these equations yields

$$\left(\frac{\partial}{\partial T} - \frac{\partial^2}{\partial X^2}\right)\left[\left(\frac{\partial}{\partial T} - 4\frac{\partial^2}{\partial X^2} + \hat{v}\frac{\partial}{\partial X}\right)^2 + 16\frac{\partial^2}{\partial X^2}\right]\psi = \mp 8\breve{a_0}^2\frac{\partial^2\psi}{\partial X^2}.$$

In addition, perturbations proportional to $\psi = \bar{\psi}e^{\mathrm{i}LX+\sigma T}$ give the dispersion relation

$$(\sigma + 4L^2 + \mathrm{i}\hat{v}L + 4L)(\sigma + 4L^2 + \mathrm{i}\hat{v}L - 4L)(\sigma + L^2) \mp 8\breve{a_0}^2L^2 = 0. \tag{4.20}$$

To approach both sides of the marginal curves, we consider the limit $\breve{a_0} \to 0$. Thus the roots of (4.20) are $-L^2 + O(\breve{a_0}^2)$ and $4L(\mp 1 - L) - i\hat{v}L + O(\breve{a_0}^2)$ and this means that all travelling waves are unstable sufficiently close to the boundary. Afterwards, we fix a nonzero value of $\breve{a_0}$ and $\hat{v}$. Then for small L we have $\sigma^3 \sim \pm 8\breve{a_0}^2L^2$, and thus to leading-order in L, $\sigma = \sigma_{2/3}L^{2/3}$ which implies $\sigma_{2/3}^3 = \pm 8\breve{a_0}^2$. This shows that these rolls are unstable for small-L disturbances. Therefore, unlike the case of the damped Nikolaevskiy equation [14], where a narrow region of stable rolls exists close to the marginal curve, near the marginal stability boundary all rolls are unstable.

4.7 Amplitude equations with dispersion

In this section we shall derive the amplitude equations which describe slow modulations in space and time of solutions of the Nikolaevskiy equation with dispersion, in particular for

weak dispersion. To derive these equations, we use a weakly nonlinear analysis and hence we set $\alpha = \epsilon\hat{\alpha}$, $\beta = \epsilon\hat{\beta}$, $\hat{c} = \hat{\alpha} - \hat{\beta}$, $\hat{v} = 3\hat{\alpha} - 5\hat{\beta}$, $X = \epsilon x$ and $T = \epsilon^2 t$ (same scaling as in weak dispersion). Therefore, by substituting in (4.1) and considering coefficients of successive powers of $O(\epsilon^{1/2})$ we get

$$u = \epsilon^{3/2} A(X,T) e^{\mathrm{i}(x-\hat{c}t)} + c.c. + \epsilon^2 f(X,T) - \epsilon^3 \frac{\mathrm{i}}{36} A^2 e^{2\mathrm{i}(x-\hat{c}t)} + c.c. + \cdots .$$

The self-consistent amplitude equations then appear from solvability conditions at $O(\epsilon^{7/4})$ and $O(\epsilon^4)$ (respectively) as follows:

$$\begin{aligned} \frac{\partial A}{\partial T} &= r_2 A + 4\frac{\partial^2 A}{\partial X^2} - \mathrm{i} f A - \hat{v}\frac{\partial A}{\partial X}, \\ \frac{\partial f}{\partial T} &= \frac{\partial^2 f}{\partial X^2} - \frac{\partial |A|^2}{\partial X}. \end{aligned}$$

By setting $\bar{T} = r_2 T$, $\bar{X} = -r_2^{1/2} X$, $\bar{f} = -f/r_2$, $\bar{A} = r_2^{-3/4} A^*$ and $\bar{v} = r_2^{-1/2}\hat{v}$ we can eliminate r_2 and obtain the same equations but with $\bar{v}$ instead of $-\hat{v}$. The latter shows that the behaviour of these amplitude equations is essentially the same for positive and negative $\bar{v}$; and thus we can restrict our attention to positive $\bar{v}$. The rescaled amplitude equations are

$$\frac{\partial A}{\partial T} = A + 4\frac{\partial^2 A}{\partial X^2} - \mathrm{i} f A + v\frac{\partial A}{\partial X}, \tag{4.21}$$

$$\frac{\partial f}{\partial T} = \frac{\partial^2 f}{\partial X^2} - \frac{\partial |A|^2}{\partial X}. \tag{4.22}$$

Note that for simplicity, we have written the variables in these new equations without the bars.

The amplitude equations (4.21) and (4.22) are the same as in [40] but with an extra advection term resulting from dispersion. In the absence of dispersion, numerical investigations have been carried out in [47, 48, 52] for different domain sizes. Moreover, we have numerically simulated these equations but with a general coefficient of the diffusion term (in the first equation) in §3.3.2. We are interested in investigating the influence of dispersion on the properties of the solution to these equations. In the next subsection we shall perform numerical calculations regarding these equations for different values of v with a fixed domain size.

4.7.1 Numerical results

This subsection is dedicated to numerically simulating (4.21) and (4.22) in a finite domain ($l = 150$) for various values of v. The numerical code is pseudo-spectral [21, 67], and employs an exponential time differencing fourth-order Runge-Kutta method for time integration [13, 30] (see appendix C). The initial conditions are $A = 0$ and $f = -10\sin(2\pi(X - l/2)/l)$ with small perturbations [52]. We have seen in §3.3.1, in the numerical simulations of the

amplitude equations with no dispersion, that there is a coexistence of an amplitude-death state and a single-front state for A and f, respectively. Moreover, these states fluctuate during the simulations due to spatiotemporal chaos [47, 48, 52]. For the amplitude equations (4.21) and (4.22), we have an extra term involving v, therefore we expect the front to move with a certain speed. Figure 4.18(a) is a numerical simulation of (4.21) and (4.22) with $v = 0.2$ demonstrating the temporal evolutions of $|A|$ and f (from top to bottom). Similarly to the case of $v = 0$, there are chaotic fluctuations. In addition, there are amplitude-death and single-front structures; however, they are drifting with some speed. We are going to compute the speed of the front for various values of v. As it is hard to calculate the speed from such figures, we shall position the front in the middle of the domain during the simulation (as in §3.3) and then calculate the speed of the front from the graph of the displacement of the front about $X = l/2$ (see figure 4.19). The plots presented in figure 4.19 are not straight lines, therefore the speed is estimated by the slope of the graph calculated from two points away from initial transients.

It is worth mentioning that it is very difficult to track the front (aligning it in the middle of the spatial domain) by using our numerical code, especially for long-time simulations. As we increase v, the speed of the front also increases; and therefore this problem becomes more severe in contrast with the case of $v = 0$. Either we lose the front in the beginning of the simulation or after a period of time as exhibited in figure 4.18(b) for $v = 0.4$. The reason why sometimes the code might not be able to track the front is that it positions the front in the middle of the domain by using the values where f is immediately above and below zero and it might confuse them with values of f very close to zero. As a result the front is no longer in the middle of the domain, as in figure 4.18(b). For larger values of v, the numerical simulation is carried out in a short time (see for example figure 4.19(j)). This is because in this case the speed of the front increases and it is difficult to position the front in the middle of the domain for a long-time simulation. Another important point is that the $max(\langle f \rangle)$ will not be calculated because we need simulations to be done for a long time in order to allow the front to settle; and again the code might not be suitable for this procedure.

We have done several numerical simulations of (4.21) and (4.22) in a domain of size 150 for different values of v ranging from 0.05 to 0.5. The plots of the displacement of the front about $X = l/2$ are given in figure 4.19. The graph of the total shifting of the front fluctuates owing to the spatiotemporal chaos of the amplitude equations in addition to the influence of the advection term involving v. We have estimated the speed of the front from these graphs (ignoring initial transients) and plotted the result in figure 4.20. As shown in the graph there is an almost linear relationship with a positive slope between the speed of the front and the value of v. Indeed, the graph is close to a straight line with slope 0.066.

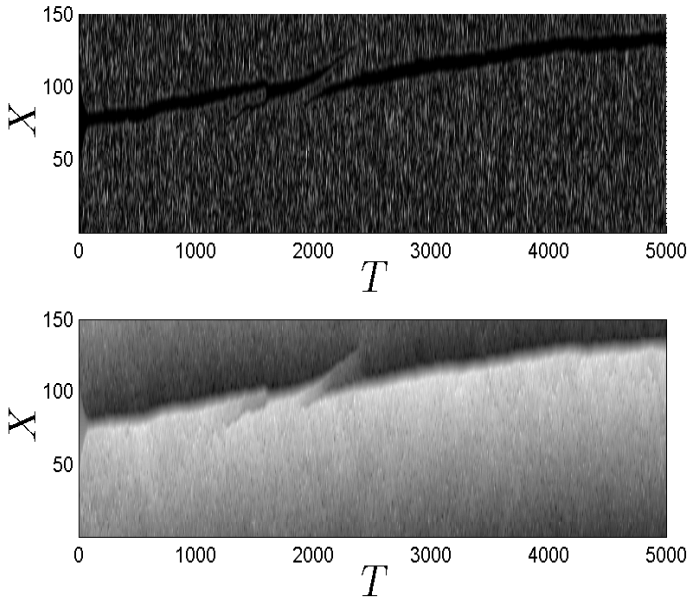

(a)

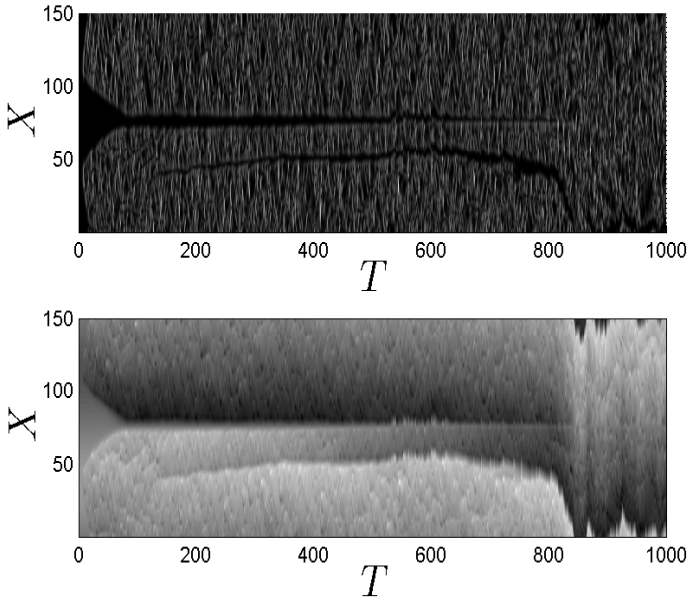

(b)

Figure 4.18: Numerical simulations of (4.21) and (4.22) exhibiting the temporal evolutions of $|A|$ and f (from top to bottom) in grey scale plots with (a) $v = 0.2$ and (b) $v = 0.4$. (a) is an example of a numerical simulation without tracking the front, while in (b) the front is positioned in the middle of the domain. However, after a while the front is no longer in the centre of the domain, due to a breakdown of our simple front-tracking algorithm.

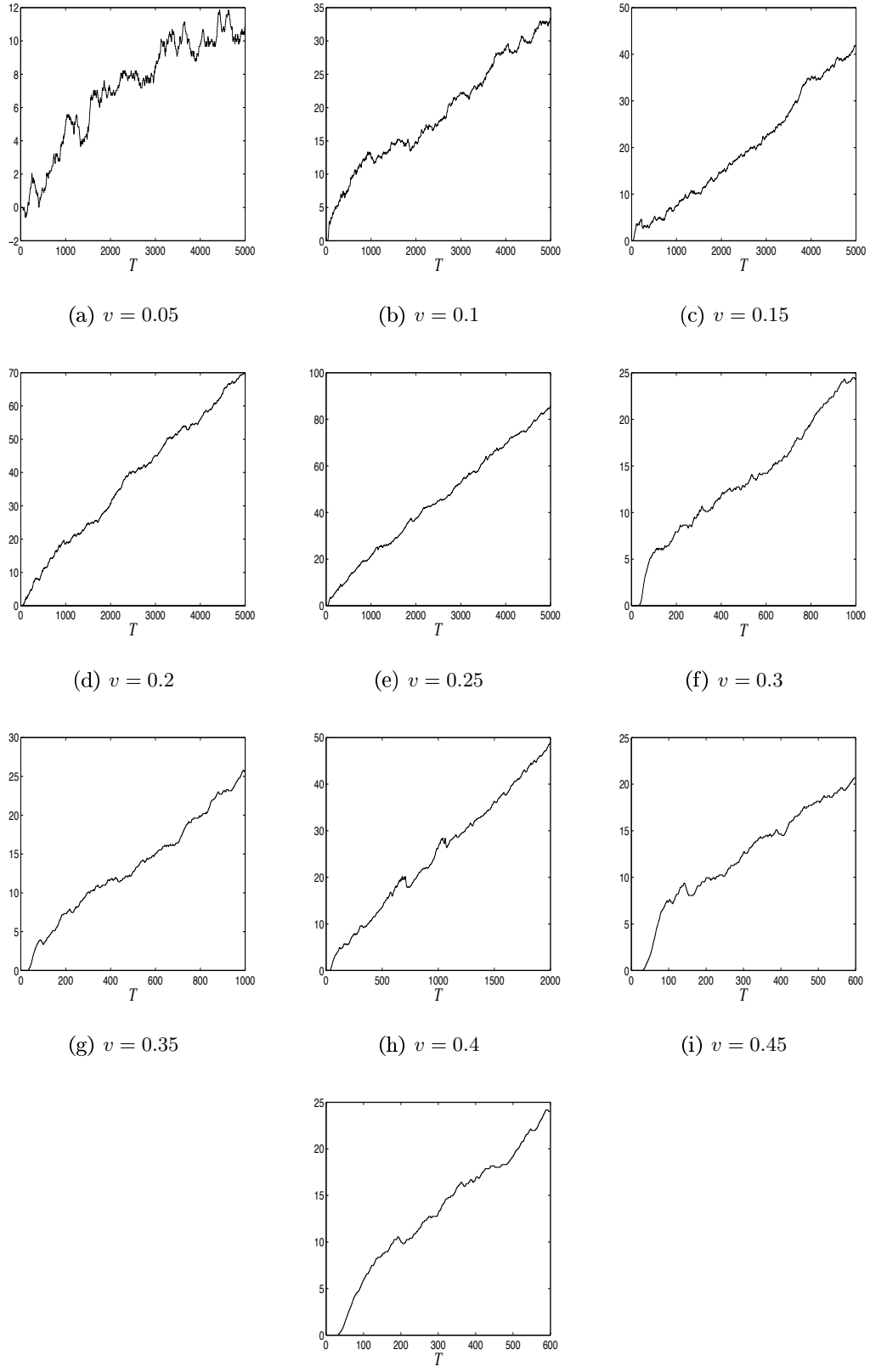

(a) $v = 0.05$ (b) $v = 0.1$ (c) $v = 0.15$

(d) $v = 0.2$ (e) $v = 0.25$ (f) $v = 0.3$

(g) $v = 0.35$ (h) $v = 0.4$ (i) $v = 0.45$

(j) $v = 0.5$

Figure 4.19: The front displacement about $X = l/2$ during the simulations of (4.21) and (4.22), where $l = 150$ and for different values of v as indicated under each graph.

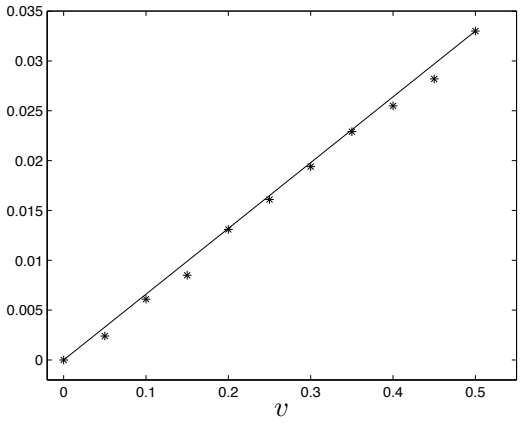

Figure 4.20: The asterisks stand for the speed of the front of f, calculated from figure 4.19, against different values of v for $l = 150$. The solid line has the slope 0.066.

In conclusion, the amplitude equations of the dispersive Nikolaevskiy equation exhibit a similar behaviour to the non-dispersive equation, where there are amplitude-death and single-front states. However, these fronts drift with a certain speed depending on the value of v. We have estimated the speed of the front for different values of v through numerical simulations in a fixed domain size. The result of these calculations indicates that there is an almost linear relationship between the front speed and v.

4.8 Numerical simulations

After analysing the dispersive Nikolaevskiy equation, for three degrees of dispersion in §4.4, §4.5 and §4.6, we now carry out numerical simulations to validate these asymptotic results. The simulations were developed using a pseudo-spectral method [21, 67] with a second-order exponential time differencing [13] for the time derivative (the *Matlab* code is given in appendix B). The initial condition is a travelling wave with wavenumber k plus small random noise and domain size $\frac{100\pi}{k}$. In particular, the initial data for strong dispersion are given by

$$u(x_0) = 2\epsilon \left[(r_2 - 4q^2)\left(36 + (\alpha - 5\beta)^2\right)\right]^{1/2} \cos(kx) \equiv b_0 \cos(kx),$$

plus small random noise. Here the amplitude is taken from (4.8). For the intermediate dispersion: $b_0 = 12\epsilon\sqrt{r_2 - 4q^2}$, and finally for the weak dispersion we have $b_0 = 12\epsilon\sqrt{r_2}$.

Figure 4.21 illustrates in order (a) strong, (b) intermediate and (c)–(e) weak dispersion. The values of α, β, r and k are chosen in the simulations to correspond to travelling waves predicted to be unstable according to the asymptotic analysis. For the sake of comparison with the analytical results we assume that $r = \epsilon^2 r_2$, where $r_2 = 1$ unless otherwise stated.

Figure 4.21(a) demonstrates the case of strong dispersion, where $\alpha = 2$ and $\beta = 1$ are

chosen with wavenumber $k = 1$ and $r = 0.01$. The stability analysis of (4.9) predicts that the rolls are unstable, since $\alpha = 2$ and $\beta = 1$ lie in the unstable region in figure 4.8. The numerical simulation agrees with this asymptotic result.

In figure 4.21(b) an example of intermediate dispersion is simulated, where $\alpha = 2\epsilon^{3/4}$ and $\beta = \epsilon^{3/4}$, $r = \epsilon^2$ and $k = 1 + \epsilon q$ for $q = 0.2$ and $\epsilon = 0.1$. It is known from the asymptotic result in §4.5 that α and β being $O(\epsilon^{3/4})$ with wavenumber $k = 1 + \epsilon q$ will result in unstable travelling wave solutions. This agrees with the simulations shown in figure 4.21(b).

Regarding weak dispersion with wavenumber $k = 1 + \epsilon^2 q$, the effect of only one dispersive term has been studied in §4.6. In figures 4.21(c) and (d) we simulate rolls with parameter values taken from this analysis with $r = 0.01$ and $\epsilon = 0.1$. In particular, in figure 4.21(c) we choose $\alpha = 2\epsilon$, $\beta = 0$ and $q = 0.87$ and this results in unstable rolls as shown in the simulation. Similarly, in figure 4.21(d), we have $\alpha = 0$, $\beta = 5\epsilon$ and $q = 2.5$ which also produce unstable rolls in the simulation. These two simulations support the predictions given in §4.6, since the parameter values of these two simulations are chosen from the unstable region in figures 4.14(b) and 4.15(g), respectively.

Figure 4.21(e) represents weak dispersion with fixed values of dispersion, namely $\alpha = \epsilon$ and $\beta = 0$. The wavenumber is $k = 1 + \epsilon^2 q$ and $r = \epsilon^2 r_2$, where $\epsilon = 0.25$, $q = 0.02$ and $r_2 = 0.04$. These values of r_2 and q lie in the unstable region given in figure 4.16(a), and this is confirmed by the numerical result in figure 4.21(e).

The finding to emerge from this section is that the stability analysis agrees with the numerical computations. We have performed several numerical simulations with parameter values taken from the stability analysis of three degrees of dispersion. Indeed, the parameter values correspond to rolls predicted to be unstable in the asymptotics; and the simulations exhibit consistency with this analysis.

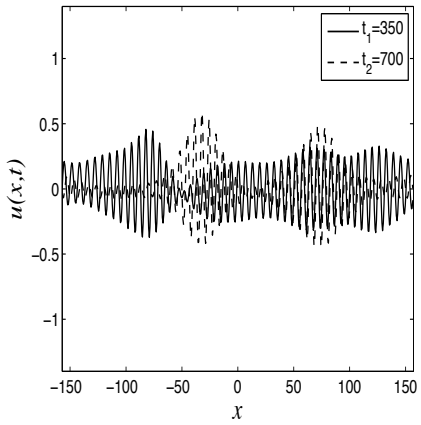

(a) $\alpha = 2$, $\beta = 1$, $r = 0.01$ and $k = 1$.

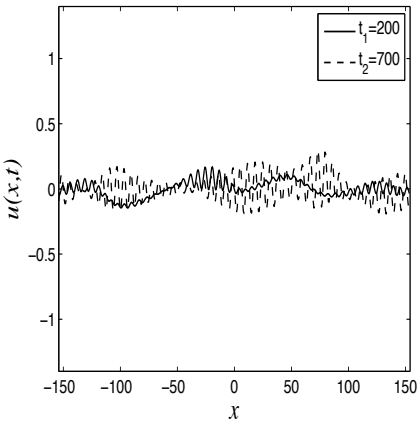

(b) $\alpha = 0.3557$, $\beta = 0.1778$, $r = 0.01$ and $k = 1.02$.

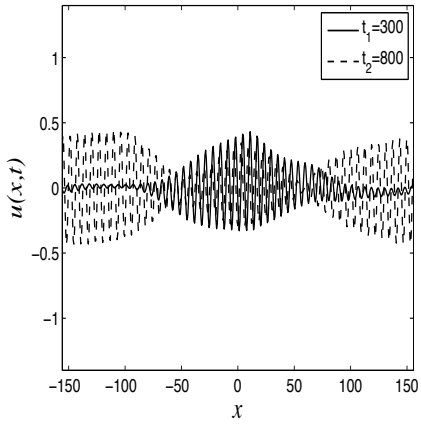

(c) $\alpha = 0.2$, $\beta = 0$, $r = 0.01$ and $k = 1.0087$.

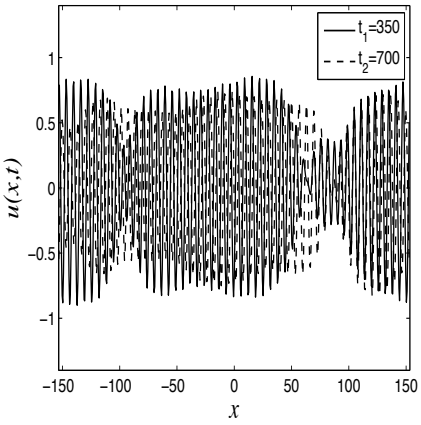

(d) $\alpha = 0$, $\beta = 0.5$, $r = 0.01$ and $k = 1.025$.

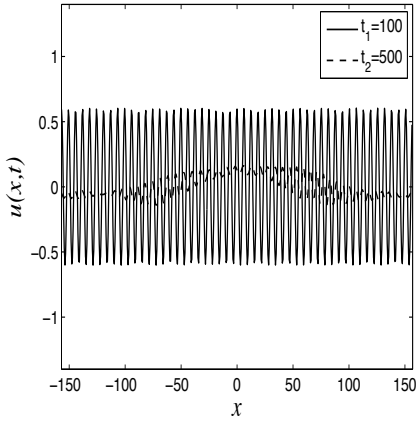

(e) $\alpha = 0.25$, $\beta = 0$, $r = 0.0025$ and $k = 1.00125$.

Figure 4.21: Snap shots of the numerical simulations of (4.1) with parameter values as indicated under each graph corresponding to (a) strong, (b) intermediate and (c)–(e) weak dispersion. The snap shots are taken at two different times as given in the insets.

4.9 Discussion

In this chapter we examined the stability of travelling wave solutions to the dispersive Nikolaevskiy equation. We found that dispersion stabilises the spatially periodic solutions at onset of pattern formation. This result was achieved by calculating the secondary stability plots numerically and by an asymptotic treatment of three particular scalings in ϵ for the dispersion coefficients. For weaker dispersion than these scalings, namely if α and β are of order ϵ^2, dispersion does not have any effect on the stability of waves. This is because after applying a weakly nonlinear analysis on (4.1), we found that dispersion does not appear in the leading-order amplitude equations. In this case (4.1) possesses the same property as the non-dispersive Nikolaevskiy equation, which is that all travelling wave solutions are unstable.

In the case of strong dispersion ($\alpha, \beta = O(1)$), the result relates to the numerical stability plots found in the (k, r) plane if r is small and α and β are fixed. Accordingly, we have two circumstances: either all rolls are unstable at the bottom of the diagram, or there is an Eckhaus-like symmetrical region of stability for small values of r. The ratio of the width of this stable region to the width of the existence region of rolls is different from the usual Eckhaus case.

In the other case of weak dispersion, the analytical result can be interpreted as giving information about the upper part of the stability diagrams in the (k, r) plane for fixed α and β. It was concluded that there can be a narrow region of stability near wavenumber $k = 1$.

The asymptotic results provide some information about the secondary stability plots. However, the numerical results revealed the complicated nature of these plots, highly dependent on the degree of dispersion, which cannot be fully explained by the asymptotics. This is because in the numerical calculations, finite-wavelength instabilities may be present, in contrast to the analytical methods where only long-wavelength instabilities are included.

The dispersive amplitude equations show similar behaviour to the non-dispersive equations. This behaviour is manifested through the coexistence of amplitude-death and single-front structures; however, dispersion makes the fronts drift with a certain speed. We concluded from numerical simulations that there is a linear relation between this speed and the group velocity.

Finally, the numerical simulation of the dispersive Nikolaevskiy equation with waves predicted to be unstable in the analytical results revealed the spatiotemporal chaotic state of the solution. This behaviour is similar to that found in the non-dispersive Nikolaevskiy equation [32, 40, 71].

Chapter 5

Other Nikolaevskiy-like systems

5.1 Introduction

In this chapter we introduce a system of coupled partial differential equations similar to the Nikolaevskiy equation, and with the same symmetries. This system, which consists of modified Swift-Hohenberg and Burgers' equations, again describes the interaction of finite-wavelength and large-scale modes. We want to discover whether the solution of this system will have the same qualitative behaviour as the Nikolaevskiy equation. We are interested in investigating what features of the solution of the Nikolaevskiy equation will follow from the symmetries. We already expect the symmetries to lead to a generalised form of the amplitude equations in [40].

The coupled system we are going to study, which has certain properties given later, is

$$\frac{\partial w}{\partial t} + u\frac{\partial w}{\partial x} = \left[r - \left(1 + \frac{\partial^2}{\partial x^2}\right)^2\right] w - sw^2 - w^3, \tag{5.1}$$

$$\frac{\partial u}{\partial t} + u\frac{\partial u}{\partial x} = \sigma\frac{\partial^2 u}{\partial x^2} + bw\frac{\partial w}{\partial x}. \tag{5.2}$$

Here $x \in [0, l]$ with periodic boundary conditions in the numerical simulations. These equations have Galilean symmetry: $x \mapsto x + Vt$, $u \mapsto u + V$ and $w \mapsto w$ (V is a constant) and reflection symmetry: $x \mapsto -x$, $u \mapsto -u$ and $w \mapsto w$. Furthermore, we have another symmetry: $s \to -s$ and $w \to -w$; and hence we can restrict our attention to the case $s \geq 0$. On the other hand, we need to consider the full range of values for $b \neq 0$. The restriction $b \neq 0$ is because when $b = 0$ and $u = 0$, we only have the Swift-Hohenberg equation. Note that the coefficient of the viscous diffusion term in (5.2) (σ) is always positive. Finally, the spatial average of u may be set as zero. This is because from (5.2) $\dfrac{d}{dt}\displaystyle\int_0^l u dx = 0$; and hence $\langle u \rangle = \dfrac{1}{l}\displaystyle\int_0^l u dx =$ constant. Thus in view of the Galilean symmetry of the system, this constant may be set to zero by transforming to a moving frame of reference.

Note that (5.1) is the Swift-Hohenberg equation with an additional nonlinear term involving u. In addition, omitting the nonlinear term involving w in (5.2) gives Burgers' equation. Other coupled systems involving a Swift-Hohenberg equation coupled to a Goldstone mode (some terms are similar to our system) have been studied in a different context. These studies include stability analysis and numerical computations. Golovin *et al.* [25] studied a system of the complex Swift-Hohenberg equation coupled to a Goldstone mode for flame fronts. It was concluded that strong coupling destabilises the travelling wave solutions, which leads to the transition to dynamical chaos. Another example of such coupling was also considered in [51], where the coupling resulted in the zigzag instability of periodic patterns and a chaotic behaviour arises. In addition to these results, the coupling of the Swift-Hohenberg model for lasers to a large-scale mode leads to the appearance of higher order instabilities [38] and the shrinkage of the Busse balloon [9] for the stability of travelling wave solutions.

The major goal of this chapter is to analyse the effect of the coupling between the Swift-Hohenberg equation and a Goldstone mode on the stability of stationary roll solutions for small r. This will be done by a combination of analytical and numerical calculations. Due to the qualitative similarities of (5.1) and (5.2) with the Nikolaevskiy equation, we shall use the same scalings in the asymptotic procedure. However, in the Nikolaevskiy equation we have only one variable which represents both the pattern and large-scale modes, whereas in this system we have two variables, namely w and u. Due to the coupling between (5.1) and (5.2), both u and w have large-scale aspects and pattern-scale variations. However, we shall see later, in the weakly nonlinear analysis, that the pattern is the dominant term in w and the large-scale mode is the dominant term in u.

This chapter is divided into nine sections. In §5.2, we introduce the dispersion relation, then we will be concerned with calculating the roll solutions of (5.1) and (5.2) in §5.3. In §5.4 we shall find the amplitude equations representing slow modulations in space and time of patterns out of equilibrium. In §5.5, there will be numerical calculations of the secondary stability of rolls, supported by numerical simulations (§5.6). Afterwards, in §5.7 and §5.8, we shall study the secondary stability of stationary rolls with two different scalings in order to compare the theory with the secondary stability plots. Conclusions drawn from this study and comparisons with the Nikolaevskiy equation will be given at the end of this chapter (§5.9).

5.2 Dispersion relation

In this section we linearise the system (5.1) and (5.2) in order to study the stability of the zero solution $u \equiv 0$ and $w \equiv 0$. Then for modes proportional to $e^{ikx+\lambda t}$, we obtain two

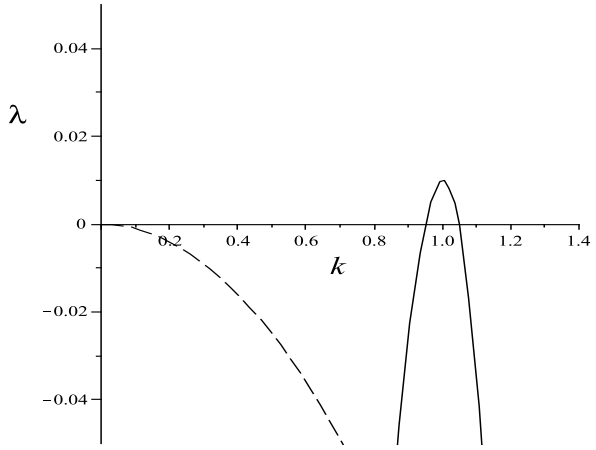

Figure 5.1: The growth rate of the instability: λ_1 (solid line) and λ_2 (dashed line) plotted against the perturbation wavenumber for $r = 0.01$ and $\sigma = 0.1$.

dispersion relations

$$\begin{aligned} \lambda_1 &= r - (1-k^2)^2, \\ \lambda_2 &= -\sigma k^2, \end{aligned}$$

corresponding, respectively, to infinitesimal disturbances in w and u (which decouple).

Figure 5.1 represents the growth rates λ_1 and λ_2 for $r = 0.01$ and $\sigma = 0.1$. As shown in this figure there exists a band of wavenumbers centred around $k_c = 1$ experiencing linear growth; and thus if $r > 0$, λ_1 will result in instability. On the other hand, there is a slowly decaying mode (Goldstone mode) near $k = 0$ for λ_2, which never gives rise to instability. Consequently, $r_c = 0$ is a threshold value for the onset of instability, where patterns grow as r exceeds zero.

The dispersion relation is qualitatively similar to the one for the Nikolaevskiy equation in these respects, thus we next examine whether the nonlinear behaviour is qualitatively the same as the Nikolaevskiy equation; for example, that all rolls are unstable at onset.

5.3 Roll solutions

In this section we intend to calculate the roll solutions near the onset of pattern formation with wavenumber close to 1. This will be done without considering the spatial modulations of the rolls.

Now we introduce the weakly nonlinear expansions, where $r = \epsilon^2 r_2$ ($\epsilon \ll 1$)

$$\begin{aligned} w &= \epsilon w_1 + \epsilon^2 w_2 + \epsilon^3 w_3 + \cdots, \\ u &= \epsilon u_1 + \epsilon^2 u_2 + \epsilon^3 u_3 + \cdots. \end{aligned}$$

From substituting these equations in (5.1) and (5.2), respectively, we obtain at $O(\epsilon)$

$$\begin{aligned} \frac{\partial w_1}{\partial t} + \left(1 + \frac{\partial^2}{\partial x^2}\right)^2 w_1 &= 0, \\ \frac{\partial u_1}{\partial t} - \sigma \frac{\partial^2 u_1}{\partial x^2} &= 0. \end{aligned}$$

From this it follows that w_1 is of the form $A(T)e^{\mathrm{i}(1+\epsilon q)x} + c.c.$ The complex amplitude $A(T)$ evolves on the slow time scale $T = \epsilon^2 t$, since the growth rate λ_1 is of order ϵ^2. In addition, u_1 is chosen to be a large-scale mode, which also evolves with T: $u_1 = u_1(T)$. Note that $\langle u \rangle = \epsilon \langle u_1 \rangle + O(\epsilon^2) = \epsilon u_1 + O(\epsilon^2)$ and hence, since $\langle u \rangle = 0$, we set $u_1 = 0$.

At the next order we obtain the two equations

$$\begin{aligned} \frac{\partial w_2}{\partial t} + \left(1 + \frac{\partial^2}{\partial x^2}\right)^2 w_2 + sA^2 e^{2\mathrm{i}(1+\epsilon q)x} + c.c. + 2s|A|^2 &= 0, \\ \frac{\partial u_2}{\partial t} - \sigma \frac{\partial^2 u_2}{\partial x^2} - \mathrm{i}bA^2 e^{2\mathrm{i}(1+\epsilon q)x} + c.c. &= 0. \end{aligned}$$

Therefore, we choose

$$\begin{aligned} w_2 &= -\frac{sA^2}{9} e^{2\mathrm{i}(1+\epsilon q)x} + c.c. - 2s|A|^2, \\ u_2 &= \frac{\mathrm{i}bA^2}{4\sigma} e^{2\mathrm{i}(1+\epsilon q)x} + c.c. \end{aligned}$$

Note that w_2 contains both pattern ($e^{\pm 2\mathrm{i}(1+\epsilon q)x}$) and large-scale ($|A|^2$) contributions. On the other hand, u_2 contains only the pattern ($e^{\pm 2\mathrm{i}(1+\epsilon q)x}$) because of the constraint $\langle u \rangle = 0$. Thus the leading term in w and u is the pattern.

The amplitude equation then appears at $O(\epsilon^3)$ (from (5.1)) from a solvability condition as follows:

$$\frac{\partial A}{\partial T} = (r_2 - 4q^2)A + \left(-3 + \frac{38s^2}{9} - \frac{b}{4\sigma}\right) A|A|^2. \tag{5.3}$$

This equation shows that the equilibrium amplitude of the rolls is given by $|A|^2 = a_0^2$, where

$$\begin{aligned} a_0^2 &= \frac{r_2 - 4q^2}{D}, \\ D &= 3 - \frac{38s^2}{9} + \frac{b}{4\sigma} = \frac{108\sigma - 152s^2\sigma + 9b}{36\sigma}. \end{aligned}$$

It is worth mentioning that in the Swift-Hohenberg equation, if $|s|$ is sufficiently small (or is zero) we then have supercritical rolls. However, rolls become subcritical for large enough s^2, in particular when $s^2 > 27/38$ [5, 24, 27]. In the present case, there is a similar trend, from (5.3) if the coefficient of $A|A|^2$ is negative, then it produces supercritical rolls and subcritical rolls if it is positive. Unlike the Swift-Hohenberg equation, there is a new parameter combination, b/σ, which affects the direction of bifurcation and the stability of the rolls.

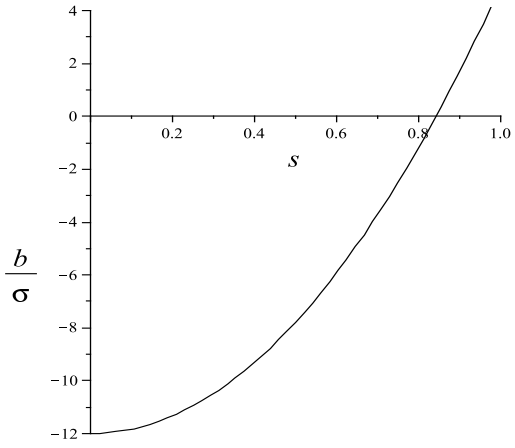

Figure 5.2: Plot of $9b/\sigma = 4(38s^2 - 27)$. The region above the curve is where $D > 0$, which is the supercritical case.

In the subcritical case, rolls are unstable at onset to amplitude disturbances. By contrast, in the supercritical case rolls are stable at onset to amplitude disturbances. Hence we only need to study the supercritical case to examine what happens to these rolls for more general disturbances. In such a case, from (5.3) we assume $-3 + \dfrac{38s^2}{9} - \dfrac{b}{4\sigma} < 0$, or, equivalently, $D > 0$. Figure 5.2 shows where in $(b/\sigma, s)$ parameter space $D > 0$, in other words where $9b/\sigma > 4(38s^2 - 27)$. If $s > \sqrt{27/38} \approx 0.8429$, then we can choose only positive values of b (since $\sigma > 0$).

In conclusion, in the stability analysis of rolls we need to consider the case $D > 0$ and since $a_0^2 = \dfrac{r_2 - 4q^2}{D} > 0$, it follows that supercritical rolls exist only for wavenumbers satisfying $-\dfrac{\sqrt{r_2}}{2} < q < \dfrac{\sqrt{r_2}}{2}$.

5.4 Amplitude equations

In §5.3 we found the roll solutions near the onset of pattern formation, whereas in this section we are interested in characterising the dynamics of the solution of (5.1) and (5.2); and thus we calculate amplitude equations, which accommodate modulation of the pattern envelope. Due to the presence of the Galilean symmetry in (5.1) and (5.2), we expect the amplitude equation for the rolls to be coupled to a large-scale mode [40].

To find the amplitude equations we consider using the same scaling as in [40], in which the pattern, which is modulated by the envelope $A(X, T)$, is of order $\epsilon^{3/2}$ and the large-scale mode is of order ϵ^2. Furthermore, $r = \epsilon^2 r_2$ and the temporal and spatial scales are replaced with the slow variables $T = \epsilon^2 t$ (the same order as the growth rate λ_1) and $X = \epsilon x$. This particular scaling is necessary to balance the diffusion term in the amplitude equations.

After applying this scaling to (5.1) and (5.2) in a weakly nonlinear regime, we find from

successive powers of $O(\epsilon^{1/2})$ that

$$w = \epsilon^{3/2}Ae^{\mathrm{i}x} + c.c. + \epsilon^3(-\frac{sA^2}{9}e^{2\mathrm{i}x} + c.c. - 2s|A|^2) + \cdots, \tag{5.4}$$

$$u = \epsilon^2 f + \epsilon^3\frac{\mathrm{i}bA^2}{4\sigma}e^{2\mathrm{i}x} + c.c. + \cdots. \tag{5.5}$$

Here A and f appear at leading-orders in w and u, respectively. They both remain at the same order as they were originally in [40]. We will examine these scalings later in this section by means of numerical calculations.

The self-consistent amplitude equations, which arise from solvability conditions at $O(\epsilon^{7/2})$ from (5.1) and $O(\epsilon^4)$ from (5.2), respectively, are

$$\begin{aligned}\frac{\partial A}{\partial T} &= r_2 A + 4\frac{\partial^2 A}{\partial X^2} - \mathrm{i}fA,\\ \frac{\partial f}{\partial T} &= \sigma\frac{\partial^2 f}{\partial X^2} + b\frac{\partial |A|^2}{\partial X}.\end{aligned}$$

These equations are the same as those found in [40] but with different coefficients in the equation for f because of the parameters appearing in (5.2). In fact, by rescaling we can eliminate r_2 and b by taking $\hat{T} = r_2 T$, $\hat{X} = r_2^{1/2}X$, $\hat{f} = f/r_2$ and $\hat{A} = A\sqrt{|b|r_2^{-3/2}}$. Then we have

$$\begin{aligned}\frac{\partial A}{\partial T} &= A + 4\frac{\partial^2 A}{\partial X^2} - \mathrm{i}fA,\\ \frac{\partial f}{\partial T} &= \sigma\frac{\partial^2 f}{\partial X^2} + \frac{b}{|b|}\frac{\partial |A|^2}{\partial X}.\end{aligned}$$

Note that for simplicity, we have dropped the hats on the variables in these new equations. The last term in the second equation is either positive or negative depending on the sign of b. We next show that the sign of this term does not affect the behaviour of the solution.

Consider the case of $b < 0$, then we have

$$\begin{aligned}\frac{\partial A}{\partial T} &= A + 4\frac{\partial^2 A}{\partial X^2} - \mathrm{i}fA,\\ \frac{\partial f}{\partial T} &= \sigma\frac{\partial^2 f}{\partial X^2} - \frac{\partial |A|^2}{\partial X}.\end{aligned}$$

Let $\hat{A} = A^*$ and $\hat{f} = -f$. Hence we obtain

$$\begin{aligned}\frac{\partial \hat{A}}{\partial T} &= \hat{A} + 4\frac{\partial^2 \hat{A}}{\partial X^2} - \mathrm{i}\hat{f}\hat{A},\\ \frac{\partial \hat{f}}{\partial T} &= \sigma\frac{\partial^2 \hat{f}}{\partial X^2} + \frac{\partial |\hat{A}|^2}{\partial X}.\end{aligned}$$

Therefore, by rescaling we can change the sign of the last term in the second equation. Hence the behaviour of the solution of the amplitude equations in the two cases is essentially the same and does not depend on b. Therefore, the amplitude equations can be written (with

no loss of generality) as

$$\begin{aligned}\frac{\partial A}{\partial T} &= A + 4\frac{\partial^2 A}{\partial X^2} - \mathrm{i}fA,\\ \frac{\partial f}{\partial T} &= \sigma\frac{\partial^2 f}{\partial X^2} - \frac{\partial |A|^2}{\partial X}.\end{aligned}$$

In these equations, we cannot remove σ by rescaling; however, we can eliminate it from the second equation by choosing $\tilde{X} = \sigma^{-1/2}X$ and $\tilde{A} = \sigma^{-1/4}A$. Thus we obtain

$$\frac{\partial \tilde{A}}{\partial T} = \tilde{A} + \frac{4}{\sigma}\frac{\partial^2 \tilde{A}}{\partial \tilde{X}^2} - \mathrm{i}f\tilde{A}, \tag{5.6}$$

$$\frac{\partial f}{\partial T} = \frac{\partial^2 f}{\partial \tilde{X}^2} - \frac{\partial |\tilde{A}|^2}{\partial \tilde{X}}. \tag{5.7}$$

In the special case $\sigma = 1$, we obtain the same behaviour as the Nikolaevskiy equation (see [40, 47, 48, 52]). In the general case, (5.6) and (5.7) are identical to those in §3.3, where n is equivalent to $4/\sigma$ (refer to (3.2) and (3.3)). Detailed numerical simulations have already been given in §3.3.

After finding the amplitude equations, we now calculate the rms of w using (5.1) and (5.2) for $b = -10$, $s = 0.8$ and $\sigma = 10$. This will be done in order to validate the scaling used to derive the amplitude equations. We calculate the rms of w averaged over 5000–150000 time units in a box of length 200π and ignore initial transients. It appears that for small r ($0.001 < r < 0.4$) w is almost proportional to $r^{3/4}$ (see figure 5.3). This means that the pattern is of order $\epsilon^{3/2}$. Therefore, the amplitude equations are verified for $0.001 < r < 0.4$, and this result is compatible with the Nikolaevskiy equation for $0.001 < r < 0.1$ [40, 62].

From this example we checked that the scaling used to derive the amplitude equations is valid. However, in our system there are several parameters and it is difficult to conclude a general result. We can say that for some values of the parameters these equations are valid and in some cases they are not; for example, when the parameters result in stable rolls.

In this section we have found the amplitude equations which describe the dynamics once rolls have become unstable; however, these equations do not capture the rolls themselves (see numerical simulations in §3.3). This is because the rolls are of $O(\epsilon)$ (§5.3) and thus the scaling used here is not appropriate for studying the stability of rolls, whereas these equations can be used to describe the rolls after they become unstable and time dependent. The correct scaling for finding the amplitude equations which characterise the stability of rolls will be presented in §5.7 after examining the secondary stability problem numerically.

5.5 Secondary stability of rolls calculated numerically

The first step in analysing the stability of stationary wave solutions of (5.1) and (5.2) is calculating the secondary stability boundaries numerically for some samples of the parameters.

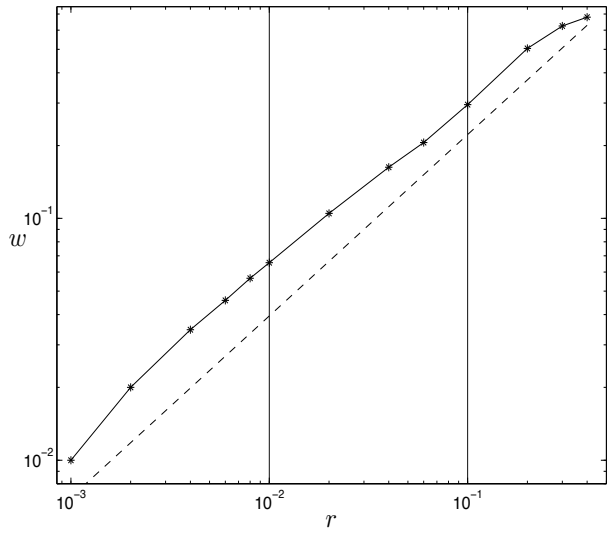

Figure 5.3: Log-log plot of the rms of w averaged over 5000–150000 time units, where $b = -10$, $s = 0.8$, $\sigma = 10$. The dashed line has the slope 3/4.

The numerical code (details given in §4.3.1) first calculates the roll solution with fixed values of the parameters in (5.1) and (5.2) and wavenumber k. Next, it linearises about the roll solution, for perturbations with wavenumber p, where $-\frac{k}{2} < p < \frac{k}{2}$. Afterwards, it finds the maximum value of the real part of all growth rates of the perturbations. If the maximum value is negative, then the original roll solution is considered to be stable. According to this numerical calculation we first find the secondary stability plots in the (k, r) plane for fixed b, s and σ. To generate these plots we fix a value of $r > 0$ and take enough samples in k between $\sqrt{1-\sqrt{r}}$ and $\sqrt{1+\sqrt{r}}$ in order to find the stable region, if it exists. Similarly, we find the secondary stability plot in the (k, s) plane for fixed b, σ and r. In the following examples, the number of samples for k and p is 200 and 800, respectively; and the number of Fourier modes used to represent the rolls, and the perturbations, is 12. We have checked that this resolution is sufficient so as not to miss any small stable region.

The first examples we introduce in the (k, r) plane are for ($b = -1$, $s = 0$ and $\sigma = 2$), ($b = -1$, $s = 0$ and $\sigma = 10$) and ($b = 1$, $s = 0.2$ and $\sigma = 1$). These are displayed in figures 5.4(a)–(c), where the lower part of the secondary stability boundary is a half Eckhaus-like stable region. To be precise, the stable region is a right-hand side of an Eckhaus-like stable region for $b > 0$ and a left-hand side for $b < 0$, for small r.

The stability regions in figures 5.4(a)–(c) seem to be similar and we shall now illustrate the types of instabilities presented in figure 5.4(c) ($b = 1$, $s = 0.2$ and $\sigma = 1$) as an example. Accordingly, we plot the growth rate (real part) of the perturbation against the wavenumber p for different values of k and r (see figure 5.5). In each graph we fix a value of r and plot for three values of k taken from the stable and unstable regions in figure 5.4(c). The dashed and dotted curves, in figure 5.5, correspond to values of k taken from the unstable region in

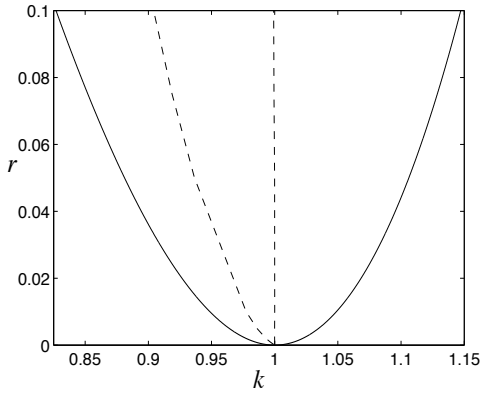

(a) $b = -1$, $s = 0$ and $\sigma = 2$.

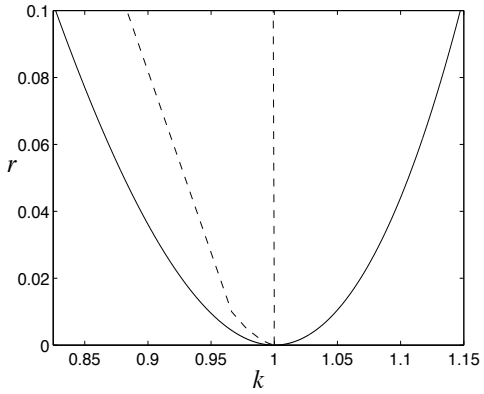

(b) $b = -1$, $s = 0$ and $\sigma = 10$

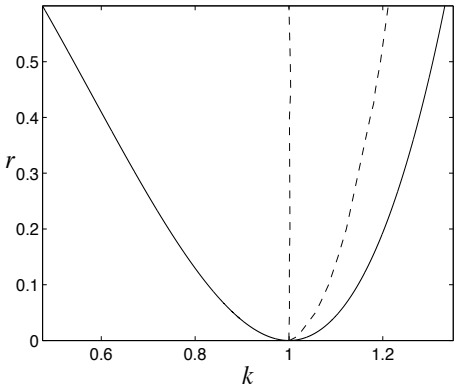

(c) $b = 1$, $s = 0.2$ and $\sigma = 1$

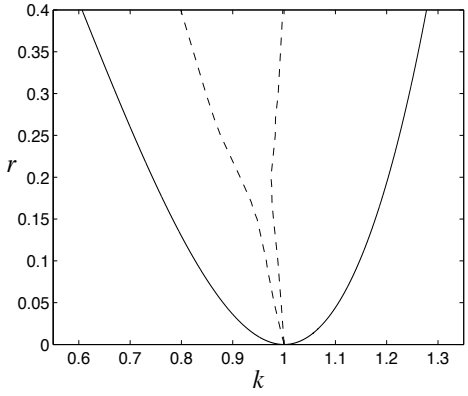

(d) $b = -5$, $s = 0.1$ and $\sigma = 1$

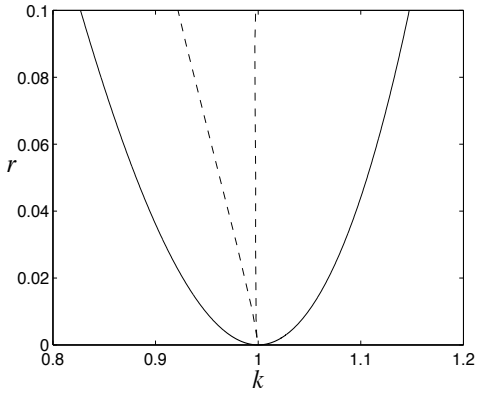

(e) $b = -10$, $s = 0.8$ and $\sigma = 10$

Figure 5.4: The secondary stability region for rolls of (5.1) and (5.2) calculated numerically for b, s and σ as given under each graph. The stable region is enclosed by the dashed curves and the marginal stability curve is $r = (1 - k^2)^2$ (solid curve). When $b < 0$ the dashed curve on the left hand side is an oscillatory instability boundary and the dashed curve on the right hand side is a monotonic instability boundary, and vice versa for $b > 0$. Note that in (e) the stable band does not extend down to $r = 0$, where all rolls are unstable for $r < 0.0021$.

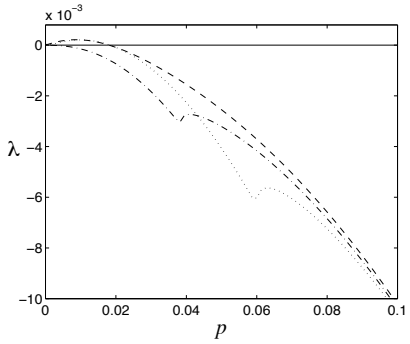

(a) $r = 0.001$, $k = 0.999$, $k = 1.002$ and $k = 1.01$.

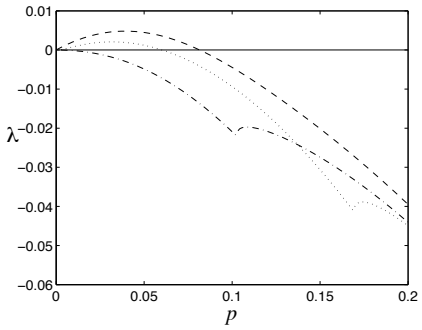

(b) $r = 0.01$, $k = 0.975$, $k = 1.01$ and $k = 1.04$.

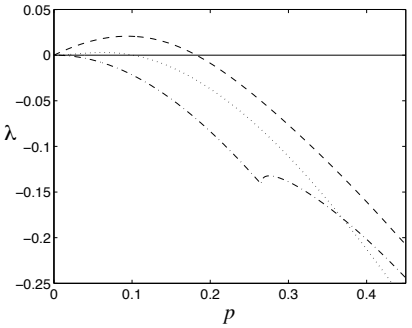

(c) $r = 0.1$, $k = 0.92$, $k = 1.04$ and $k = 1.1$.

Figure 5.5: The real part of the growth rate of the perturbation plotted against the wavenumber p for $b = 1$, $s = 0.2$, $\sigma = 1$. The dashed curve corresponds to the first value of k, the dash-dotted curve corresponds to the second value of k and the dotted curve corresponds to the third value of k. The dashed and the dotted curves exhibit long-wavelength instability.

figure 5.4(c) and the dash-dotted curve corresponds to k taken from the stable region. As shown in figure 5.5, the growth rate of the perturbation with wavenumber k taken from the stable region in figure 5.4(c) (dash-dotted curve) is negative for all values of p. On the other hand, there is a band of unstable wavenumbers when k is chosen from the unstable region in 5.4(c) (dashed and dotted curves); and this is a long-wavelength instability. In particular, we have monotonic instability regarding the dashed curves and oscillatory instability regarding the dotted curves.

Another example, exhibited in figure 5.4(d), is for $b = -5$, $s = 0.1$ and $\sigma = 1$. The stable region is a narrow strip, which becomes wider when $r > 0.15$. In figure 5.6, the growth rate (real part) of the perturbation is plotted against p for different values of r and k. Again we have a fixed value of r in each graph, and we plot for three different values of k taken from the stable and unstable regions in figure 5.4(d). The dashed and dotted curves correspond to values of k taken from the unstable region in figure 5.4(d). In addition,

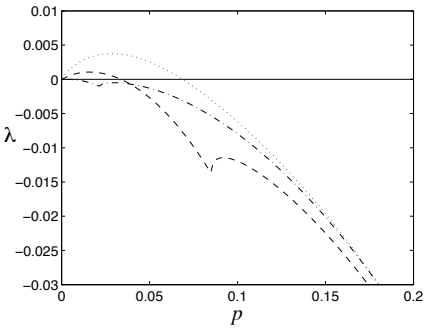

(a) $r = 0.001$, $k = 0.9888$, $k = 0.9997$ and $k = 1.01$.

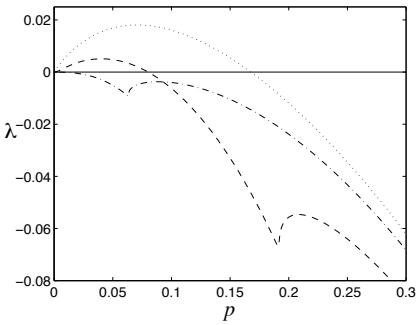

(b) $r = 0.01$, $k = 0.965$, $k = 0.9975$ and $k = 1.02$.

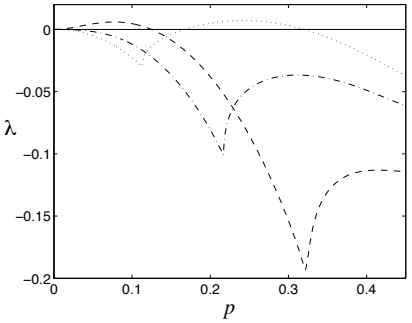

(c) $r = 0.1$, $k = 0.93$, $k = 0.97$ and $k = 0.992$.

Figure 5.6: The real part of the growth rate of the perturbation plotted against the wavenumber p for $b = -5$, $s = 0.1$, $\sigma = 1$. The dashed curve corresponds to the first value of k, the dash-dotted curve corresponds to the second value of k and the dotted curve corresponds to the third value of k. The dashed and the dotted curves exhibit long-wavelength instability in (a) and (b). On the other hand, in (c) the dashed curve exhibits long-wavelength instability and the dotted curve exhibits finite-wavelength instability.

the dash-dotted curve corresponds to k chosen from the stable region in 5.4(d). The dashed curve exhibits long-wavelength instability in figures 5.6(a)–(c) (oscillatory instability). On the other hand, the dotted curve exhibits long-wavelength instability in figures 5.6(a) and (b) and finite-wavelength instability in figure 5.6(c) (all are monotonic instability).

The final example in the (k, r) plane is for $b = -10$, $s = 0.8$ and $\sigma = 10$ (see figure 5.4(e)). In this figure, there is a region of stable rolls for $r > 0.0021$. Beyond this value as we increase r the stable region becomes wider.

After providing some regions of stability in the (k, r) plane, we now calculate the domain of stability in the (k, s) plane for $r = 0.01$ and fixed values for b and σ. In this case the value of s is limited by the condition $s^2 < \frac{9}{152}(b/\sigma + 12)$ (see figure 5.2). In addition, rolls exist if $0.9487 < k < 1.0488$. Accordingly two plots are given in figure 5.7 for $b = -5$

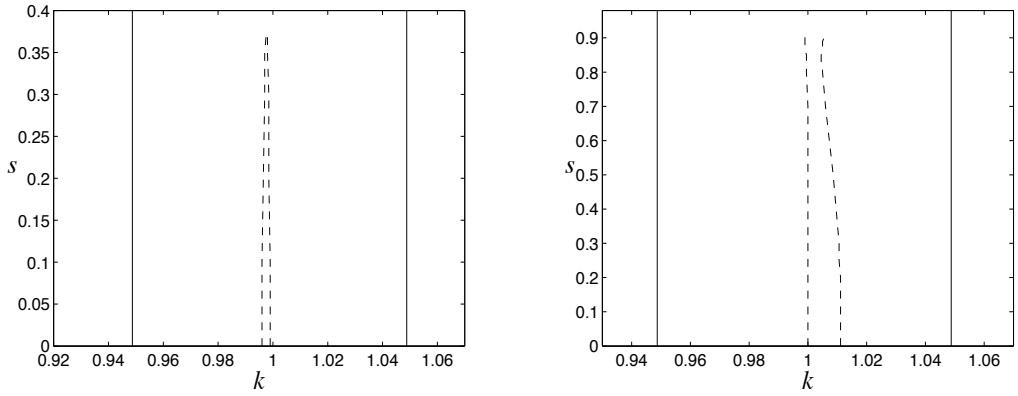

(a) $b = -5$, $\sigma = 1$ (b) $b = 4$ and $\sigma = 2$

Figure 5.7: The secondary stability region for rolls of (5.1) and (5.2) calculated numerically for $r = 0.01$, where b and σ are indicated under each graph. The stable region is bounded by the dashed curves and the solid curve is the marginal stability curve. When $b < 0$ the dashed curve on the left hand side is an oscillatory instability boundary and the dashed curve on the right hand side is a monotonic instability boundary, and vice versa for $b > 0$. Note that the stable region is delimited from above by $s = 0.37$ and $s = 0.9105$ in (a) and (b), respectively.

and $\sigma = 1$, and for $b = 4$ and $\sigma = 2$. In figure 5.7(a) we must choose the values of s such that $s < \frac{3}{76}\sqrt{266} \approx 0.6438$, because if $s > \frac{3}{76}\sqrt{266}$, then rolls become subcritical. In figure 5.7(a), the stable region becomes a narrow strip with an upper bound, where rolls are unstable if $s > 0.37$. The stable region in figure 5.7(b) is also a narrow strip bounded by $s = \frac{3}{38}\sqrt{133} \approx 0.9105$. We cannot go further than this value of s because rolls become subcritical if $s > \frac{3}{38}\sqrt{133}$.

In the previous examples we have illustrated stability regions in the (k, r) and (k, s) planes. Unfortunately, given the number of parameters in the problem, the secondary stability plots found here are only indicative and do not allow us to draw many general conclusions about the secondary stability problem. Indeed, as we change the values of the parameters, different topologies of the stability regions occur, which are challenging to describe analytically. Later in §5.7 and §5.8 we attempt to investigate the secondary stability of rolls analytically. An important observation from these plots is that near the marginal stability curve $r = (1 - k^2)^2$ there are no stable rolls. In addition to this, a half Eckhaus-like stable region may appear for small values of r.

In the following section we illustrate some numerical simulations of (5.1) and (5.2) with parameter values taken from the secondary stability plots.

5.6 Numerical simulations

Having calculated the secondary stability diagrams numerically, here we perform some numerical simulations of (5.1) and (5.2) with certain values of the parameters. In particular, we test the results illustrated in figures 5.4 and 5.7. The numerical code used here employs a pseudo-spectral method for spatial discretisation [21, 67] and an exponential time differencing fourth-order Runge-Kutta method [13, 30] for time stepping. The initial conditions for w and u are

$$\begin{aligned} w &= 2\epsilon a_0 \cos(kx), \\ u &= -\frac{\epsilon^2 b a_0^2}{2\sigma} \sin(2kx), \end{aligned}$$

plus small random noise for both and $a_0^2 = r_2/D$ ($D = \frac{108\sigma - 152s^2\sigma + 9b}{36\sigma}$ and $r_2 = 1$). The initial conditions are chosen from the dominant terms in the weakly nonlinear analysis in §5.3. The domain size is $l = 500$ and $r = \epsilon^2$. The values of k are selected from the regions which are expected to be stable or unstable in figures 5.4 and 5.7. For each simulation in figures 5.8–5.12, w (which represents the pattern) is plotted.

Figure 5.8 provides an example of numerical simulations with $b = -1$, $s = 0$, $\sigma = 2$ and $r = 0.1$. The wavenumber is taken from either the stable or unstable region in figure 5.4(a). In figures 5.8(a) and (c) the wavenumber is chosen from the unstable region in figure 5.4(a); and the numerical simulations are in agreement with this stability graph. In addition, the unstable rolls are eventually replaced by rolls with wavenumber from the band of stability, as can be seen in figures 5.8(a) and (c), which exhibits the Eckhaus instability. In figure 5.8(b) we have a numerical simulation of rolls with wavenumber selected from the stable region in figure 5.4(a); also we have consistency with the secondary stability plot. A similar result is given in figure 5.9, where the parameter values are taken from figure 5.4(c) ($b = 1$, $s = 0.2$, $\sigma = 1$ and $r = 0.5$). The similarities between the numerical simulations in figures 5.8 and 5.9 are due to the fact that the parameter values are selected from figures 5.4(a) and (c), respectively, which have similar stability regions.

In the next example we choose $b = -5$, $s = 0.1$, $\sigma = 1$ and $r = 0.4$. If the wavenumbers are chosen from the unstable region in figure 5.4(d), then the simulations in figures 5.10(a) and (c) for $k = 0.7$ and $k = 1.1$, respectively, exhibit extremely complicated behaviour of the time dependent solution. On the other hand, if we choose a wavenumber predicted to be stable in figure 5.4(d), then the simulation in figure 5.10(b) illustrates stable rolls.

If we fix $b = -10$, $s = 0.8$, $\sigma = 10$ and $r = 0.1$ and select unstable wavenumbers from figure 5.4(e), this results in instability in the simulations (see figures 5.11(a) and (c)). These simulations show similar behaviour to the Nikolaevskiy chaos in which there is no formation

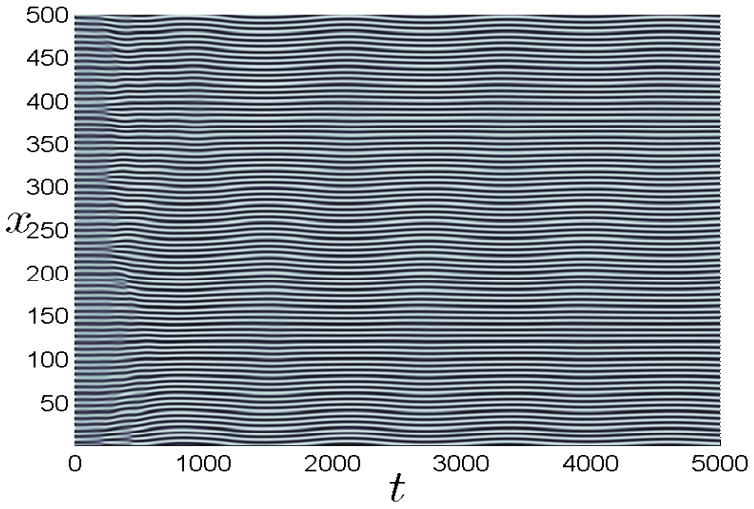

(a) $k = 0.8656$

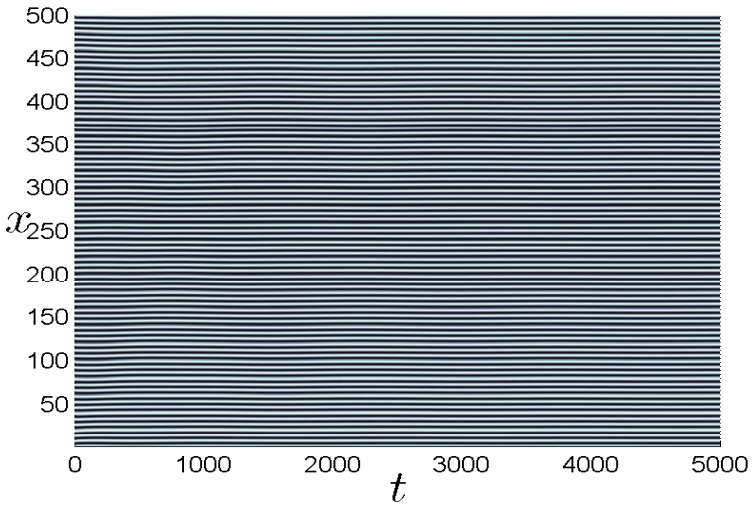

(b) $k = 0.9517$

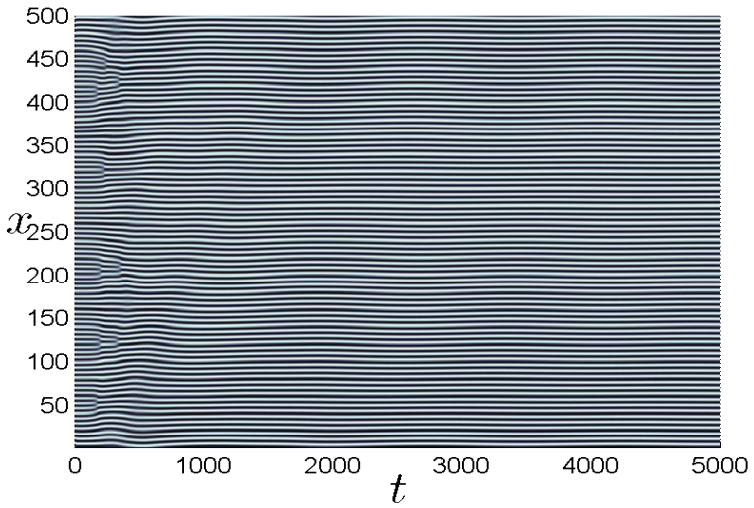

(c) $k = 1.0733$

Figure 5.8: Space-time numerical simulation of (5.1) and (5.2) for different values of k as indicated under each graph, where w is plotted. The parameter values are $b = -1$, $s = 0$, $\sigma = 2$ and $r = 0.1$.

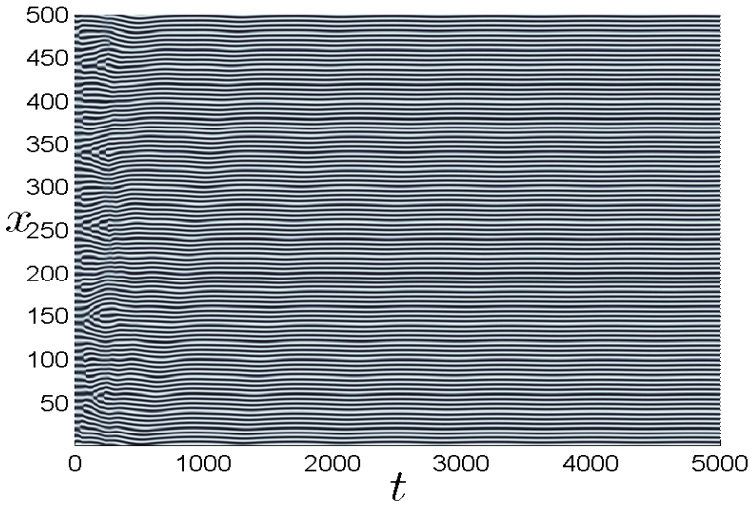

(a) $k = 0.7719$

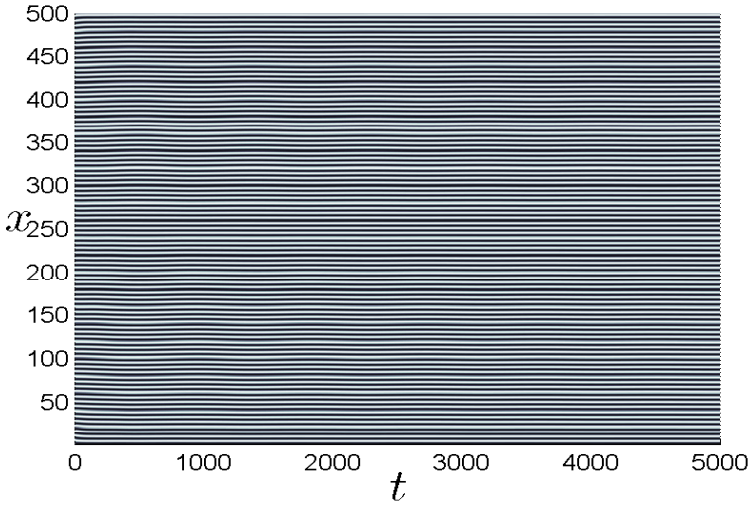

(b) $k = 1.0989$

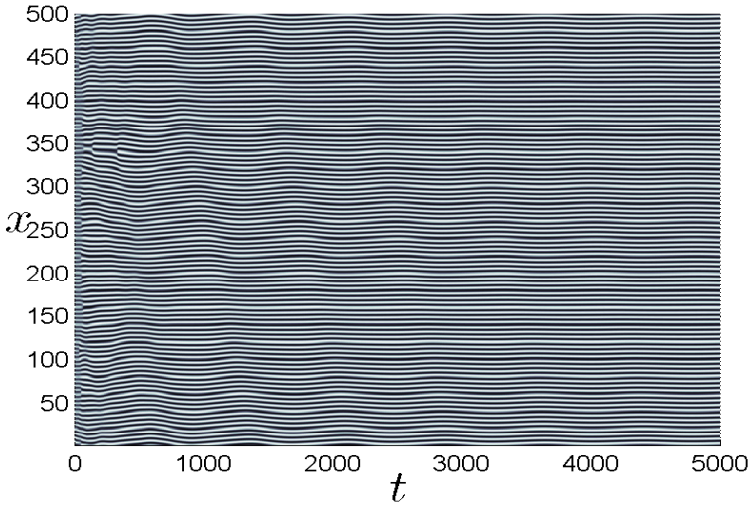

(c) $k = 1.2508$

Figure 5.9: Same as figure 5.8 with parameter values $b = 1$, $s = 0.2$, $\sigma = 1$ and $r = 0.5$.

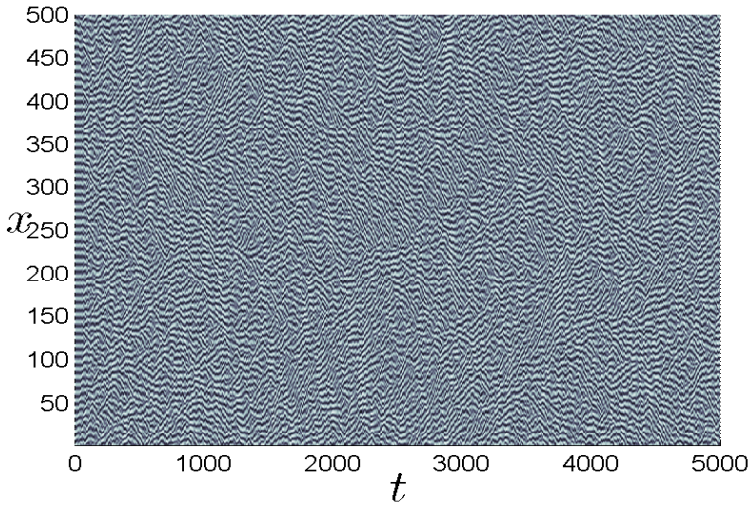

(a) $k = 0.7$

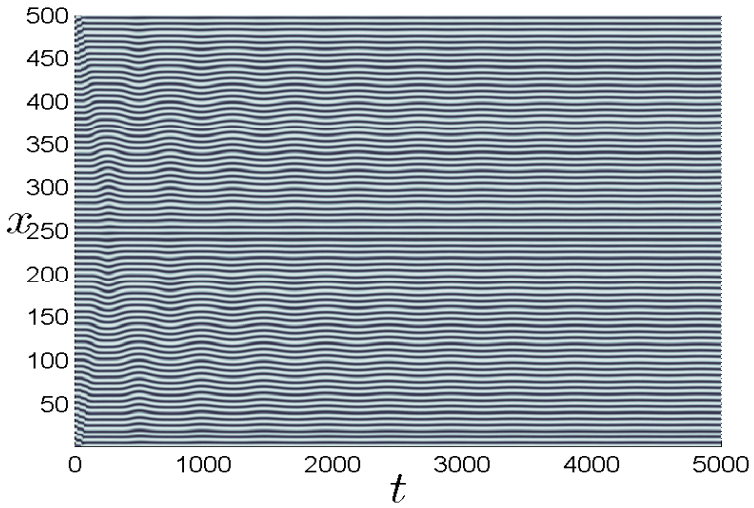

(b) $k = 0.9$

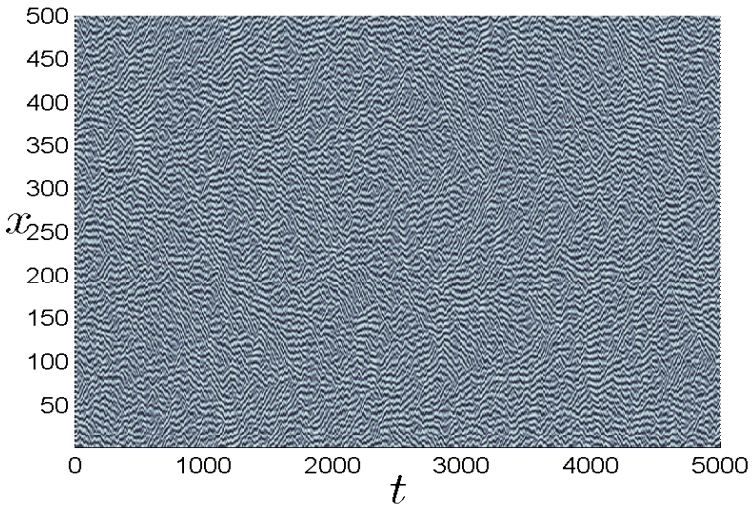

(c) $k = 1.1$

Figure 5.10: Same as figure 5.8 with parameter values $b = -5$, $s = 0.1$, $\sigma = 1$ and $r = 0.4$.

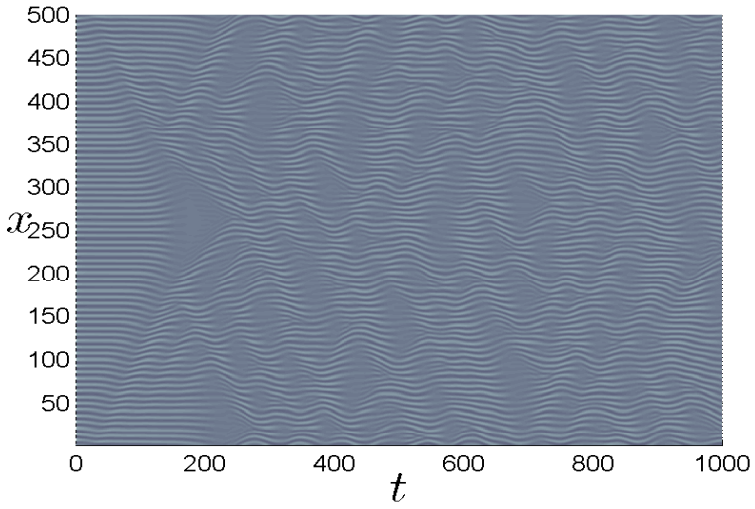

(a) $k = 0.8744$

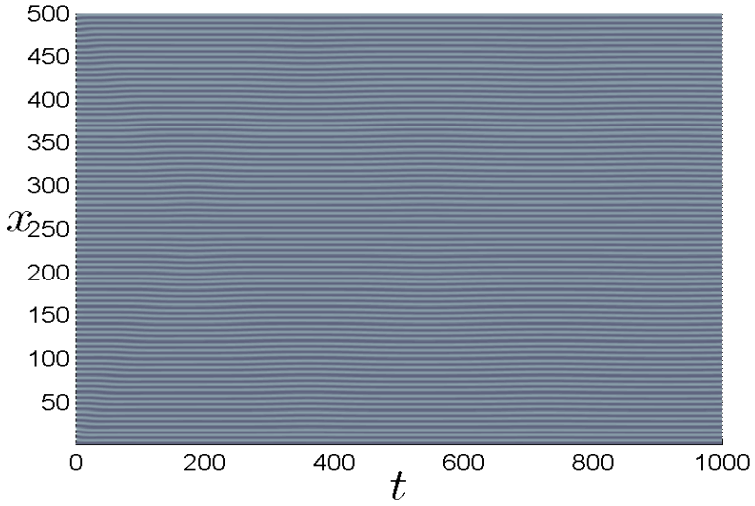

(b) $k = 0.9599$

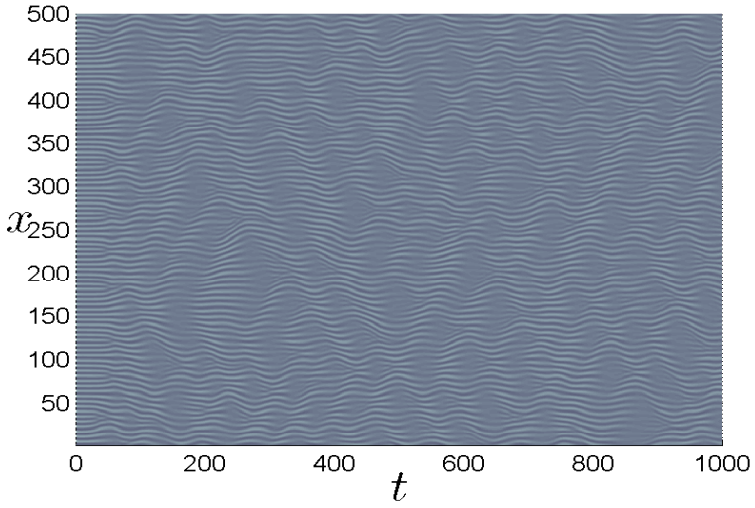

(c) $k = 1.0724$

Figure 5.11: Same as figure 5.8 with parameter values $b = -10$, $s = 0.8$, $\sigma = 10$ and $r = 0.1$.

of an arranged structure (see figure 1.3). If we choose k from the stable region in figure 5.4(e), then the numerical simulation gives stable rolls as can be seen in figure 5.11(b).

The final simulations we have are presented in figure 5.12, where $b = 4$, $s = 0.2$, $\sigma = 2$ and $r = 0.01$ (the parameter values are taken from figure 5.7(b)). In figures 5.12(a) and (c) the simulations exhibit unstable rolls and this agrees with figure 5.7(b) since the wavenumbers are taken from the unstable region. Also the simulation in figure 5.12(b) is consistent with the result in figure 5.7(b). This is because the wavenumber is predicted to be stable from figure 5.7(b) and the simulation shows the stability of rolls. In the unstable case, rolls do not settle down and are persistently time dependent. This behaviour is different from the extremely chaotic state exhibited in figure 5.10.

It can be concluded from the previous graphs that for certain values of the parameters the system (5.1) and (5.2) exhibits a similar behaviour to that of the Nikolaevskiy equation. Now we are going to move to the next step, which is analytically investigating the stability of roll solutions of (5.1) and (5.2) and examining how the result is applicable to the secondary stability plots.

5.7 Secondary stability of stationary rolls

Now we derive nonlinear amplitude equations and then we use them to study the stability of rolls. Therefore, we apply a weakly nonlinear analysis on (5.1) and (5.2) and introduce the slow temporal and spatial variables $T = \epsilon^{3/2}t$ and $X = \epsilon^{3/4}x$ ($r = \epsilon^2 r_2$). This scaling is motivated by [72], which was also used in [14] and §4.5 in the same framework as here. As is always the case, this scaling is appropriate to allow the development of asymptotically self-consistent amplitude equations.

Now we substitute this scaling of time and space with the following expansions in (5.1) and (5.2)

$$\begin{aligned} w &= \epsilon w_1 + \epsilon^{5/4} w_2 + \epsilon^{3/2} w_3 + \cdots, \\ u &= \epsilon u_1 + \epsilon^{5/4} u_2 + \epsilon^{3/2} u_3 + \cdots. \end{aligned}$$

After taking into account coefficients of powers of $\epsilon^{1/4}$ and applying solvability conditions, this leads to the following:

$$\begin{aligned} w &= \epsilon(a_0 + \epsilon^{1/2} a(X,T))e^{\mathrm{i}M} + c.c. + \cdots, \\ u &= \epsilon^{7/4} f + \epsilon^2 \frac{\mathrm{i}ba_0^2}{4\sigma} e^{2\mathrm{i}M} + c.c. + \cdots, \end{aligned}$$

where $M = (1 + \epsilon q)x + \epsilon^{1/4}\psi(X,T)$. The amplitude is given by $a_0^2 = \frac{r_2 - 4q^2}{D}$ where $D = \frac{108\sigma - 152s^2\sigma + 9b}{36\sigma}$ (as in §5.3). In addition, $a(X,T)$ represents disturbances to the amplitude of

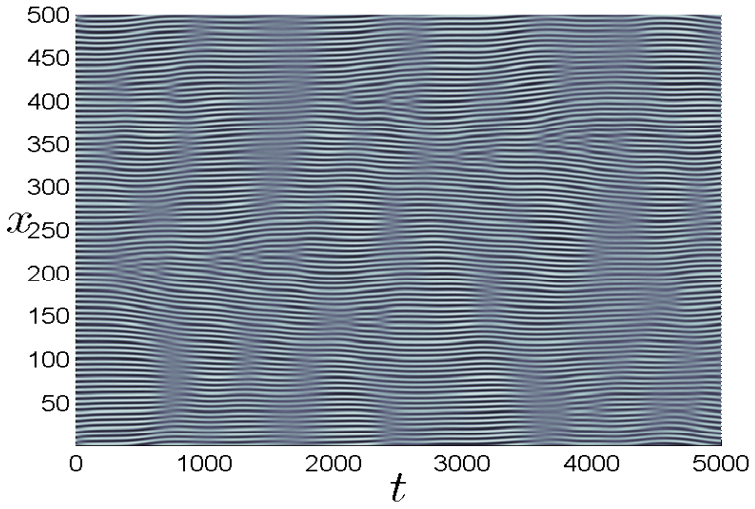

(a) $k = 0.96$

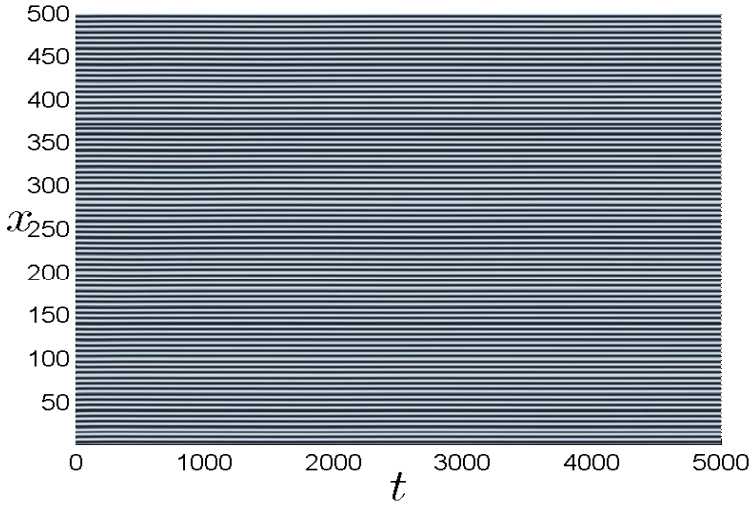

(b) $k = 1.005$

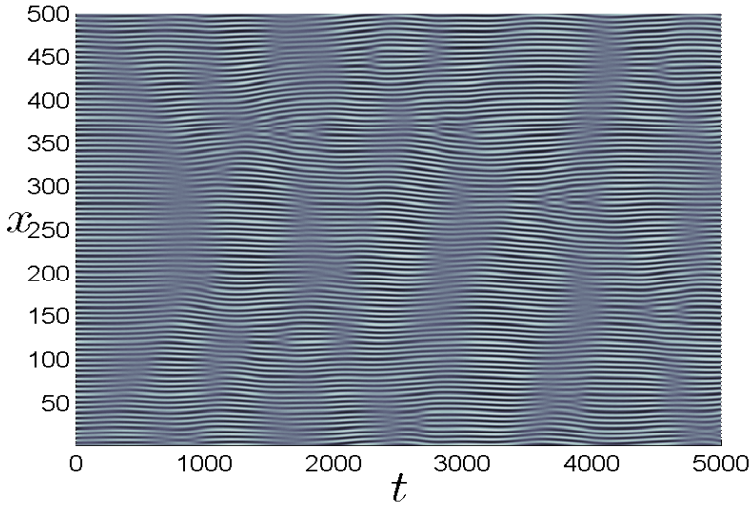

(c) $k = 1.04$

Figure 5.12: Same as figure 5.8 with parameter values $b = 4$, $s = 0.2$, $\sigma = 2$ and $r = 0.01$.

the pattern, $\psi(X,T)$ represents corresponding disturbances to the phase of the pattern and $f(X,T)$ is a large-scale mode. From the expansions of w and u, the pattern and large-scale modes are the leading terms in w and u, respectively.

The coupled amplitude equations appear at $O(\epsilon^{11/4})$, $O(\epsilon^{13/4})$ and $O(\epsilon^3)$ (from solvability conditions) as follows:

$$\begin{aligned}\frac{\partial\psi}{\partial T} &= 4\frac{\partial^2\psi}{\partial X^2} - f,\\ \frac{\partial f}{\partial T} &= \sigma\frac{\partial^2 f}{\partial X^2} + 2ba_0\frac{\partial a}{\partial X},\\ \frac{\partial a}{\partial T} &= 4\frac{\partial^2 a}{\partial X^2} - 4a_0\left(\frac{\partial\psi}{\partial X}\right)^2 - 8a_0q\frac{\partial\psi}{\partial X}.\end{aligned}$$

These equations are similar to the amplitude equations in [14, 40, 54] but with the absence of damping and dispersion. In fact by taking $b=-1$ and $\sigma=1$ we obtain the same equations (see §4.5).

In order to study the stability of rolls, we first write the above amplitude equations as follows:

$$\begin{aligned}\left(\frac{\partial}{\partial T} - 4\frac{\partial^2}{\partial X^2}\right)\psi &= -f,\\ \left(\frac{\partial}{\partial T} - \sigma\frac{\partial^2}{\partial X^2}\right) f &= 2ba_0\frac{\partial a}{\partial X},\\ \left(\frac{\partial}{\partial T} - 4\frac{\partial^2}{\partial X^2}\right) a &= -4a_0\left(\frac{\partial\psi}{\partial X}\right)^2 - 8a_0q\frac{\partial\psi}{\partial X}.\end{aligned}$$

Then we reduce them to the following nonlinear phase equation:

$$\left(\frac{\partial}{\partial T} - 4\frac{\partial^2}{\partial X^2}\right)^2\left(\frac{\partial}{\partial T} - \sigma\frac{\partial^2}{\partial X^2}\right)\psi = 16ba_0^2\left(\frac{\partial\psi}{\partial X} + q\right)\frac{\partial^2\psi}{\partial X^2}. \tag{5.8}$$

Linearising this equation and putting $\psi = \bar{\psi}e^{\mathrm{i}LX+\Lambda T}$, gives the dispersion relation

$$\Lambda^3 + (\sigma+8)\Lambda^2L^2 + (8\sigma+16)\Lambda L^4 + 16\sigma L^6 + 16ba_0^2qL^2 = 0. \tag{5.9}$$

It is useful for the following analysis to note that L appears at even powers and thus we can restrict our attention to positive L. However, for q and b this is not the case (odd powers occur), hence we need to consider all possible values.

In order to study the stability of rolls we need to consider the dispersion relation (5.9) for general L. Before proceeding to this, we shall begin by considering the two limiting cases of small and large L, which provide helpful information about the stability. If L is small, then $\Lambda^3 \sim -16ba_0^2qL^2$. Thus to leading-order in L, $\Lambda = \Lambda_{2/3}L^{2/3}$ and hence $\Lambda_{2/3}^3 = -16ba_0^2q$. This means that we expect stationary instability if $bq<0$ and oscillatory instability if $bq>0$. This analysis shows that rolls are unstable to small-L disturbances, provided a_0^2q is not small.

However, we will see in the next section that some rolls are stable with wavenumber close to 1 and with certain values of the parameters.

On the other hand, if L is sufficiently large, then we have $\Lambda^3 + (\sigma+8)\Lambda^2 L^2 + (8\sigma + 16)\Lambda L^4 + 16\sigma L^6 \approx 0$. Thus $\Lambda \approx -\sigma L^2$ or $-4L^2$ (twice), which shows that rolls are stable to large-L disturbances (since $\sigma > 0$).

Now we provide more information about the stability by considering general L and finding the secondary stability boundaries. Firstly, we find the oscillatory instability boundary, thus we set $\Lambda = \mathrm{i}\Omega$ and substitute in the dispersion relation (5.9). After comparing the real and imaginary parts, the following is obtained:

$$\begin{aligned} \Omega^3 - (8\sigma+16)\Omega L^4 &= 0, \\ \Omega^2 - \frac{16\sigma L^4}{\sigma+8} - \frac{16ba_0^2 q}{\sigma+8} &= 0. \end{aligned}$$

Eliminating Ω between these two equations gives

$$2ba_0^2 q - (\sigma+4)^2 L^4 = 0. \tag{5.10}$$

Therefore

$$L^4 = \frac{2bqa_0^2}{(\sigma+4)^2}.$$

When $b > 0$, there is oscillatory instability of rolls with $0 < q < \frac{\sqrt{r_2}}{2}$ with unstable disturbances satisfying $0 < L < \left(\frac{2bqa_0^2}{(\sigma+4)^2}\right)^{1/4}$. On the other hand, if $b < 0$, then there is oscillatory instability to disturbances having $0 < L < \left(\frac{2bqa_0^2}{(\sigma+4)^2}\right)^{1/4}$, where $-\frac{\sqrt{r_2}}{2} < q < 0$. Thus the stability of rolls with a particular wavenumber depends on the sign of b.

Secondly, we find the monotonic instability boundary. Hence let $\Lambda = 0$ and substitute in the dispersion relation (5.9), then we obtain

$$\sigma L^4 + ba_0^2 q = 0. \tag{5.11}$$

Thus

$$L^4 = \frac{-bqa_0^2}{\sigma}.$$

Therefore, if $b < 0$, then the monotonic instability exists if $0 < q < \frac{\sqrt{r_2}}{2}$ with the unstable disturbances $0 < L < \left(\frac{-bqa_0^2}{\sigma}\right)^{1/4}$. If $b > 0$, then we have monotonic instability if $-\frac{\sqrt{r_2}}{2} < q < 0$ with unstable disturbances satisfying $0 < L < \left(\frac{-bqa_0^2}{\sigma}\right)^{1/4}$. Here also the result depends on b. Table 5.1 summarises the monotonic and oscillatory instability regions for $b < 0$ and $b > 0$.

Note that these results agree with the Nikolaevskiy equation when $b = -1$ and $\sigma = 1$ (see §2.3.2).

	$-\sqrt{r_2}/2 < q < 0$	$0 < q < \sqrt{r_2}/2$
$b < 0$	oscillatory instability for $0 < L < \left(\frac{2bqa_0^2}{(\sigma+4)^2}\right)^{1/4}$	monotonic instability for $0 < L < \left(\frac{-bqa_0^2}{\sigma}\right)^{1/4}$
$b > 0$	monotonic instability for $0 < L < \left(\frac{-bqa_0^2}{\sigma}\right)^{1/4}$	oscillatory instability for $0 < L < \left(\frac{2bqa_0^2}{(\sigma+4)^2}\right)^{1/4}$

Table 5.1: The instability regions of (5.8) for $b < 0$ and $b > 0$.

In (5.10) and (5.11), it is useful to put $a_0 = b_0 r_2^{1/2}$, $L = L' r_2^{3/8}$ and $q = q' r_2^{1/2}$ to obtain a general result, which does not depend on r_2. Then these equations can be rewritten as

$$\begin{aligned} 2bb_0^2 q' - (\sigma+4)^2 L'^4 &= 0, \\ \sigma L'^4 + bb_0^2 q' &= 0. \end{aligned}$$

Accordingly, the monotonic and oscillatory instability boundaries are shown in (q', L') parameter space in figures 5.13 and 5.14. The values of the parameters are $s = 0.2$ and $\sigma = 1$, where $b = -1$ and $b = 1$ in figures 5.13 and 5.14, respectively. As can be seen in these two figures, when b changes sign the two instability boundaries (monotonic and oscillatory) exchange places, which is also the case in the numerical secondary stability plots in §5.5. Furthermore, for small-L' disturbances rolls are unstable regardless of the values of b and σ. Also for large-L' disturbances, where rolls are stable, the result does not depend on the values of b and σ. By contrast the instability boundaries for general L' are affected by the sign of b. If $b < 0$, then the position of the instability boundaries is the same as the Nikolaevskiy equation.

In conclusion, the stability analysis in this section predicts that all rolls are unstable at onset, provided that $a_0^2 bq \neq 0$. This result is universal, meaning that it is insensitive to the parameter values b, s and σ; this also applies to the Nikolaevskiy equation [72]. In addition to this, the result agrees with that of chapter 3 for systems similar to the Nikolaevskiy equation. However, this analysis is strictly valid only if $a_0^2 bq$ is not small; if $a_0^2 bq$ is small, then the scaling used here needs to be reconsidered. In the next section we investigate the case of small $a_0^2 bq$ by considering the situation of q being small. We will see that some rolls with wavenumber close to 1 with certain choices of the parameters are stable. We are not

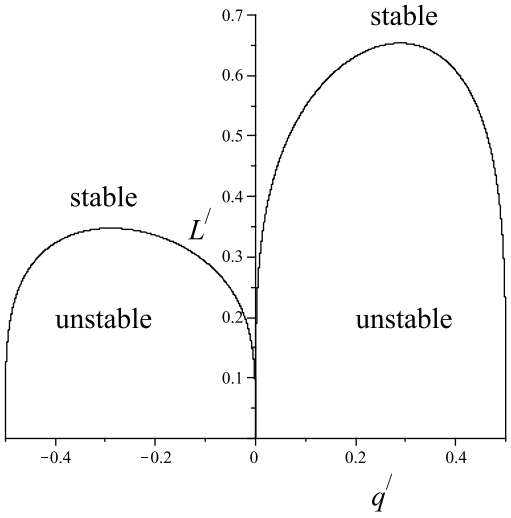

Figure 5.13: The stability boundaries of rolls according to (5.8) with $b = -1$, $s = 0.2$ and $\sigma = 1$. We have monotonic instability on the right and oscillatory on the left.

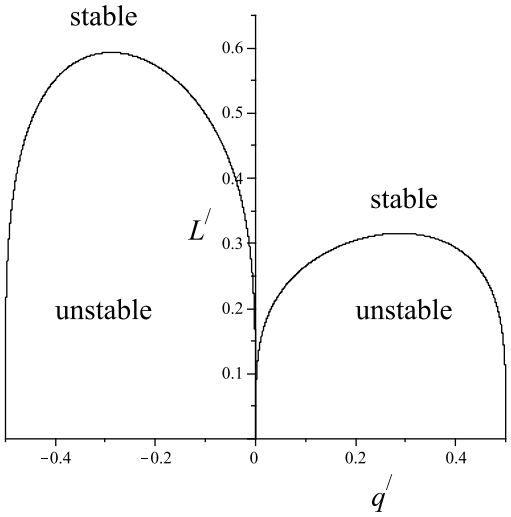

Figure 5.14: The stability boundaries of rolls according to (5.8) with $b = 1$, $s = 0.2$ and $\sigma = 1$. We have oscillatory instability on the right and monotonic on the left.

going to study the case of a_0^2 being small, since the secondary stability diagrams calculated numerically, in §5.5, provide us with the fact that there are no stable rolls close to the marginal stability curve.

5.8 Secondary stability of stationary rolls with wavenumber close to the critical value

In the previous section we found that all rolls with wavenumber $k = 1 + \epsilon q$ are expected to be unstable. However, this prediction is no longer valid for wavenumbers much closer to 1,

when q in this expression is small. Thus in this section we investigate the stability of such rolls by considering a different scaling which was originally used in [72], and then in [14, 54] (see also §4.6.1). Accordingly, the wavenumber is $k = 1 + \epsilon^2 q$.

First, we introduce the following expansions, which provide a distinguished balance in the weakly nonlinear regime

$$\begin{aligned} w &= \epsilon(a_0 + \epsilon^2 a(X,T))e^{\mathrm{i}M} + c.c. + \cdots, \\ u &= \epsilon^2 \frac{\mathrm{i}ba_0^2}{4\sigma} e^{2\mathrm{i}M} + c.c. + \epsilon^3 f(X,T) + \cdots, \end{aligned}$$

with $X = \epsilon x$ and $T = \epsilon^2 t$. In addition, the amplitude is now given by $a_0^2 = \frac{36r_2\sigma}{108\sigma - 152s^2\sigma + 9b}$ and $M = (1+\epsilon^2 q)x + \epsilon\psi(X,T)$.

After substituting these expansions in (5.1) and (5.2), the system is solved at successive powers of $O(\epsilon)$. Subsequently, the amplitude equations result from solvability conditions as follows:

$$\begin{aligned} &\frac{\partial \psi}{\partial T} = 4\frac{\partial^2 \psi}{\partial X^2} - f, \\ &\frac{\partial f}{\partial T} = \sigma \frac{\partial^2 f}{\partial X^2} + 2ba_0 \frac{\partial a}{\partial X}, \\ &\frac{\partial a}{\partial T} = 4\frac{\partial^2 a}{\partial X^2} - 4a_0 \left(\frac{\partial \psi}{\partial X}\right)^2 - 2r_2 a + 4a_0 \left(-2q + \frac{\partial^2}{\partial X^2} - \frac{8}{27}s^2 a_0^2\right)\frac{\partial \psi}{\partial X}. \end{aligned}$$

Unlike the amplitude equations found in [14, 54], the term involving f_X does not arise in the third equation, which results from (5.1). This is because in the Nikolaevskiy equation we had only one variable (u), which contains both the pattern and large-scale modes. Therefore, the term uu_x, in the Nikolaevskiy equation, and the particular order of f will result in the appearance of the term f_X in the third amplitude equation in [14, 54]. On the other hand, in (5.1) and (5.2) we have two variables w and u, where in the expansion of u, f appears at one of the leading-orders. Moreover, the third amplitude equation results from (5.1), which does not have the term uu_x. Therefore, the term f_X will not arise in the third amplitude equation. Other than this missing term, the other ones found in [14, 54] appear in our equations.

The next step in studying the stability of stationary waves is to combine these amplitude equations into the nonlinear phase equation

$$\begin{aligned} &\left(\frac{\partial}{\partial T} - 4\frac{\partial^2}{\partial X^2}\right)\left(\frac{\partial}{\partial T} - 4\frac{\partial^2}{\partial X^2} + 2r_2\right)\left(\frac{\partial}{\partial T} - \sigma\frac{\partial^2}{\partial X^2}\right)\psi = 16ba_0^2 \frac{\partial \psi}{\partial X}\frac{\partial^2 \psi}{\partial X^2} \\ &+ 8ba_0^2\left(2q - \frac{\partial^2}{\partial X^2} + \frac{8}{27}s^2 a_0^2\right)\frac{\partial^2 \psi}{\partial X^2}. \end{aligned} \tag{5.12}$$

Then we linearise and seek solutions proportional to $e^{\mathrm{i}LX + \Lambda T}$ to obtain the dispersion relation

$$\begin{aligned} &\Lambda^3 + (8+\sigma)\Lambda^2 L^2 + 2r_2\Lambda^2 + 8(2+\sigma)\Lambda L^4 + 2r_2(4+\sigma)\Lambda L^2 + 16\sigma L^6 + 8r_2\sigma L^4 + 8ba_0^2 L^4 \\ &+ 16ba_0^2 q L^2 + \frac{64}{27}s^2 ba_0^4 L^2 = 0. \end{aligned} \tag{5.13}$$

In this equation we can restrict attention to positive L. However, we must consider positive and negative values for q and b.

In the following analysis, we investigate the stability of stationary wave solutions according to (5.13). Before answering the stability question for general L, it is instructive to consider the two cases of large and small-L disturbances. For large-L disturbances, we have stability (the same as in §5.7).

Before giving details of the analysis regarding small-L disturbances, we elucidate the result in figure 5.15, which shows where rolls are expected to be unstable for $b<0$ and $b>0$ for small L. Let L be small, expand $\Lambda=\Lambda_1 L+\Lambda_2 L^2+\cdots$ and substitute in (5.13). Thus we obtain

$$\begin{aligned}\Lambda_1 &= \pm\frac{2a_0\sqrt{-6r_2b(27q+4a_0^2s^2)}}{9r_2},\\ \Lambda_2 &= \frac{2ba_0^2(27q+4s^2a_0^2)}{27r_2^2}-\frac{\sigma+4}{2}.\end{aligned}$$

From Λ_1, if $b(27q+4a_0^2s^2)<0$, then the rolls are unstable. Since b is allowed to take either sign, then we have two cases. If $b<0$, then the rolls are unstable ($b(27q+4a_0^2s^2)<0$) provided that $q>-\frac{4a_0^2s^2}{27}$. If $b>0$, then $b(27q+4a_0^2s^2)<0$ (unstable rolls) only if $q<-\frac{4a_0^2s^2}{27}$.

Otherwise, if $b(27q+4a_0^2s^2)>0$, then Λ_1 is purely imaginary and hence we need to consider Λ_2. At the borderline case $q=-\frac{4a_0^2s^2}{27}$, $\Lambda_2=-\frac{\sigma+4}{2}$, which will result in stability. Let us consider first the case $b<0$, so that $q<-\frac{4a_0^2s^2}{27}$. As we decrease q, Λ_2 increases because $b(27q+4a_0^2s^2)>0$. Correspondingly, Λ_2 will change its sign and thus the rolls will develop instability. On the other hand, let $b>0$ and $q>-\frac{4a_0^2s^2}{27}$. If we increase q, then Λ_2 increases because $b(27q+4a_0^2s^2)>0$. Ultimately, again Λ_2 will change its sign for sufficiently large q; and thus we get instability. In conclusion, if $b(27q+4a_0^2s^2)>0$, then rolls are unstable if $b<0$ and $q<-\frac{4a_0^2s^2}{27}+\frac{r_2^2(\sigma+4)}{4ba_0^2}$ or if $b>0$ and $q>-\frac{4a_0^2s^2}{27}+\frac{r_2^2(\sigma+4)}{4ba_0^2}$. This result is illustrated in figure 5.15.

After predicting that all rolls are stable to disturbances for large L and that some are stable for small L, we now consider general L to find the stability boundaries. To calculate the oscillatory instability boundary let $\Lambda=\mathrm{i}\Omega$ and substitute in (5.13), therefore we obtain from the real and imaginary parts

$$\begin{aligned}\Omega^3-8(\sigma+2)\Omega L^4-2r_2(4+\sigma)\Omega L^2 &= 0,\\ (2r_2+(\sigma+8)L^2)\Omega^2-16\sigma L^6-8r_2\sigma L^4-8ba_0^2L^4-16ba_0^2qL^2-\frac{64}{27}s^2ba_0^4L^2 &= 0.\end{aligned}$$

Eliminating Ω between these two equations gives

$$\begin{aligned}&-864\sigma L^4-432r_2\sigma L^2+108ba_0^2L^2+216ba_0^2q+32s^2ba_0^4-108\sigma^2L^4-1296r_2L^2-1728L^4\\ &-216r_2^2-54r_2^2\sigma-27r_2\sigma^2L^2=0.\end{aligned}\tag{5.14}$$

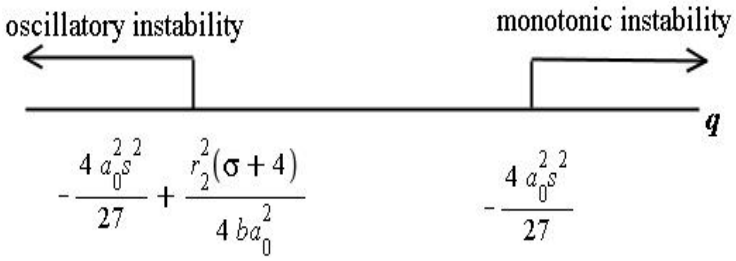

(a) $b < 0$.

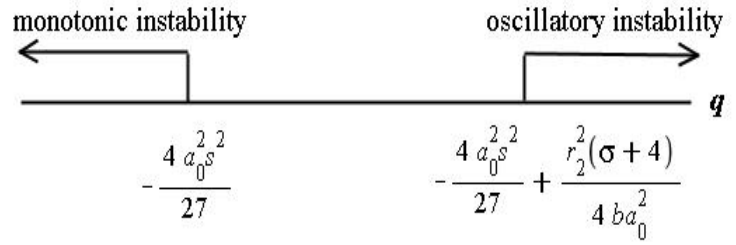

(b) $b > 0$.

Figure 5.15: Diagram showing for small-L disturbances where the rolls are unstable according to (5.12) for the two cases of (a) $b < 0$ and (b) $b > 0$.

It is convenient to eliminate r_2 from the previous equation by introducing $b_0^2 = a_0^2/r_2$, $L' = L/\sqrt{r_2}$ and $q' = q/r_2$. Thus (5.14) may be rewritten in the form

$$q' = A + BL'^2 + CL'^4 \equiv q'_o(L'), \tag{5.15}$$

where the parameters are given by

$$\begin{aligned} A &= -\frac{4s^2b_0^2}{27} + \frac{\sigma+4}{4bb_0^2}, \\ B &= \frac{(\sigma+8)^2-16}{8bb_0^2} - \frac{1}{2}, \\ C &= \frac{(\sigma+4)^2}{2bb_0^2}. \end{aligned}$$

This equation gives the oscillatory stability boundary of the rolls.

For calculating the monotonic instability boundary, let $\Lambda = 0$ and substitute in (5.13), which implies

$$2\sigma L^4 + r_2\sigma L^2 + ba_0^2L^2 + 2ba_0^2q + \frac{8}{27}s^2ba_0^4 = 0.$$

Similarly to (5.15), this equation can also be rescaled as follows:

$$q' = \bar{A} + \bar{B}L'^2 + \bar{C}L'^4 \equiv q'_m(L'), \tag{5.16}$$

but here

$$\begin{aligned}\bar{A} &= -\frac{4s^2b_0^2}{27},\\ \bar{B} &= -\frac{bb_0^2+\sigma}{2bb_0^2},\\ \bar{C} &= -\frac{\sigma}{bb_0^2}.\end{aligned}$$

Depending on all of the aforementioned analysis we are now interested in finding the domain of stability for general L'. Therefore, we must study the properties of the oscillatory and monotonic instability boundaries. We begin by considering large and small-L' disturbances. We already know that if L' is large, then all rolls are stable and the oscillatory instability boundary satisfies

$$q_o'(L') \to \begin{cases} \infty & \text{if } b>0\\ -\infty & \text{if } b<0,\end{cases}$$

whereas for the monotonic instability boundary we have

$$q_m'(L') \to \begin{cases} \infty & \text{if } b<0\\ -\infty & \text{if } b>0.\end{cases}$$

This means that when $b>0$, the oscillatory instability boundary will point to the right and the monotonic instability boundary will point to the left, and vice versa for $b<0$ (see figure 5.16). Note that this result agrees with the previous scaling in §5.7 (middle parts of figures 5.13 and 5.14). On the other hand, for small L' rolls are stable provided that $-\frac{4s^2b_0^2}{27}+\frac{\sigma+4}{4bb_0^2} < q' < -\frac{4b_0^2s^2}{27}$ for $b<0$ (see figure 5.15(a)). If $b>0$, then rolls are stable if $-\frac{4b_0^2s^2}{27} < q' < -\frac{4s^2b_0^2}{27}+\frac{\sigma+4}{4bb_0^2}$ (see figure 5.15(b)).

Now we consider general L' and examine the shape of the stability boundaries, which will result in determining the condition for a stable interval to exist. To do this, first suppose that $b<0$, thus in (5.15) the point of intersection with the q'-axis is $q'=-\frac{4s^2b_0^2}{27}+\frac{\sigma+4}{4bb_0^2}$ (negative). Moreover, B and C are negative and therefore the oscillatory instability boundary is a curve similar to the dashed curve in figures 5.16(a), (b) and (c). Now in (5.16) the monotonic instability boundary intersects the q'-axis at the point $q'=-\frac{4s^2b_0^2}{27}$ (negative), which lies to the right of the oscillatory instability boundary. In addition, $\bar{C}$ is positive, and hence if $\bar{B}$ is positive we obtain a curve similar to the solid curve in figure 5.16(a). On the other hand, if $\bar{B}$ is negative we obtain a curve similar to the solid curves in figures 5.16(b) and (c).

If instead $b > 0$, by considering the point of intersection with the q'-axis in (5.15) and (5.16), the monotonic instability boundary is now on the left of the oscillatory instability boundary. Indeed, the point of intersection with the q'-axis is always negative for the monotonic instability boundary and either positive or negative for the oscillatory instability boundary. In addition, in (5.15), C is positive and therefore if B is positive we obtain a curve similar to the dashed curve in figure 5.16(d). By contrast, if B is negative we obtain a curve similar to the dashed curves in figures 5.16(e) and (f). In (5.16), $\bar{B}$ and $\bar{C}$ are negative, and hence we obtain a curve similar to the solid curve in figures 5.16(d), (e) and (f).

It is convenient to summarise the results by sketching all possible types of stability boundaries; and these are demonstrated in figure 5.16. In all cases we need to consider the minimum and the maximum values of q on these boundaries, by using (5.15) and (5.16), in order to find the stable region. We are going to give the condition of stability first for $b < 0$. In the straightforward case, in figure 5.16(a) the band of stability lies between the minimum and the maximum points of the right and left instability boundaries. This region simply lies between the points of intersection with the q'-axis ($-\frac{4s^2b_0^2}{27} + \frac{\sigma+4}{4bb_0^2} < q' < -\frac{4s^2b_0^2}{27}$). On the other hand, if we want to find the stable region in figures 5.16(b) and (c), then we need to calculate the minimum value of the monotonic instability boundary curve and the maximum value of the oscillatory instability. The latter is given by the point of intersection of the oscillatory instability with the q'-axis. If the minimum value of the monotonic instability is greater than the point of intersection of the oscillatory instability with the q'-axis, then the stable region exists (see figure 5.16(b)). On the other hand, if the minimum value of the monotonic instability is less than the point of intersection of the oscillatory instability with the q'-axis, then there is no stable region, as shown in figure 5.16(c).

To summarise, either the stable region is clear, as in figure 5.16(a), or does not exist (see figure 5.16(c)) or needs to be calculated as in figure 5.16(b). The result is similar when $b > 0$, which is illustrated in figures 5.16(d)–(f). It can be concluded that regardless of the sign of b, we have three cases of instabilities, as demonstrated in figure 5.16. We shall refer to the type of stability boundary exhibited in figure 5.16(a) as "type (a) stability boundary" and the type of stability boundary shown in figure 5.16(b) as "type (b) stability boundary" and so on.

After studying the stability of rolls, we now provide some examples to clarify the analysis. The first example given is of type (c) stability boundary. Let $b = -10$, $s = 0.8$ and $\sigma = 10$ (see figures 5.17(a)–(c)). Therefore, from the previous analysis we expect rolls to be stable for large L' and the stable region for small L' exists if $-2.0012 < q' < -1.9845$. However, from (5.16) $\bar{B}$ and $\bar{C}$ have different signs and so we expect that this region may not be valid for general L'. Therefore, we need to calculate the minimum value of the monotonic

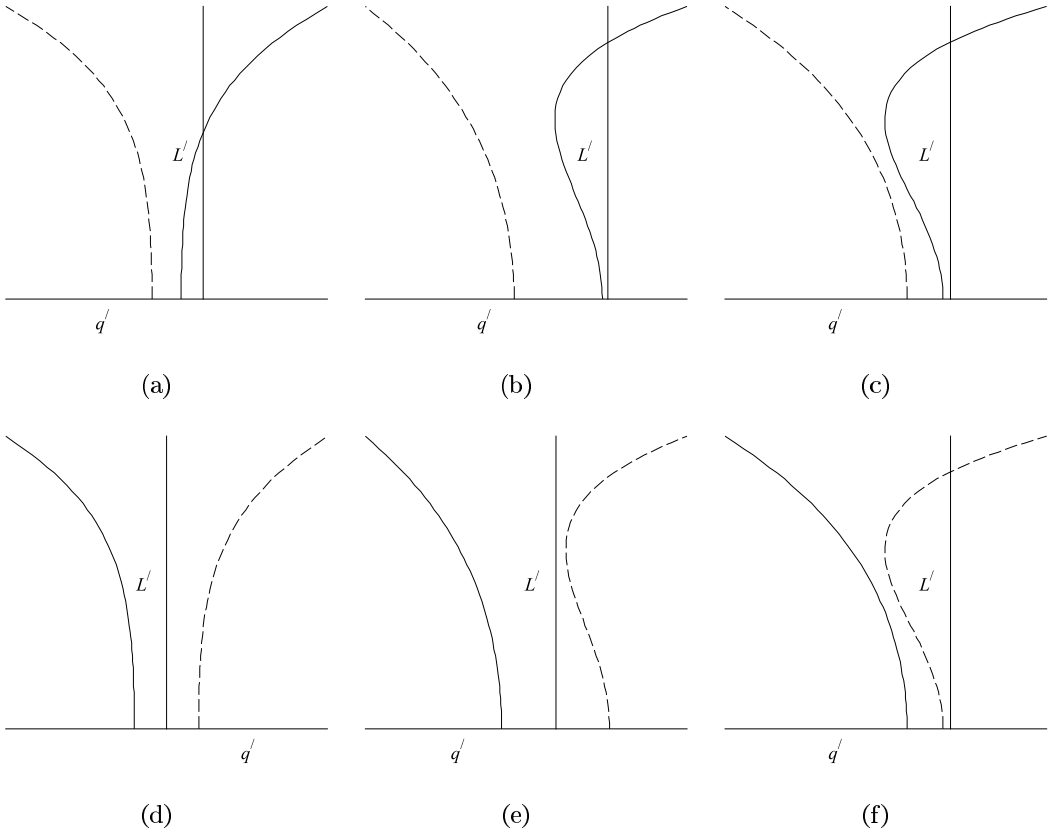

Figure 5.16: General plots which are indicative of the possible forms of the stability boundaries of rolls regarding (5.12), where the stable region lies between the dashed and solid lines. Here the solid curves represent the monotonic instability boundaries and the dashed curves represent the oscillatory instability boundaries. Graphs (a)–(c) correspond to the case $b < 0$ and graphs (d)–(f) correspond to the case $b > 0$. In each of the two cases we have three forms of the stability boundaries.

instability boundary, which is $q' = -3.1706$ when $L' = 2.2322$. This means that in the region $-2.0012 < q' < -1.9845$ some rolls are unstable. Hence for general L' there are no stable rolls, and this is demonstrated in figures 5.17(a)–(c).

On the other hand, if we change the sign of b ($b = 10$), then we get type (d) stability boundary where the stable region lies between the two points of intersection with the q'-axis. This implies that rolls are stable for general L' if $-0.1731 < q' < 0.0186$. This is confirmed by the shape of stability boundary in figure 5.17(d).

We now give some examples with $s = 0$ and $\sigma = 1$. First, in figures 5.17(e)–(g), we choose $b = -5$, then for small L' the stable region exists for $-0.4375 < q' < 0$. However, this is a type (b) stability boundary and we need to calculate the minimum point of the monotonic instability boundary, which is $q' = -0.0754$ when $L' = 0.6814$. Thus the stable region for general L' is $-0.4375 < q' < -0.0754$. If instead we take $b = -1$, from figure

5.17(h), the stable region lies between the points of intersections with the q'-axis (type (a) stability boundary). Thus the stable region exists for $-3.4375 < q' < 0$.

The final two examples we take, to cover all types of stability boundaries, are for a fixed $s = 1$ (see figures 5.17(i) and (j)). In this case we must choose positive values of b to get supercritical rolls (see figure 5.2). Let $b = 20$ and $\sigma = 4$, then the stable region for small L' is $-5.3333 < q' < -5.3306$. The minimum value of the oscillatory instability boundary occurs at the point $q' = -6.6146$ and $L' = 2.3184$, whereas the maximum value of the monotonic instability boundary is the point $q' = -5.3333$ and $L' = 0$. This implies that there are no stable rolls, and this is shown in figure 5.17(i) (type (f) stability boundary). If we choose $b = 40$ and $\sigma = 5$, then the stable region for small L' exists for $-0.1905 < q' < -0.1467$; and this is a type (e) stability boundary (see figure 5.17(j)). Therefore, the stable region for general L' is valid when $-0.1905 < q' < -0.1519$.

In conclusion, the theoretical results found here agree with the stability diagrams in §5.5 for small r, where the numerical plots are covered by all types of stability boundaries found in this section. Indeed, figures 5.4(a)–(c) correspond to type (a) and (d) stability boundaries. The stability analysis reflects on the lower part of these plots, which are a half Eckhaus-like stable region. Moreover, the secondary stability plots are expected to develop long-wavelength instability (see figure 5.5). On the other hand, in figure 5.4(d) we have type (b) stability boundary and the secondary stability plots are expected to develop long-wavelength and finite-wavelength instabilities (see figure 5.6). Finally, figure 5.4(e) is a type (c) stability boundary, which predicts that there are no stable rolls. This agrees with figure 5.4(e) for small r, since in this figure the stable region exists for $r > 0.0021$.

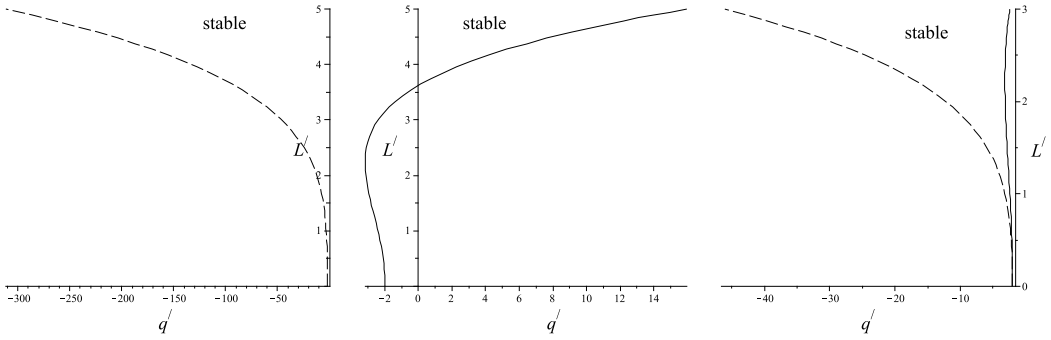

(a) $b = -10$, $s = 0.8$, $\sigma = 10$.

(b) $b = -10$, $s = 0.8$, $\sigma = 10$.

(c) $b = -10$, $s = 0.8$, $\sigma = 10$.

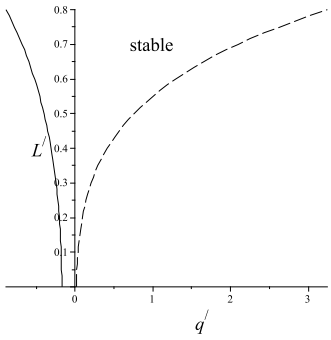

(d) $b = 10$, $s = 0.8$, $\sigma = 10$.

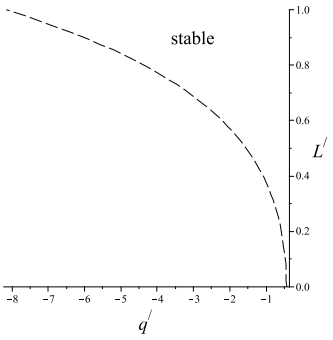

(e) $b = -5$, $s = 0$, $\sigma = 1$.

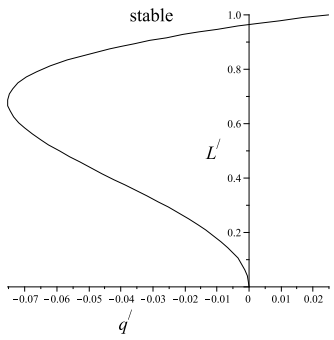

(f) $b = -5$, $s = 0$, $\sigma = 1$.

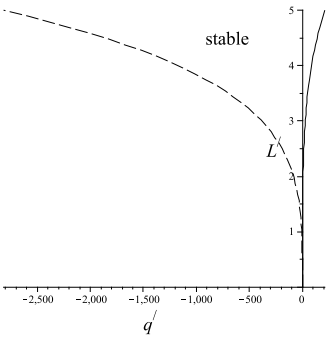

(g) $b = -5$, $s = 0$, $\sigma = 1$.

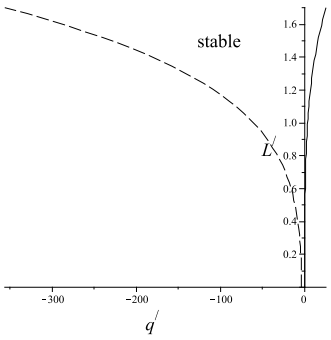

(h) $b = -1$, $s = 0$, $\sigma = 1$.

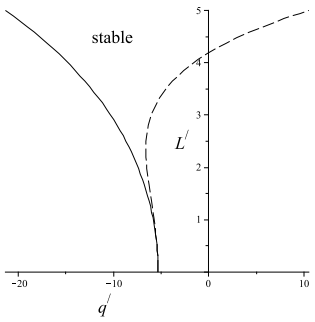

(i) $b = 20$, $s = 1$ and $\sigma = 4$.

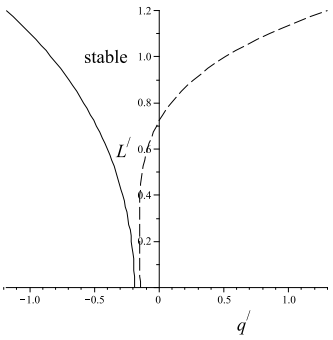

(j) $b = 40$, $s = 1$ and $\sigma = 5$.

Figure 5.17: The stability boundaries obtained from (5.12) with parameter values as indicated under each figure. The dashed curves represent the oscillatory instability boundary and the solid curves represent the monotonic instability boundary.

5.9 Discussion

In this chapter we found that the nonlinear behaviour of the Swift-Hohenberg equation is strongly influenced by the coupling with the Goldstone mode. This result was achieved through asymptotic and numerical calculations.

After applying a weakly nonlinear regime to (5.1) and (5.2) and using the same scaling as the Nikolaevskiy equation, we derived amplitude equations for chaotic dynamics, which are similar to those found in [40]. However, they depend on the value of the diffusion term (σ) in (5.2) and we know from chapter 3 that this can significantly influence the behaviour of the solutions.

The secondary stability plots were calculated numerically. Due to the numerous parameters in (5.1) and (5.2) which control the stability, it is difficult to construct general plots covering all possible cases. Instead, some plots were generated for specific values of the parameters. The secondary stability diagrams were compared to some numerical simulations, which provide remarkably good agreement. Furthermore, some of the simulations manifest features similar to the Nikolaevskiy chaos.

In our analytical treatment of the secondary stability of rolls we concluded that, for small enough r, all rolls are predicted to be unstable, expect those with wavenumber close to 1; for such rolls there may be a thin region of stability. This result agrees with the secondary stability plots calculated numerically.

Our analysis of the stability of rolls reveals stability boundaries different from those present in the Nikolaevskiy equation. By carefully considering all possible values of the parameters we found three types of stability boundaries, regardless of the sign of b. Type (a) and (b) stability boundaries predict that stable rolls exist. By contrast, this type of stability boundary is not present in the Nikolaevskiy equation, since all rolls are unstable at onset. On the other hand, also we have type (c) stability boundary which predicts that all rolls are unstable at onset, and this agrees with the Nikolaevskiy equation. To summarise, for certain values of the parameters, stable rolls may be observed, in contrast to the Nikolaevskiy equation.

Chapter 6

Conclusions

The current study set out to analyse the Nikolaevskiy equation, which satisfies continuous symmetries and represents a coupling between finite-wavelength instability and a Goldstone mode. Moreover, it has rich dynamical properties and is considered as a simple model exhibiting spatiotemporal chaos. Therefore, studying this equation sheds light on our understanding of such systems exhibiting chaos and complexity. We studied a dispersive version of this equation in addition to similar systems with the same symmetries and possessing the property that finite-wavelength patterns are coupled to a large-scale mode. The results are corroborated by numerical calculations in addition to asymptotic treatments of this equation and similar models.

In chapter 3 we generalised the instability of all roll solutions of the Nikolaevskiy equation at onset to any model having the same symmetries with coupling between finite-wavelength patterns and a Goldstone mode; and this result is only applicable to wave solutions of such systems with wavenumbers neither close to the marginal stability curve nor close to the critical wavenumber. Furthermore, we also generalised the amplitude equations of the Nikolaevskiy equation by replacing the coefficient of the diffusion term in these equations by a general positive variable n. We concluded from numerical simulations, in relatively small domains, that the behaviour of these general amplitude equations is analogous to amplitude equations of the Nikolaevskiy equation. This behaviour is manifested through a concurrent existence of amplitude-death and single-front states. However, the statistical measures of these states are highly dependent on the value of n. This research has thrown up a question in need of further investigation, which is about examining these amplitude equations analytically and exploring how the result is applicable to full numerical simulations of Nikolaevskiy-like PDEs.

The key point of this study is the Nikolaevskiy equation with dispersion. In contrast to most studies of the Nikolaevskiy equation, we restored the dispersive terms and studied

the influence on the behaviour and properties of the solution in chapter 4. Indeed, the research consists of analysing the stability of travelling wave solutions for different degrees of dispersion through asymptotic expansions. One of the significant findings to emerge from this research is that the instability of all spatially periodic solutions at the onset of pattern formation in the non-dispersive version is modified by the presence of dispersion. To be more specific, there exists an Eckhaus-like stability region near the onset of instability if the dispersion is sufficiently strong. However, the ratio of the width of this stable region to the width of the existence region of rolls is not the same as the usual Eckhaus case. On the other hand, concerning weak dispersion there is a thin region of stability in the vicinity of the critical wavenumber. The asymptotic results agree well with the secondary stability diagrams computed numerically. Furthermore, the numerical stability results show the complicated nature of the secondary stability boundaries, which sensitively depend on the magnitude of the dispersive terms. In fact, rolls predicted to be stable by the asymptotics may turn out to be unstable when the full numerical calculation is performed. This is because the asymptotics concern only long-wavelength instabilities and other finite-wavelength instabilities may arise.

Another investigation point, considered in chapter 4, is the amplitude equations of the dispersive Nikolaevskiy equation. This produced results showing that these equations are similar to the non-dispersive case where there are amplitude-death and single-front states manifested through numerical simulations. However, these structures drift with a certain speed depending on the group velocity, which results from dispersion. We deduced from several numerical simulations done for these amplitude equations, with different values of the group velocity, that there is an almost linear relationship between the front speed and the group velocity. Further studies are suggested on this topic where the results could be achieved analytically and compared to the numerical calculations. In addition to this, more advanced numerical simulations are encouraged, in order to observe other statistical measures regarding the dispersive amplitude equations.

A system coupling a Swift-Hohenberg equation to a large-scale mode, which exhibits the same symmetries as the Nikolaevskiy equation, was studied in chapter 5 by means of numerical and asymptotic approaches. The result of this analysis shows that the Swift-Hohenberg equation is strongly influenced by the coupling with the Goldstone mode. It was expected that the symmetries might force all rolls to be unstable at onset; however, we found that this is not the case with this system. Indeed, there can be stable stationary wave solutions of this system with wavenumber close to the threshold. The numerical stability diagrams show different topologies corresponding to different parameter values; and therefore it is difficult to draw general conclusions from these graphs. Moreover, these graphs are not fully explained by the asymptotic results, which involve only long-wavelength instabilities.

The Nikolaevskiy equation is a very rich model and there are many unanswered questions that should be addressed; therefore further studies on this topic are recommended. One of the significant issues for future research is to consider a two-dimensional version of the Nikolaevskiy equation. Another research interest is applying this equation to other physical phenomena than the known ones. Another open question includes focusing on explaining the numerical behaviour of the Nikolaevskiy equation presented in this thesis, as the analytical results are strictly valid only close to the threshold. Finally, performing further numerical simulations with different boundary conditions is proposed as a future research topic.

Appendix A

Numerical schemes

In this section we introduce numerical schemes used in this thesis to solve the Nikolaevskiy equation and other related systems. We shall present the Fourier spectral method for spatial discretisation along with the exponential time differencing (ETD) method or the exponential time differencing Runge-Kutta (ETDRK) method for time integration of a general nonlinear partial differential equation (PDE). Note that we always impose periodic boundary conditions.

Consider the nonlinear PDE whose solution varies in time and space:

$$\frac{\partial u}{\partial t} = \frac{\partial^m u}{\partial x^m} + F(u,t).$$

Here F is the nonlinear term. In order to solve this system accurately we spatially discretise it by using the Fourier spectral method [7, 10, 21, 67], where the error decreases exponentially as we increase the resolution. This will result in a system of coupled ODEs (ordinary differential equations) in time t:

$$\frac{d\hat{u}_n}{dt} = c\hat{u}_n + \hat{F}(u,t), \tag{A.1}$$

where the discrete Fourier transform of u is

$$u = \sum_{-N/2+1}^{N/2} \hat{u}_n e^{inkx}.$$

Here $k = 2\pi/l$, for some domain length l, and $c = (ink)^m$, which is represented by a diagonal matrix in the Fourier basis. This matrix consists of real values for dissipative systems and imaginary values for dispersive systems.

The nonlinear term $\hat{F}$ is calculated, using the pseudo-spectral procedure, by transforming first to physical space and then carrying out the multiplication before transforming back to spectral space. This is done using the *Matlab* commands *fft* and *ifft*, where *fft* is the fast Fourier transform and *ifft* is the inverse fast Fourier transform. The *fft* reduces the number of operations from $O(N^2)$ (for the discrete Fourier transform) to $O(N \log N)$ [11].

The system of ODEs (A.1) is coupled through the nonlinear term and the linear part is diagonal. If the differentiation matrix (resulting from discretisation) has a wide range of eigenvalues for all Fourier modes or if the system has a spatial derivative higher than the second order, then it is more likely to be stiff. This means that the solution consists of slow and fast components. For example, in the dispersive Nikolaevskiy equation the nonlinear part (uu_x) evolves on a long time scale while u_{xxxxxx} results in a rapid linear decay of the high-wavenumber modes and u_{xxx} causes a rapid linear oscillation of the high-wavenumber modes. Therefore, the dispersive Nikolaevskiy equation is considered stiff; and this also applies to the Nikolaevskiy equation with no dispersion. As a remedy for this problem we need to consider a numerical method with a small step size to cover the range of different time scales of the solution. This results in increasing the number of integration steps and this generates an accumulation of the error. Therefore, we need a procedure that handles the stiffness without requiring a small step size.

For simplicity we shall drop the hats from the variables in (A.1) and write the "n-th" equation as follows:

$$\frac{du}{dt} = cu + F(u,t).$$

One of the methods for solving such a stiff ODE, where the linear part is responsible for stiffness and the nonlinear term evolves on a longer time scale than the linear part, is the ETD method [13]. This scheme permits using a large time step which in turn does not affect the stability (magnification of the error as the calculation proceeds); however, it influences the accuracy. In order to maintain good stability and accuracy we shall consider a higher order ETD scheme which is the ETD2 scheme [4, 13] as a numerical solution for the Nikolaevskiy equation together with the spectral approach.

The formula of the ETD2 method is given by

$$u_{n+1} = u_n e^{ch} + \{[(ch+1)e^{ch} - 2ch - 1]F_n + (-e^{ch} + ch + 1)F_{n-1}\}/(c^2 h).$$

Here h is the time step. For some modes we might have $c = 0$ and in this case we cannot use this scheme directly, since we then divide by zero. Instead we use the limiting form of these coefficients as $c \to 0$. This circumstance actually arises for the zero modes in the Nikolaevskiy equation. A similar case appears for modes with $|ch| \ll 1$; and in this situation we replace the coefficients with their Taylor series.

Another suitable numerical solution for stiff systems is the ETDRK method [13]. Unlike the high-order ETD (multistep) scheme, the ETDRK method does not require the calculation of the previous nonlinear term. In addition to this advantage, it is more accurate, with larger stability regions than the multistep schemes [13]. In some numerical calculations (presented

in this thesis) we shall consider the exponential time differencing fourth-order Runge-Kutta ETD4RK method for better accuracy and stability along with the pseudo-spectral method.

The ETD4RK formula [4, 13, 30] is given as follows:

$$\begin{aligned}
a_n &= u_n e^{ch/2} + (e^{ch/2} - 1)F(u_n, t_n)/c, \\
b_n &= u_n e^{ch/2} + (e^{ch/2} - 1)F(a_n, t_n + h/2)/c, \\
c_n &= a_n e^{ch/2} + (e^{ch/2} - 1)(2F(b_n, t_n + h/2) - F(u_n, t_n))/c, \\
u_{n+1} &= u_n e^{ch} + \{F(u_n, t_n)[-4 - hc + e^{ch}(4 - 3ch + h^2c^2)] \\
&\quad +2(F(a_n, t_n + h/2) + F(b_n, t_n + h/2))[2 + hc + e^{ch}(-2 + hc)] \\
&\quad +F(c_n, t_n + h)[-4 - 3hc - h^2c^2 + e^{ch}(4 - hc)]\}/h^2c^3.
\end{aligned}$$

As with the ETD2 scheme, for some modes we might have $c = 0$ or $|ch| \ll 1$ and in this case we replace the coefficients by their limit as $c \to 0$ if $c = 0$ and by their Taylor series if $|ch| \ll 1$.

To summarise, the Nikolaevskiy equation is considered as a stiff system since it consists of spatial derivatives up to the sixth order in conjunction with a nonlinear term. Therefore, after spatially discretising it we use the ETD2 method in order to generate numerical simulations. In addition to this, we also use the ETD4RK method for the related amplitude equations and systems similar to the Nikolaevskiy equation.

Appendix B

Numerical code for simulating the Nikolaevskiy equation with dispersion

This *Matlab* code numerically simulates the Nikolaevskiy equation with dispersion (4.1) and also with no dispersion (1.2) (a similar code is found in [75]). Note that for the Nikolaevskiy equation with no dispersion we set the parameters *alpha* and *beta*, in the code, to zero. Also note that the parameter values should be changed accordingly to generate the numerical simulations given in this thesis.

```
% Set equation coefficients
r2 = 1;
q = 0;
epsilon = 0.1;
r = epsilon^2*r2;
alpha = 2;
beta = 1;
% Set system parameters
n = 50;            % Winding number for 'tw' initial condition no. of waves
K = 1+epsilon*q;   % wave no.
L = 2*n*pi/K;      % Domain size or length of the box it should be a multiple of
                   % $2*pi$
Tmax = 1000;       % Simulation time
N = 512;           % Number of grid points
dT = 0.05;         % Time step (choose between 0.01 and 0.05)
dps = 1000;        % Number of stored times
ic = 'tw';         % Initial condition: choose 'zero', 'tw', 'uniform' or 'pulse'
```

```
% Whether to continue simulation from final values of previous simulation
co = 0;
% Calculate some further parameters
nmax = round(Tmax/dT);
X = (L/N)*(-N/2:N/2-1)';
nplt = floor(nmax/dps);
% Define initial conditions
if co == 0
Tdata = zeros(1,dps+1);
if strcmp(ic, 'zero')
U = zeros(size(X)) + 10^(-2)*randn(size(X));
elseif strcmp(ic, 'tw')
U = 2*epsilon*sqrt(r2-4*q^2)*sqrt(36+(5*beta-alpha)^2)*cos(K*X)...
   +10^(-2)*randn(size(X));
elseif strcmp(ic, 'uniform')
U = ones(size(X)) + 0.01*randn(size(X));
elseif strcmp(ic, 'pulse')
U = sech((X+10).^2) + 0.8*sech((X-30).^2) + 10^(-2)*randn(size(X));
else
error('invalid initial condition selected')
end
Tdata(1) = 0;
else
U = Udata(:,end);
starttime = Tdata(end);
Tdata = zeros(1,dps+1);
Tdata(1) = starttime;
disp('    CARRYING OVER...')
end
U = U-mean(U);
% Set wavenumbers and data arrays
k = [0:N/2-1 0 -N/2+1:-1]'*(2*pi/L);
k2 = k.*k; k2(N/2+1) = ((N/2)*(2*pi/L))^2;
Udata = zeros(N,dps+1);
U_hatdata = zeros(N,dps+1);
U_hat = fft(U);
```

```
Udata(:,1) = U;
U_hatdata(:,1) = U_hat;
% Compute exponentials and nonlinear factors for ETD2 method
cU = (-1+r)*k2  +2*k2.^2-k2.^3-alpha*i*k2.*k+beta*i*k2.^2.*k;
expU = exp(dT*cU);
nlfacU = (exp(dT*cU).*(1+1./cU/dT)-1./cU/dT-2)./cU;
nlfacUp = (exp(dT*cU).*(-1./cU/dT)+1./cU/dT+1)./cU;
nlfacU(1) = 3*dT/2;
nlfacUp(1) = -dT/2;
% Solve PDE
dataindex = 2;
for n = 1:nmax
T = Tdata(1) + n*dT;
U = real(ifft(U_hat));
U2 = U.*U;
U2hat = fft(U2);
dU2hat = -i*k.*U2hat/2;
% Find nonlinear component in Fourier space
nlU  = dU2hat;
% Setting the first values of the previous nonlinear coefficients
if n == 1
nlUp = nlU;
    end
% Time-stepping
U_hat = U_hat.*expU + nlfacU.*nlU + nlfacUp.*nlUp;
nlUp  = nlU;
U_hat(1) = 0;
% Saving data
if mod(n,nplt) == 0
U = real(ifft(U_hat));
Udata(:,dataindex) = U;
U_hatdata(:,dataindex) = U_hat;
Tdata(dataindex) = T;
dataindex = dataindex + 1;
        plot(X,U);axis([-L/2,L/2,-1.4,1.4]);drawnow;
    end
```

```
% Commenting on time elapsed
if mod(n,floor(nmax/10)) == 0
outp = strcat('  n= ', num2str(n), ' completed'); disp(outp);
end
end
% Plot evolution
figure('position', [200 200 300 350])
surf(X,Tdata,real(Udata).')
view(0,90), shading interp, axis tight
xlabel('x','fontname','courier','fontsize', 20,'color',[0.6 0.6 0.6])
ylabel('t','fontname','courier','fontsize', 20,'color',[0.6 0.6 0.6],...
'rotation', 0)
```

Appendix C

Numerical code for simulating the amplitude equations

This code simulates the generalised amplitude equations (3.2) and (3.3) ($n = 4$ for the Nikolaevskiy equation). It also simulates the amplitude equation of the Nikolaevskiy equation with dispersion (4.21) and (4.22).

```
% modified by SM Cox from...
% AK Kassam and LN Trefethen, July 2002
% Spatial grid and initial condition:
N = 1024;
Le=  150;
rval = 1;    % ALWAYS set to 1
vval = 0;    % group velocity parameter
nval=4;      % the coefficient of A_XX (nval=4 for the Nikolaevskiy equation)
x = Le*(1:N)'/N;
A = 0.01*rand(N,1);
% f = 0.01*rand(N,1);
f = -10*sin(2*pi*(x-Le/2)/Le)+0.01*rand(N,1);
v = fft(A);
w = fft(f);w(1)=0;
% Precompute various ETDRK4 scalar quantities:
h = 0.02;                              % time step
k = [0:N/2-1 0 -N/2+1:-1]'*2*pi/Le;   % wave numbers
antialias = (abs(k)>=2/3*N/2*2*pi/Le);
antialias(N/2+1)=1;
```

```
L01 = rval-nval*k.^2-vval*i*k;        % Fourier multipliers for A
L02 = -k.^2;                          % Fourier multipliers for f
L = [L01;L02];
E = exp(h*L); E2 = exp(h*L/2);        % exponentials
M = 16;                               % no. of points for complex means
r = exp(2i*pi*((1:M)-.5)/M);          % roots of unity
LR = h*L(:,ones(M,1)) + r(ones(2*N,1),:);
Q  = h*(mean(           (exp(LR/2)-1)./LR              ,2));
f1 = h*(mean(  (-4-LR+exp(LR).*(4-3*LR+LR.^2))./LR.^3  ,2));
f2 = h*(mean(    (4+2*LR+exp(LR).*(-4+2*LR))./LR.^3    ,2));
f3 = h*(mean(  (-4-3*LR-LR.^2+exp(LR).*(4-LR))./LR.^3  ,2));
pspec = zeros(N,1);
tmax =1000;
b=100; % the average is calculated after this time unit
Z=b/h;
dps=1000;
nmax = round(tmax/h); nplt = floor((tmax/dps)/h);
g = -i*k; arewethereyet = waitbar(0,'please wait...');
Aave=0;fave=0;
AA=zeros(N,dps+1);AA(:,1)=ifft(v);tt2=zeros(1,dps+1);
ff=zeros(N,dps+1);ff(:,1)=real(ifft(w));
tt=(1:nmax)*h;
shiftv=zeros(nmax,1);
% first loop
for n = 1:Z
    t = n*h;
    Ais = ifft(v);fis = real(ifft(w));
    Nv = -i*fft(Ais.*fis);
    Nw = g.*fft(abs(Ais).^2);
    vw=[v;w]; Nt=[Nv;Nw];
    a = E2.*vw + Q.*Nt; a1=a(1:N); a2=a(N+1:end);
    Ais = ifft(a1);fis = real(ifft(a2));
    Na1= -i*fft(Ais.*fis);Na2= g.*fft(abs(Ais).^2);Na=[Na1;Na2];
    b = E2.*vw + Q.*Na; b1=b(1:N); b2=b(N+1:end);
    Ais = ifft(b1);fis = real(ifft(b2));
    Nb1= -i*fft(Ais.*fis);Nb2= g.*fft(abs(Ais).^2);Nb=[Nb1;Nb2];
```

```
    c = E2.*a + Q.*(2*Nb-Nt); c1=c(1:N); c2=c(N+1:end);
    Ais = ifft(c1);fis = real(ifft(c2));
    Nc1= -i*fft(Ais.*fis);Nc2= g.*fft(abs(Ais).^2);Nc=[Nc1;Nc2];
    vw = E.*vw + Nt.*f1 + (Na+Nb).*f2 + Nc.*f3;
    v=vw(1:N);w=vw(N+1:end);
    v(antialias)=0;
    w(antialias)=0;
    if (max(isnan(real(v)))==1) break,end
    if (max(isnan(imag(v)))==1) break,end
    if (max(isnan(real(w)))==1) break,end
    if (max(isnan(imag(w)))==1) break,end
    % pspec(1) is the long-time average of |v_0|^2/length (square of zero mode)
    fphys=real(ifft(w));[YYY,III]=min(abs(fphys((N/2-5):(N/2+5))));
    shiftv(n)=(III-1-5)*Le/N;
    w=exp(i*k*(III-1-5)*Le/N).*w;
    v=exp(i*k*(III-1-5)*Le/N).*v;
    Aabs2=abs(ifft(v));
    pspec = pspec+((abs(v)).^2)/nmax/Le;
    if mod(n,nplt)==0
    A=ifft(v); AA(:,n/nplt+1)=A;
    f=real(ifft(w)); ff(:,n/nplt+1)=f;
    tt2(n/nplt+1)=n*h;
    figure(2),plot(x,f,x,Aabs2),shg
    end
    waitbar(n/nmax,arewethereyet)
end
% the average is calculated in the second loop
for n = Z+1:nmax
    t = n*h;
    Ais = ifft(v);fis = real(ifft(w));
    Nv = -i*fft(Ais.*fis);
    Nw = g.*fft(abs(Ais).^2);
    vw=[v;w]; Nt=[Nv;Nw];
    a = E2.*vw + Q.*Nt; a1=a(1:N); a2=a(N+1:end);
    Ais = ifft(a1);fis = real(ifft(a2));
    Na1= -i*fft(Ais.*fis);Na2= g.*fft(abs(Ais).^2);Na=[Na1;Na2];
```

```
    b = E2.*vw + Q.*Na; b1=b(1:N); b2=b(N+1:end);
    Ais = ifft(b1);fis = real(ifft(b2));
    Nb1= -i*fft(Ais.*fis);Nb2= g.*fft(abs(Ais).^2);Nb=[Nb1;Nb2];
    c = E2.*a + Q.*(2*Nb-Nt); c1=c(1:N); c2=c(N+1:end);
    Ais = ifft(c1);fis = real(ifft(c2));
    Nc1= -i*fft(Ais.*fis);Nc2= g.*fft(abs(Ais).^2);Nc=[Nc1;Nc2];
    vw = E.*vw + Nt.*f1 + (Na+Nb).*f2 + Nc.*f3;
    v=vw(1:N);w=vw(N+1:end);
    v(antialias)=0;
    w(antialias)=0;
    if (max(isnan(real(v)))==1) break,end
    if (max(isnan(imag(v)))==1) break,end
    if (max(isnan(real(w)))==1) break,end
    if (max(isnan(imag(w)))==1) break,end
    % pspec(1) is the long-time average of |v_0|^2/length (square of zero mode)
    fphys=real(ifft(w));[YYY,III]=min(abs(fphys((N/2-5):(N/2+5))));
    shiftv(n)=(III-1-5)*Le/N;
    w=exp(i*k*(III-1-5)*Le/N).*w;
    v=exp(i*k*(III-1-5)*Le/N).*v;
    Aabs2=abs(ifft(v));
    Aave=Aave+abs(ifft(v).^2);fave=fave+real(ifft(w));
    pspec = pspec+((abs(v)).^2)/nmax/Le;
    if mod(n,nplt)==0
    A=ifft(v); AA(:,n/nplt+1)=A;
    f=real(ifft(w)); ff(:,n/nplt+1)=f;
    tt2(n/nplt+1)=n*h;
    % The plot of |A| (solid curve) and f (dashed curve) at the end of the
    % simulation
    figure(2),plot(x,f,'--',x,Aabs2,'black'),shg
    set (gca,'FontSize',13)
    xlabel('X','FontSize',20,'Interpreter','latex')
    end
    waitbar(n/nmax,arewethereyet)
end
Aave=Aave/(nmax-Z);fave=fave/(nmax-Z);
close(arewethereyet);
```

```
% Plot results:
% The temporal evolutions of |A| and f in grey scale plots (from top to bottom)
figure(1),clf(1)
view(2), colormap(gray);
subplot(2,1,1)
surf(tt2,x,abs(AA)), shading interp, lighting phong, axis tight
xlabel('$T$','FontSize',16,'Interpreter','latex')
ylabel('$X$','FontSize',16,'Interpreter','latex')
view(2), colormap(gray);
subplot(2,1,2)
pcolor(tt2,x,ff), shading flat,
colormap(gray)
xlabel('$T$','FontSize',16,'Interpreter','latex')
ylabel('$X$','FontSize',16,'Interpreter','latex')
shg
figure(3),clf(3)
subplot(1,2,1)
plot(x,Aave,'black')
xlim([0     Le])
set (gca,'FontSize',13)
xlabel('$X$','FontSize',20,'Interpreter','latex')
ylabel('$\langle|A|^2\rangle$','FontSize',20,'Interpreter','latex')
subplot(1,2,2)
plot(x,fave,'black')
xlim([0     Le])
set (gca,'FontSize',13)
xlabel('$X$','FontSize',20,'Interpreter','latex')
ylabel('$\langle f \rangle$','FontSize',20,'Interpreter','latex')
shg
% The front displacement about X=Le/2 during the simulation
figure(4),clf(4)
plot(tt,cumsum(shiftv),'black'),shg
set (gca,'FontSize',13)
xlabel('$T$','FontSize',20,'Interpreter','latex')
ylabel('','FontSize',20,'Interpreter','latex')
```

Appendix D

Numerical code for calculating the secondary stability of rolls

In this part we introduce the numerical code used in *Matlab* to calculate the secondary stability of rolls (§4.3) for the Nikolaevskiy equation with dispersion (4.1).

```
% set the parameters
global N rval alp beta basic_wavenumber k;
N  = 16;
rval = 0.1;  % r
alp = 1;     % alpha
beta = 2;    % beta
% calculate the minimum and maximum values for the wavenumber
wvalmin=sqrt(1-sqrt(rval));
wvalmax=sqrt(1+sqrt(rval));
% how many steps to take to get from min to max wavenumber
nwvals = 200;
% set the list of wavenumbers
wvals = linspace(wvalmin,wvalmax,nwvals);
for jct = 1:nwvals
% find the rolls
basic_wavenumber=wvals(jct);
Le = 2*pi/basic_wavenumber;
x = (0:N-1)'/N*2*pi/basic_wavenumber;
k = [0:N/2-1 0 -N/2+1:-1]'*basic_wavenumber;
u = 2*(sqrt(36+(alp-5/2*beta)^2)*sqrt(rval)*cos(basic_wavenumber*x)...
```

```
   +rval*sin(2*basic_wavenumber*x));
v = fft(u);vin0=v(2:end/2);vinri=[real(vin0);imag(vin0)];
% option to display output
options=optimset('Display','iter');
% option to display output
options=optimset('Display','off','TolFun',1e-10);
[v,fval] = fsolve(@myfun,vinri,options);  % Call optimizer
v=v(1:end/2)+i*v(end/2+1:end);
v=[0;v;0;conj(v(end:-1:1))];
% compute the phase speed
cnumer01 = 0.5*i*k.*fft(real(ifft(v)).^2);
cnumer02 = i*k.*v;
cnumer03 = -(k.^2).*v;
cnumer06 = -i*(k.^3).*v;
cnumer04 = fft(real(ifft(cnumer01)).*real(ifft(cnumer02)));
cnumer05 = fft(real(ifft(cnumer03)).^2);
cnumer07 = fft(real(ifft(cnumer06)).^2);
cdenom01 = fft(real(ifft(cnumer02)).^2);
cphase = (cnumer04(1)+alp*cnumer05(1)-beta*cnumer07(1))/cdenom01(1);
% compute the stability
gonetozero = 0;
 if (gonetozero == 0)
   vfinal = [v(N/2+2:end)' v(1:N/2)']/N;
   extra_bit = zeros(N-1,N-1);
  for ict = -(N/2-2):(N/2-2)
    extra_bit = extra_bit+diag(vfinal(ict+N/2)*ones(N-1-abs(ict),1),ict);
  end
  % set the perturbation wavenumber
  maxeig = -10.0;
  for p = linspace(-pi/Le,pi/Le,300)
      wavenumbers = [-(N/2-1):(N/2-1)]'*2*pi/Le+p;
      linear_terms = wavenumbers.^2.*(rval-1+2*wavenumbers.^2 ...
      - wavenumbers.^4)-alp*i*wavenumbers.^3 ...
      +i*cphase*wavenumbers+beta*i*wavenumbers.^5;
      stability_matrix = diag(linear_terms)-diag(wavenumbers)*i*extra_bit;
      eigenvalues = eig(stability_matrix);
```

```
      [eii,ii] = sort(-real(eigenvalues));
      eigenvalues = eigenvalues(ii);
      firstfew = eigenvalues(1:5);
      [maxff,ifff] = max(real(firstfew));
    if (maxff>maxeig)
       maxeig = maxff;
       eigis = firstfew(ifff);
    end
  end
% output columns are:
% r   alpha   beta   k   max(Re(eigenvalue))  c   eigenvalue
  disp([num2str(rval) '    ' num2str(alp) '    ' num2str(beta) '    ' ...
  num2str(basic_wavenumber,8) '    ' num2str(maxeig,8) '    ' ...
  num2str(cphase,8) '    ' num2str(eigis)])
 else
% here the solution has gone to the trivial state
  disp([num2str(rval) '    ' num2str(alp) '    ' num2str(beta) '    ' ...
  num2str(basic_wavenumber) '    ' num2str(-999)])
 end
end
```

This code uses the following function:

```
function F = myfun(vinri)
global N rval alp beta basic_wavenumber k;
vin = vinri(1:end/2)+i*vinri(end/2+1:end);
v = [0;vin;0;conj(vin(end:-1:1))];
% COMPUTE THE PHASE SPEED
cnumer01 = 0.5*i*k.*fft(real(ifft(v)).^2);
cnumer02 = i*k.*v;
cnumer03 = -(k.^2).*v;
cnumer06 = -i*(k.^3).*v;
cnumer04 = fft(real(ifft(cnumer01)).*real(ifft(cnumer02)));
cnumer05 = fft(real(ifft(cnumer03)).^2);
cnumer07 = fft(real(ifft(cnumer06)).^2);
cdenom01 = fft(real(ifft(cnumer02)).^2);
cphase = (cnumer04(1)+alp*cnumer05(1)-beta*cnumer07(1))/cdenom01(1);
```

```
g = -0.5i*k;
linear_terms = k.^2.*(rval-1+2*k.^2-k.^4)-alp*i*k.^3+beta*i*k.^5+i*cphase*k;
nonlinear_term = g.*fft(real(ifft(v)).^2);
nik = linear_terms.*v+nonlinear_term;
Fri = nik(2:end/2);
F = [real(Fri);imag(Fri)];
F(end/2+1) = imag(v(2));
```

References

[1] S. I. Anisimov, M. I. Tribel'skii, and Y. G. Épel'baum. Instability of plane evaporation front in interaction of laser radiation with a medium. *Sov. Phys. JETP*, 51:802–806, 1980.

[2] R. Anugraha, Y. Hidaka, N. Oikawa, and S. Kai. A transition to spatiotemporal chaos under a symmetry breaking in a homeotropic nematic system. *J. Phys. Soc. Jpn.*, 77:073001, 2008.

[3] I. S. Aranson and L. Kramer. The world of the complex Ginzburg-Landau equation. *Rev. Mod. Phys.*, 74:99–143, 2002.

[4] H. Ashi. *Numerical Methods for Stiff Systems*. PhD thesis, University of Nottingham, 2008.

[5] P. Becherer, A. N. Morozov, and W. van Saarloos. Probing a subcritical instability with an amplitude expansion: An exploration of how far one can get. *Physica D*, 238:1827–1840, 2009.

[6] I. A. Beresnev and V. N. Nikolaevskiy. A model for nonlinear seismic waves in a medium with instability. *Physica D*, 66:1–6, 1993.

[7] J. P. Boyd. *Chebyshev and Fourier Spectral Methods*. Dover, New York, second edition, 2001.

[8] P. Brunet. Stabilized Kuramoto-Sivashinsky equation: A useful model for secondary instabilities and related dynamics of experimental one-dimensional cellular flows. *Phys. Rev. E*, 76:017204, 2007.

[9] F. H. Busse. Non-linear properties of thermal convection. *Rep. Prog. Phys.*, 41:1929–1967, 1978.

[10] C. Canuto, M. Y. Hussaini, A. Quarteroni, and T. A. Zang. *Spectral Methods in Fluid Dynamics*. Springer-Verlag, Berlin and New York, 1988.

[11] J. W. Cooley and J. W. Tukey. An algorithm for the machine calculation of complex Fourier series. *Math. Comp.*, 19:297–301, 1965.

[12] P. Coullet and S. Fauve. Propagative phase dynamics for systems with Galilean invariance. *Phys. Rev. Lett.*, 55:2857–2859, 1985.

[13] S. M. Cox and P. C. Matthews. Exponential time differencing for stiff systems. *J. Comput. Phys.*, 176:430–455, 2002.

[14] S. M. Cox and P. C. Matthews. Pattern formation in the damped Nikolaevskiy equation. *Phys. Rev. E*, 76:056202, 2007.

[15] S. M. Cox, P. C. Matthews, and S. L. Pollicott. Swift-Hohenberg model for magnetoconvection. *Phys. Rev. E*, 69:066314, 2004.

[16] M. C. Cross and P. C. Hohenberg. Pattern formation outside of equilibrium. *Rev. Mod. Phys.*, 65:851–1112, 1993.

[17] J. Duan, H. V. Ly, and E. S. Titi. The effect of nonlocal interactions on the dynamics of the Ginzburg-Landau equation. *ZAMP*, 47:432–455, 1996.

[18] W. Eckhaus. *Studies in Non-Linear Stability Theory*, volume 6. Springer-Verlag, Berlin, 1965.

[19] K. R. Elder, J. D. Gunton, and N. Goldenfeld. Transition to spatiotemporal chaos in the damped Kuramoto-Sivashinsky equation. *Phys. Rev. E*, 56:1631–1634, 1997.

[20] F. J. Elmer. Nonlinear and nonlocal dynamics of spatially extended systems: stationary states, bifurcations and stability. *Physica D*, 30:321–342, 1988.

[21] B. Fornberg. *A Practical Guide to Pseudospectral Methods*. Cambridge University Press, Cambridge, 1996.

[22] H. Fujisaka, T. Honkawa, and T. Yamada. Amplitude equation of higher-dimensional Nikolaevskii turbulence. *Prog. Theor. Phys.*, 109:911–918, 2003.

[23] H. Fujisaka and T. Yamada. Possibility of soft-mode turbulence in reaction-diffusion systems. *Prog. Theor. Phys.*, 106:315–322, 2001.

[24] L. Y. Glebsky and L. M. Lerman. On small stationary localized solutions for the generalized 1-D Swift-Hohenberg equation. *Chaos*, 5:424–431, 1995.

[25] A. A. Golovin, B. J. Matkowsky, and A. A. Nepomnyashchy. A complex Swift-Hohenberg equation coupled to the Goldstone mode in the nonlinear dynamics of flames. *Physica D*, 179:183–210, 2003.

[26] Y. Hidaka, J.-H. Hun, K. Hayashi, S. Kai, and M. I. Tribelsky. Soft-mode turbulence in electrohydrodynamic convection of a homeotropically aligned nematic layer. *Phys. Rev. E*, 56:R6256–R6259, 1997.

[27] M' F. Hilali, S. Métens, P. Borckmans, and G. Dewel. Pattern selection in the generalized Swift-Hohenberg model. *Phys. Rev. E*, 51:2046–2052, 1995.

[28] R. Hoyle. *Pattern Formation: An Introduction to Methods*. University Press, Cambridge, 2006.

[29] S. Kai, K. Hayashi, and Y. Hidaka. Pattern forming instability in homeotropically aligned liquid crystals. *J. Phys. Chem.*, 100:19007–19016, 1996.

[30] A.-K. Kassam and L.N. Trefethen. Fourth-order time-stepping for stiff PDEs. *SIAM J. Sci. Comput.*, 26:1214–1233, 2005.

[31] T. Kawahara. Formation of saturated solitons in a nonlinear dispersive system with instability and dissipation. *Phys. Rev. Lett.*, 51:381–383, 1983.

[32] I. L. Kliakhandler and B. A. Malomed. Short-wavelength instability in presence of a zero mode: anomalous growth law. *Phys. Lett. A*, 231:191–194, 1997.

[33] E. Knobloch and J. De Luca. Amplitude equations for travelling wave convection. *Nonlinearity*, 3:975–980, 1990.

[34] N. A. Kudryashov and A. V. Migita. Periodic structures developing with account for dispersion in a turbulence model. *Fluid Dyn.*, 42:463–471, 2007.

[35] Y. Kuramoto. *Chemical Oscillations, Waves, and Turbulence*. Springer-Verlag, New York, 1984.

[36] Y. Kuramoto and T. Tsuzuki. Persistent propagation of concentration waves in dissipative media far from thermal equilibrium. *Prog. Theor. Phys.*, 55:356–369, 1976.

[37] R. E. LaQuey, S. M. Mahajan, P. H. Rutherford, and W. M. Tang. Nonlinear saturation of the trapped-ion mode. *Phys. Rev. Lett.*, 34:391–394, 1975.

[38] J. Lega, J. V. Moloney, and A. C. Newell. Swift-Hohenberg equation for lasers. *Phys. Rev. Lett.*, 73:2978–2981, 1994.

[39] B. A. Malomed. Patterns produced by a short-wave instability in the presence of a zero mode. *Phys. Rev. A*, 45:1009–1017, 1992.

[40] P. C. Matthews and S. M. Cox. One-dimensional pattern formation with Galilean invariance near a stationary bifurcation. *Phys. Rev. E*, 62:R1473–R1476, 2000.

[41] C. Misbah and A. Valance. Secondary instabilities in the stabilized Kuramoto-Sivashinsky equation. *Phys. Rev. E*, 49:166–183, 1994.

[42] A. A. Nepomnhyashchy. Order parameter equations for long-wavelength instabilities. *Physica D*, 86:90–95, 1995.

[43] A. C. Newell and J. A. Whitehead. Finite bandwidth, finite amplitude convection. *J. Fluid Mech.*, 38:279–303, 1969.

[44] V. N. Nikolaevskii and G. S. Stepanova. Nonlinear seismics and the acoustic action on the oil recovery from an oil pool. *Acoust. Phys.*, 51:S131–S139, 2005.

[45] V. N. Nikolaevskiy. Dynamics of viscoelastic media with internal oscillators. In S. L. Koh and C. G Speciale, editors, *Recent Advances in Engineering Science*, Lecture Notes in Engineering, pages 210–221. Springer-Verlag, Berlin, 1989.

[46] E. Plaut and F. H. Busse. Low-Prandtl-number convection in a rotating cylindrical annulus. *J. Fluid Mech.*, 464:345–363, 2002.

[47] K.-F. Poon. *Dynamics of the Nikolaevskiy and Related Equations*. PhD thesis, Simon Fraser University, 2009.

[48] K.-F. Poon and R. W. Wittenberg. Coarsening to chaos-stabilized fronts. *Phys. Rev. E*, 83:016211, 2011.

[49] A. G. Rossberg. Three-dimensional pattern formation, multiple homogeneous soft modes, and nonlinear dielectric electroconvection. *Phys. Rev. E*, 62:8114–8132, 2000.

[50] A. G. Rossberg, A. Hertrich, L. Kramer, and W. Pesch. Weakly nonlinear theory of pattern-forming systems with spontaneously broken isotropy. *Phys. Rev. Lett.*, 76:4729–4732, 1996.

[51] H. Sakaguchi. Defect turbulence in the coupled Swift-Hohenberg-Ginzburg-Landau equations. *Prog. Theor. Phys.*, 96:1037–1042, 1996.

[52] H. Sakaguchi and D. Tanaka. Global structure in spatiotemporal chaos of the Matthews-Cox equation. *Phys. Rev. E*, 76:025201(R), 2007.

[53] L. A. Segel. Distant side-walls cause slow amplitude modulation of cellular convection. *J. Fluid Mech.*, 38:203–224, 1969.

[54] E. Simbawa, P. C. Matthews, and S. M. Cox. Nikolaevskiy equation with dispersion. *Phys. Rev. E*, 81:036220, 2010.

[55] G. I. Sivashinsky. Nonlinear analysis of hydrodynamic instability in laminar flames-I. Derivation of basic equations. *Acta Astronaut.*, 4:1177–1206, 1977.

[56] G. I. Sivashinsky. Instabilities, pattern formation, and turbulence in flames. *Ann. Rev. Fluid Mech.*, 15:179–199, 1983.

[57] G. I. Sivashinsky and D. M. Michelson. On irregular wavy flow of a liquid film down a vertical plane. *Prog. Theor. Phys.*, 63:2112–2114, 1980.

[58] D.V. Strunin. Phase equation with nonlinear excitation for nonlocally coupled oscillators. *Physica D*, 238:1909–1916, 2009.

[59] J. Swift and P. C. Hohenberg. Hydrodynamic fluctuations at the convective instability. *Phys. Rev. A*, 15:319–328, 1977.

[60] K. Tamura, Y. Hidaka, Y. Yusuf, and S. Kai. Anomalous diffusion and Lévy distribution of particle velocity in soft-mode turbulence in electroconvection. *Physica A*, 306:157–168, 2002.

[61] D. Tanaka. Chemical turbulence equivalent to Nikolaevskii turbulence. *Phys. Rev. E*, 70:015202(R), 2004.

[62] D. Tanaka. Critical exponents of Nikolaevskii turbulence. *Phys. Rev. E*, 71:025203(R), 2005.

[63] D. Tanaka. Turing instability leads oscillatory systems to spatiotemporal chaos. *Prog. Theor. Phys. Suppl.*, 161:119–126, 2006.

[64] D. Tanaka and Y. Kuramoto. Complex Ginzburg-Landau equation with nonlocal coupling. *Phys. Rev. E*, 68:026219, 2003.

[65] M. Tlidi, M. Georgiou, and P. Mandel. Transverse patterns in nascent optical bistability. *Phys. Rev. A*, 48:4605–4609, 1993.

[66] M. Tlidi, P. Mandel, and R. Lefever. Localized structures and localized patterns in optical bistability. *Phys. Rev. Lett.*, 73:640–643, 1994.

[67] L. N. Trefethen. *Spectral Methods in MATLAB*. SIAM, Philadelphia, 2000.

[68] M. I. Tribel'skii. Short-wavelength instability and transition to chaos in distributed systems with additional symmetry. *Phys. Usp.*, 40:159–180, 1997.

[69] M. I. Tribelsky. Statistical properties of chaos at onset of electroconvection in a homeotropically aligned nematic layer. *Phys. Rev. E*, 59:3729–3732, 1999.

[70] M. I. Tribelsky. Patterns in dissipative systems with weakly broken continuous symmetry. *Phys. Rev. E*, 77:035202(R), 2008.

[71] M. I. Tribelsky and K. Tsuboi. New scenario for transition to turbulence? *Phys. Rev. Lett.*, 76:1631–1634, 1996.

[72] M. I. Tribelsky and M. G. Velarde. Short-wavelength instability in systems with slow long-wavelength dynamics. *Phys. Rev. E*, 54:4973–4981, 1996.

[73] K. Tsiveriotis and R. A. Brown. Bifurcation structure and the Eckhaus instability. *Phys. Rev. Lett.*, 63:2048–2051, 1989.

[74] L. S. Tuckerman and D. Barkley. Bifurcation analysis of the Eckhaus instability. *Physica D: Nonlinear Phenomena*, 46:57–86, 1990.

[75] D. M. Winterbottom. The complex Ginzburg-Landau equation. `http://www.maths.nottingham.ac.uk/personal/pmxdmw/tutorial/`.

[76] D. M. Winterbottom. *Pattern Formation with a Conservation Law.* PhD thesis, University of Nottingham, 2005.

[77] R. W. Wittenberg. Dissipativity, analyticity and viscous shocks in the (de)stabilized Kuramoto-Sivashinsky equation. *Phys. Lett. A*, 300:407–416, 2002.

[78] R. W. Wittenberg and P. Holmes. Scale and space localization in the Kuramoto-Sivashinsky equation. *Chaos*, 9:452–465, 1999.

[79] R. W. Wittenberg and K.-F. Poon. Anomalous scaling on a spatiotemporally chaotic attractor. *Phys. Rev. E*, 79:056225, 2009.

[80] H.-W. Xi, R. Toral, J. D. Gunton, and M. I. Tribelsky. Extensive chaos in the Nikolaevskii model. *Phys. Rev. E*, 62:R17–R20, 2000.

[81] T. Yamada and Y. Kuramoto. A reduced model showing chemical turbulence. *Prog. Theor. Phys.*, 56:681–683, 1976.